SCUOLA DI DOTTORATO

UNIVERSITÀ DEGLI STUDI DI MILANO-BICOCCA

Department of Medicine and Surgery

PhD program in Translational and Molecular Medicine (DIMET)

Cycle XXXVIII

Transcriptional activators rescue Frataxin expression and downstream pathways in Friedreich's ataxia diseased cell types

Surname **MELACINI** Name **ELENA**

Registration number **896574**

Tutor: Prof.ssa Silvia Kirsten Nicolis

Co-tutor: Dr. Vania Broccoli

Supervisor: Dr. Vania Broccoli

Coordinator: Prof. Francesco Mantegazza

ACADEMIC YEAR 2024/2025

Table of contents

Abbreviations and acronyms

FA – Friedreich's Ataxia

FXN – Frataxin (gene/protein)

FA-DMR – Friedreich's Ataxia–Differentially Methylated Region

CRISPR – Clustered Regularly Interspaced Short Palindromic Repeats

CRISPRa – CRISPR activation

dCas9 – dead Cas9

VP160 / VP64 / VPR – activation domains derived from VP16 (transcriptional activator from Herpes Simplex)

sgRNA – single guide RNA

ZF / ZFA / ZFAs – Zinc Finger / Zinc Finger Activator(s)

AAV – Adeno-Associated Virus

NLS – Nuclear Localization Signal

iPSC(s) – induced Pluripotent Stem Cell(s)

NPC(s) – Neural Progenitor Cell(s)

DRG(s) – Dorsal Root Ganglion (Ganglia)

CTRL – Control (healthy donor)

DIV – Days In Vitro

hFXN/mFXN – human/murine Frataxin

ISC(s) – Iron–Sulphur Cluster(s)

ETC – Electron Transport Chain

ROS – Reactive Oxygen Species

RNA-seq – RNA sequencing

RT-qPCR – Reverse Transcription quantitative Polymerase Chain Reaction

PCA – Principal Component Analysis

FDA – Food and Drug Administration

EMA – European Medicines Agency

AAV – Adeno-Associated Virus (vettore virale)

CHAPTER 1
General introduction

1. Proprioception

Proprioception is the sense that enables the perception of body and limb position and movement in space (Sherrington CS, 1906). This “sense of self” originates in the musculoskeletal system, where proprioceptors, muscle spindles and Golgi tendon organs (GTOs), detect muscle stretch and tension (Jami L, 1992; Matthews PBC, 1972). These signals are transmitted via afferent axons of proprioceptive sensory neurons, whose cell bodies reside in the dorsal root ganglia (DRGs), to the central nervous system (CNS). In the CNS, proprioceptive signal is either transmitted to a spinal reflex circuit, for rapid and unconscious motor response, or, at the same time, to upper centers of motor control, in cerebellum and cortex, to elaborate a conscious response to the peripheral stimulus (Proske U, Gandevia SC, 2018.; Riemann BL, Lephart SM, 2002.; Tuthill JC, Azim E, 2018). Through the spinal reflex circuit, the action potential generated by the proprioceptive neurons is instantly transmitted to the α-motorneurons innervating the extrafusal fibers of the same muscle, to immediately stabilize posture and adapt to unexpected external factors. In parallel, the signal is transmitted to the upper motor centers through ascending pathways, such as the cerebello-thalamo-cortical pathway and the dorsal column–medial lemniscus cortical pathway (Horne MK, Butler EG. 1995, Ivanusic JJ et al. 2005, Loutit AJ et al. 2021). Once the target organ has been reached by the signal, this is elaborated and a response is sent back to the α-motorneurons, contacting the muscle. This feedback loop allows the muscle to contract with a strength that is directly proportional to the intensity of the stretch recorded by the proprioceptors, in order to avoid possible damages to the tissue and to ensure a proper positioning of the body in the surrounding space (Kröger S et al., 2018). Proprioceptive information tells us about the contractile state of our muscles and, therefore, it is essential for the coordination of any movement, normal gait and steady posture. Since this sense is vital for motor control, pathological conditions in which it is impaired result in prominent sensory and motor deficits, culminating in ataxic symptoms (Dietz V et al., 2002). Congenital absence of proprioception results in developmental alterations of head movements control and walking, an early impairment of fine motor skills, sensory ataxia with unsteady gait, inability to maintain balance with eyes closed (Romberg’s sign) and an absence of tendon reflexes (Behunova J et al., 2019; Delle Vedove A et al., 2016; Haliloglu G et al., 2017; Mahmud AA et al., 2017; Masingue M et al., 2019; Smith LJ et al., 2018). In this condition, secondary senses, such as visual and vestibular systems, can help compensate for proprioceptive lack, ensuring the possibility to perform coordinated voluntary movements. Interestingly, recent evidence highlighted the involvement of proprioceptive system also in the realignment and proper healing of fractured bones (Blecher R et al., 2017) as well as for the maintenance of spine alignment (Blecher R et al., 2017, 2018; Kröger S et al., 2018).

1.1 Muscle spindle

The muscle spindles are the main proprioceptors that can be found in the organism (Matthews PB, 2015; Proske U, Gandevia SC, 2012). In humans, their number is around 50000 (Banks RW, 2006). They consist of specialized incapsulated muscle fibers (called intrafusal fibers), oriented in parallel to the other (extrafusal) muscle fibers. Human intrafusal fibers can be up to 8 mm long and each spindle can be composed of 8-20 fibers (Kiehn O, 2016; Macefield VG, Knellwolf TP, 2018; Proske U, Gandevia SC, 2012). Intrafusal fibers can be distinguished as nuclear bag or nuclear chain fibers, according to the positioning of their multiple nuclei (Kröger S, Watkins B, 2021). Muscle spindle function is to sense alterations in muscle stretch and communicate this information to the CNS (Matthews PB, 2015). Indeed, the muscle spindle is innervated by multiple neuronal terminations, in particular by two kinds of neurons: afferent sensory neurons and efferent motorneurons. The sensory neurons terminals can be divided into type Ia primary fibers, that form the annulospiral wrapping around the central part (equatorial) of the intrafusal fibers, and type II secondary fibers that, when present, contact the region flanking the equatorial one. The two types display different velocity of conduction of the signal (Banks RW, 2015). Additionally, intrafusal fibers are innervated by ɣ- and β-motorneurons efferents. ɣ-motorneurons, the best characherized and more abundant, represent the 30% of motorneurons in the ventral horn of the spinal cord. These terminals enter the muscle spindle together with the sensory axons, but then they form cholinergic synapses exclusively with the polar regions of the fibers, where most of the sarcomeres are localized. The endplates formed by ɣ-moteroneurons inside the muscle spindle are different from the neuromuscular junctions formed by α-motorneurons with the extrafusal fibers, however they have common features such as their cholinergic nature, junctional folds and a basal lamina filling the synaptic clefts (Banks RW, 1994; Manuel M, Zytnicki D, 2011; Zhang Y et al., 2015).

The mechanism by which all these elements work in synergy, to control the proprioceptive inputs and generate a response, relies on a series of auto-regulatory feedback that could be explained as follows. Upon muscle stretch, an action potential is generated in the sensory neurons afferents with a frequency corresponding to the entity of the event (De-Doncker L et al., 2003). The signal is transmitted to the CNS, where a co-activation of α- and ɣ-motorneurons happens. ɣ-motorneurons induce the contraction of the sarcomeres in the polar regions of the intrafusal fibers, generating a shortening of the fibers themselves and a stretch of the non-contractile equatorial region, with a consequent increased firing rate of the sensory terminals. In the meantime, as previously said, also α-motorneurons synapses are activated and the extrafusal fibers contraction is obtained (Proske U, 1997). This complex system guarantees a continuous adjustment of the mechanical sensitivity of the spindle, throughout the succession of muscle lengths and stretch velocities that usually takes place during a movement. Muscle spindle formation starts during embryonic development. In humans, muscle spindles are detectable from week 11 of gestation (Deriu F et al., 1996; Mavrinskaya LF, 1968; Przedpelska-Ober E, 1982). Immature intrafusal fibers maturation begins with the formation

of physical contact between sensory neurons axons and primary myotube. At this point the two elements start exchanging signals that favour reciprocal survival and maturation. More in detail, axons terminals secrete Neuregulin-1 (Nrg-1) factor which, through ErbB2 receptor, activates a pathway that leads to the induction of the transcriptional program for mature intrafusal fibers (Andrechek ER et al., 2002; Cheret C et al., 2013; Hippenmeyer S et al., 2002; Zelena J, 1994;). At the same time, muscle fibers release neurotrophin-3 (NT-3) that, binding to the tropomyosin receptor kinase C (TrkC), promotes the survival of proprioceptive sensory neurons. Indeed, it was demonstrated that muscle specific NT3- overexpression results in an increased number of sensory neurons afferents and muscle spindles (Ernfors P et al., 1994; Klein R et al., 1994; Smeyne RJ et al., 1994; Wright DE et al., 1997).

1.2 Dorsal root ganglia (DRGs)

In vertebrates, all the somatosensory pathways begin with the activation of sensory neurons, which sense the input from the periphery and transmit it to the CNS. They are responsible for mechanoception (sensing pressure), nociception (feeling pain), thermoception (sensing temperature) and proprioception (sensing body position in space) (Nascimento AI et al, 2018). Their cellular bodies (somas) are grouped inside the dorsal root ganglia (DRGs), structures located alongside the spinal cord. Humans have 31 pairs of spinal nerves formed by sensory fibers whose somas are in the DRGs (Haberberger RV et al, 2019). Interestingly, sensory neurons have a peculiar pseudo-unipolar morphology, first described in 1886 by His (His W, 1886). Indeed, they have a single protrusion called stem-axon that, inside the DRG, bifurcates into a peripheral and a central axon branch. As reported above, the stimulus from the periphery generates an action potential that propagates towards the spinal cord through the peripheral axonal branch. It enters the CNS, along the central axonal branch, through the dorsal horn of the spinal cord and, once there, it follows either ascending or descending pathways (Giuffrida R, Rustioni A, 1992).

1.2.1 Somatosensory neurons subtypes

DRG neurons are a strongly heterogeneous cell population and, for this reason, still today a clear and unique classification has not been reached. According to their functionality, they can be classified as mechanoceptors, proprioceptors, nociceptors and thermoceptors (Meltzer S et al., 2021). Large-diameter axon neurons are generally defined as Aα fibers and they are mainly proprioceptors, characterized by fast conduction speed. Proprioceptors can be subdivided into other three classes. The group Iα and II proprioceptive neurons innervate muscle spindles, while group Iβ innervates Golgi tendon organs and they are sensitive respectively to changes in muscle stretch and tension

(Tuthill JC, Azim E, 2018; Zampieri N, de Nooij JC, 2021). Among the large-diameter and large-body neurons, can be found also a group of low-threshold mechanoceptors (LTMR). Their myelinated fast-conductive fibers, referred to as Aβ fibers, respond to mechanical stimuli from the skin such as skin vibration, hair deflection and skin stretch (Zimmerman A et al.,2014). Intermediate cell body size and Aδ fibers neurons, with medium velocity of conduction, are again a mixed group of sensory neurons. In this class, it is possible to find neurons sensitive to thermal stimulation, mechanical forces and chemical irritants acting on the skin or internal organs. For example, Aδ -LTMRs, belonging to this group, are sensitive to skin indentation and hair deflection. On the other hand, Aδ -high threshold mechanoceptors (Aδ -HTMR) respond to high force mechanical inputs (Sharma N et al, 2020). Finally, there are small body size and small axon diameter sensory neurons. Their axons are the ones with the slowest conduction velocity and they are called C fibers. DRG neurons with C fibers include thermoceptors, nociceptors, mechanoceptors, pruriceptors which collectively report tissue damage, thermal stimuli, soft mechanical inputs acting on hairy skin and the presence of pruritogens factor on the skin or certain internal organs (Cranfill SL, Luo W, 2021). An important group of neurons with small caliber is represented by nociceptors. Historically, nociceptors were classified as either peptidergic or non-peptidergic (Basbaum AI et al., 2009). Peptidergic nociceptors secrete the neuropeptides CGRP and substance P, while the non-peptidergic ones express the neurotrophic factor Ret. Small diameter nociceptors can also be distinguished upon the expression of several ion channels such as TRPV1, TRPA1, TRPM8 and ASICs channels. C fibers-LTMRs are responsive to hairy skin stimuli (Zotterman Y, 1939) and, in humans, to affective touch (Olausson H et al, 2010) (Figure 1).

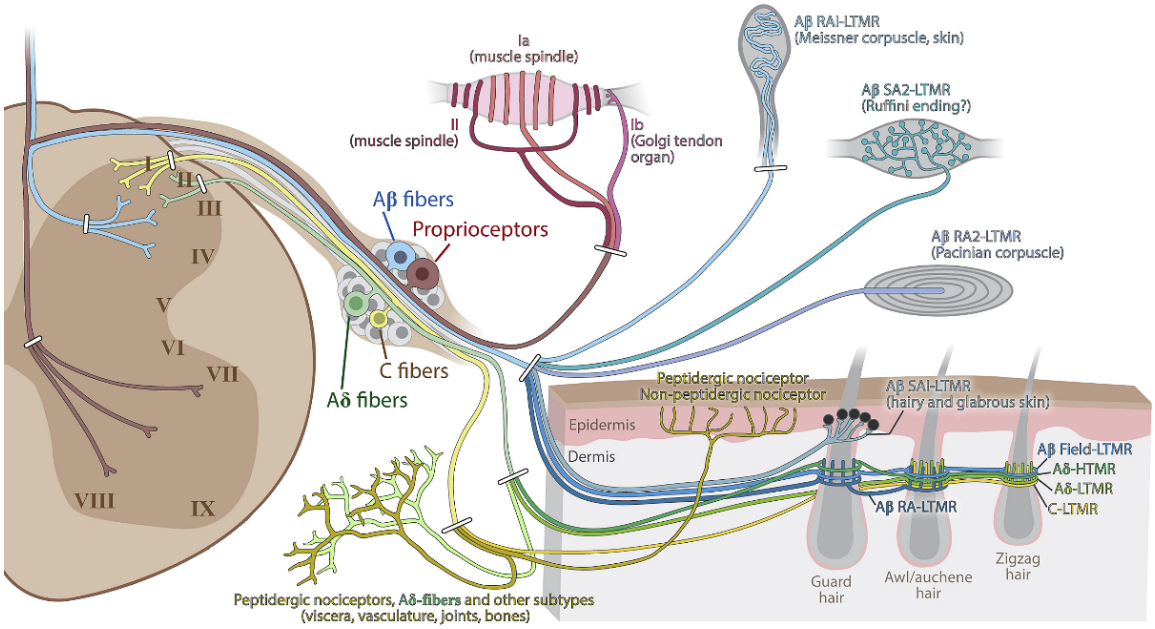

Figure 1. Somatosensory neurons projections. The cell bodies of somatosensory neurons are located in the dorsal root ganglia (DRG), positioned next to the spinal cord. These DRG neurons exhibit a pseudo-unipolar structure, with a single axon that splits into two branches, one projecting toward the periphery and the other toward the spinal cord. On the right, the main types of peripheral target tissues innervated by specific DRG neuron subtypes are illustrated. Also shown are the general, though simplified, lamination patterns of their central projections within the spinal cord. Notably, Aβ low-threshold mechanoreceptor (LTMR) fibers and proprioceptors possess central branches with multiple collaterals that extend along the rostral-caudal axis of the spinal cord, as well as an additional branch that travels upward through the dorsal column, often reaching the dorsal column nuclei in the brainstem (adapted from Meltzer S et al., 2021).

1.2.2 Somatosensory neurons development

The heterogeneity of DRG neurons and the difficulty in creating a clear and unambiguous classification is the reflection of the wide range of stimuli that the human organism can respond to. The complexity of this system rises from the developmental cues that lead the neurogenesis of somatosensory neurons. In the following paragraph, the process through which the DRG neurons acquire their mature identity will be illustrated.

DRG neurons and all the peripheral nervous system (PNS) glia originate from the neural crest cells (Le Douarin N et al.,1991). Neurons and glia in the CNS, on the other hand, originate from the neural tube (Rowitch DH, 2004). Neural crest cells are located dorsally to the neural tube and they migrate ventrally, to form the DRG, between E8.5 and E10 in mouse, in response to signaling cues from the neural tube (Kasemeier-Kulesa JC et al., 2005; Serbedzija GN et al., 1990). The identity of the future DRG neurons is determined through two specifying waves characterized by the activation of the transcription factors Neurogenin 1 and 2 (Ngn1/2). During the first wave, neural crest cells start to express Ngn2. The so defined transcriptional program gives rise mainly, but not only, to proprioceptive neurons positive for TrkC and mechanoceptive neurons positive for TrkB and Ret. The Ngn1-dependent second wave generates small diameter TrkA-positive nociceptive, mechanoceptive and thermoceptive neurons. Finally, a third and late wave of neurogenesis at E12 (in mouse) happens, starting from the progeny of the boundary cap cells which locates transiently on the top of the neural tube. This final wave brings to the specification of TrkA, TrkB and TrkC sensory neurons (Nascimento AI et al., 2018) (Figure 2). As already mentioned, from this process also PNS glia is generated. In the PNS the main glial cells are the Schwann cells and the satellite glial cells (SGCs). Similarly to DRG neurons, also glia is specified from neural crest cells and boundary cap cells. SGCs are present only in the DRGs and they interact with the body and the initial segment of the axons of the sensory neurons. Every DRG neuron is surrounded by one or multiple SGCs sheets and each neuron with its SGCs form a separate unit from the other neurons, thanks also to the presence of connective tissue among them. Conversely, Schwann cells are responsible for the wrapping of the distal portion of the neuronal axons both in the PNS and the CNS (Nascimento AI et al., 2018). One of the main features of the somatosensory neurons is their unique pseudo-unipolar morphology. During embryonic development, the not still mature DRG neurons are

bipolar, then the cell body elongates and this gives origin to the stem axon from which the two axonal terminals (central and peripheral) protrude and generate the peculiar T shape (Matsuda S et al., 2000).

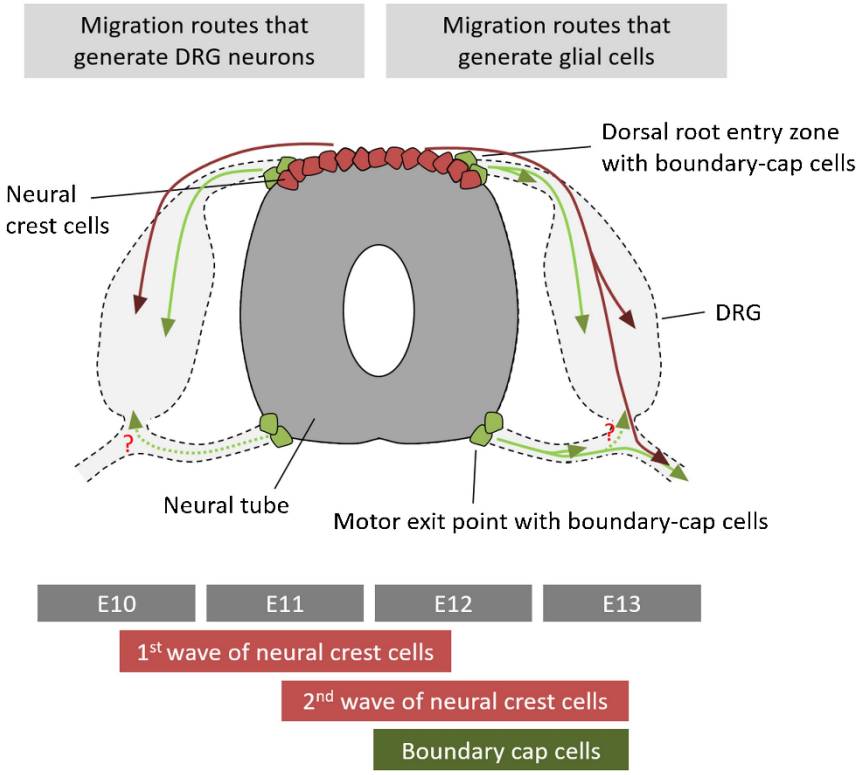

Figure 2. Somatosensory neurons development. Migration pathways of neural crest cells (shown in red) and boundary cap cells (shown in green) give rise to dorsal root ganglion (DRG) neurons (left) and glial cells (right). Neural crest cells detach from the dorsal neural tube and generate DRG neurons through two overlapping waves of neurogenesis. A third wave arises from boundary cap cells, transient intermediate progenitors located at the dorsal root entry zones and future motor exit points. Both neural crest cells and boundary cap cells contribute to the formation of DRG neurons and peripheral glial cells. The timeline of neurogenesis in lumbar DRGs of the mouse is also illustrated (From Nascimento AI et al., 2018).

1.3 Cerebellum

The human cerebellum (“little brain”) is an important part of the central nervous system (CNS) both in size and neural processing power. The cerebellum connects to the brainstem via three roots: the superior, middle, and inferior peduncles. It has a unique and perfectly organized structure. The cortex is divided into three transverse lobes: anterior and posterior lobes are separated by the primary fissure, and the smaller flocculonodular lobe is separated by the posterolateral one. The anterior and posterior lobes are folded into a series of lobules and further folded into folia. Longitudinally, it can be divided into a central part called vermis, because of its worm-like shape, and two lateral paravermis regions which give rise to the lateral emispheres (Aminoff MJ, Daroff RB, 2014).

The cerebellar cortex contains five cell types organized in layers. The most prominent cell type of the cortex is the ɣ-aminobutyric acid (GABA)ergic Purkinje cells. Their inhibitory axons, contacting the deep cerebellar nuclei, represent the only output from the cerebellar cortex. Each cortical region projects systematically to the underlying deep nuclei. The lateral hemisphere projects predominantly to the Dentate Nucleus; the paravermis projects to the Interpositus Nucleus, which in humans is divided into globose and emboliform nuclei; and the vermis projects to the fastigial nucleus. The flocculonodular cortex projects to the Dieter's Nucleus, a more lateral deep cerebellar nucleus (Aminoff MJ, Daroff RB, 2014). Charles Sherrington, in 1900, defined the cerebellum as the "head ganglion" of the proprioceptive system, considering its central role in elaborating the somatosensory information coming from the DRG neurons. Indeed, anatomically, once reached the CNS, the sensory inputs from the periphery are sent to upper centers. More precisely, two pairs of spinocerebellar tracts originate from the DRG neurons terminals exiting the spinal cord: the dorsal spinocerebellar tract (DSCT) and the ventral spinocerebellar tract (VSCT), carrying information from the hindlimbs and lower trunk, and the cuneo- and rostro-spinocerebellar tracts, carrying information from the forelimbs and upper trunk. The DSCT arises from Clarke's Nucleus, located posteriorly in the spinal cord, and provides fast-adapting cutaneous and muscle mechanoreceptor information to the cerebellum via the inferior peduncle. The VSCT arises from more lateral cells of the spinal gray matter and carries muscle spindle, cutaneous, and particularly Golgi tendon organ inputs via the superior cerebellar peduncle. In the cerebellum, mossy and climbing fibers, the terminal part of the ascending tract, form excitatory glutamatergic synapses with the Purkinje cells in the granule layer of the cerebellar cortex. The so activated Purkinje cells generate output signals that are sent to the deep cerebellar nuclei. From here some cerebellar outputs relay via the thalamus to the motor cortex, where the motor command is elaborated. Other outputs follow the indirect pathway that involves the red nucleus and vestibular nuclei in the brainstem, which in turn project to the motor cortex (Aminoff MJ, Daroff RB, 2014). At this point, the motor instructions are sent back to the spinal cord through the corticospinal (or pyramidal) tract by the pyramidal neurons in the V layer of the motor cortex. In the ventral horn of the spinal cord, the motor stimulus reaches α-, β- or ɣ-motorneurons, the last hierarchical element in movement control (Figure 3). As explained in paragraph 1.1, each type of motorneuron is responsible for contacting specific areas of the muscle fibers. As said so far, the movement is finely regulated by motor cortex outputs, but a fundamental role is also played by the simpler and faster reflex arc. The reflex arc consists in the synaptic interaction of sensory neurons directly with α-motorneurons. When the signal from the periphery travels along the central axon of the DRG neurons it can be sent not only to the Clarke's Nuclei, to follow ascending pathways, but also directly to the α-motorneurons, that immediately induce the muscle contraction. This system ensures a rapid adaptation to unexpected changes in muscular tone and prevents possible tissue damages caused by excessive stretch (Aminoff MJ, Daroff RB, 2014).

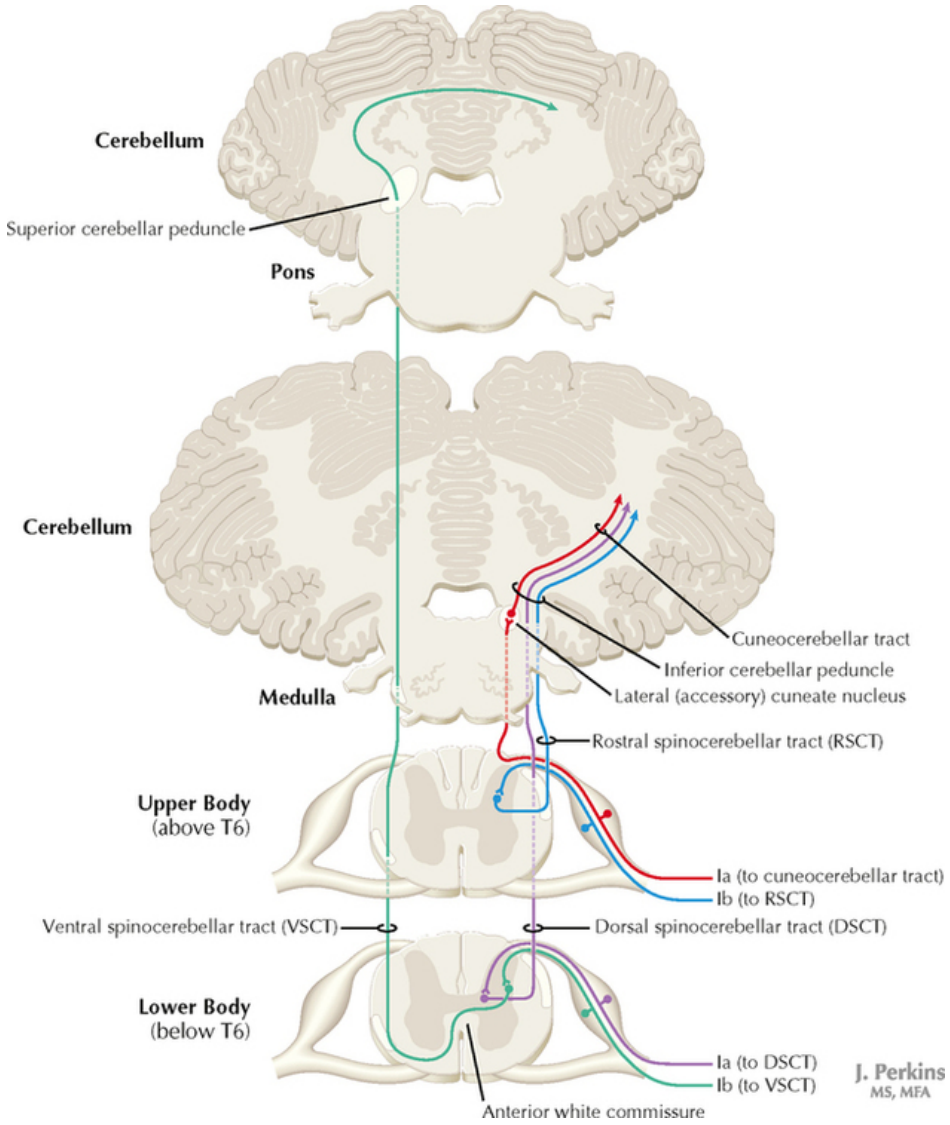

Figure 3. Spino-cerebellar pathways. Proprioceptive primary somatosensory axons originating from joints, tendons, and ligaments, represented here by group Ib afferents from Golgi tendon organs, terminate on neurons that give rise to the ventral spinocerebellar tract (VSCT) and the rostral spinocerebellar tract (RSCT), which carry information from the lower and upper body, respectively. Meanwhile, proprioceptive axons from muscle spindles, represented by group Ia afferents, synapse onto neurons located in Clarke's nucleus and the lateral (external) cuneate nucleus of the medulla, which give rise to the dorsal spinocerebellar tract (DSCT) and the cuneo-cerebellar tract for the lower and upper body, respectively. The DSCT, RSCT, and cuneo-cerebellar tracts remain on the same (ipsilateral) side of the body, while the VSCT crosses the midline twice, first at the anterior white commissure of the spinal cord and again within the cerebellum (James A. Perkins, MS, MFA-Netter Collection).

2. Friedreich’s ataxia (FA)

2.1 Clinical aspects

FA is the most prevalent autosomal recessive hereditary ataxia, with an estimated prevalence of approximately 1 in 40,000 individuals within the Caucasian population (Koeppen AH, 2011; Pandolfo M, 2009). The disease typically manifests during childhood or adolescence, with an average age of onset between 10 and 15 years. Progressive motor impairment often leads to wheelchair dependence within 10–15 years of symptom onset. The mean life expectancy is around 36 years, with cardiomyopathy representing the leading cause of mortality. The hallmark clinical features of FA include limb and gait ataxia, resulting from progressive neurodegeneration. Additional neurological manifestations comprise dysarthria, areflexia, and loss of vibration and proprioceptive senses (Corben LA, 2010). The neurodegenerative process predominantly affects large sensory neurons within the DRGs, especially proprioceptive neurons, the Dentate Nucleus of the cerebellum, and the corticospinal tracts (Harding IH, 2020). Patients may also experience visual impairment, hearing loss, urinary urgency, and neuropathic pain. Visual loss is associated with degeneration of the optic nerve and thinning of the retinal ganglion cell layer, whereas hearing loss arises from auditory neuropathy. Neuropathic pain, on the other hand, results from sensory neuron degeneration (Keita M et al., 2022). Although FA is classically defined as a neurodegenerative disorder, it is now recognized as a multisystemic disease. Cardiac involvement is particularly prominent and represents the major life-limiting complication, accounting for approximately 60% of deaths. Electrocardiographic and echocardiographic abnormalities are common, with about 85% of patients showing T-wave repolarization anomalies (Payne RM, 2011). The most frequent cardiac phenotype is concentric left ventricular hypertrophy, which may progress to myocardial fibrosis. Atrial arrhythmias, particularly atrial fibrillation, are also frequently observed (Lynch DR, 2012). In addition to cardiac and neurological symptoms, FA patients frequently present with skeletal deformities, such as scoliosis and pes cavus, which occur in approximately 55–75% of cases. Pes cavus is characterized by an exaggerated and rigid plantar arch that fails to flatten under load, thereby impairing gait and foot function (Delatycki MB, 1999). Endocrine involvement is also frequent, as up to 10% of FA patients develop diabetes mellitus over time, reflecting the systemic metabolic disturbances associated with frataxin deficiency (Keita M et al., 2022). To date, no curative therapy exists for Friedreich’s ataxia. Management remains primarily symptomatic and supportive. In 2023, the U.S. Food and Drug Administration (FDA) approved the first disease-modifying treatment, Omaveloxolone, which was subsequently approved by the European Medicines Agency (EMA) in 2024. Omaveloxolone acts downstream of frataxin deficiency by activating the transcription factor NRF2, which binds to antioxidant response elements (AREs) in DNA to induce the expression of cytoprotective and antioxidant genes (Abeti R et al., 2018). This mechanism helps mitigate oxidative

stress, one of the principal pathological hallmarks of FA. Nevertheless, despite this advancement, a definitive curative treatment remains unavailable (Keita M et al., 2022).

2.2 Frataxin gene and mutation

The Frataxin (FXN) gene, which is mutated in FA, spans approximately 95 kilobases and is located on chromosome 9q21.11. The gene comprises seven exons, of which six (exons 1, 2, 3, 4, 5a, and 5b) contain coding sequences. The major *FXN* transcript is approximately 1.3 kilobases in length and includes exons 1 through 5a, although additional minor alternatively spliced transcripts have also been identified (Campuzano V et al., 1996). *FXN* expression is ubiquitous across tissues, but its abundance varies both spatially and temporally. In adult humans, the highest transcript levels are detected in the heart and spinal cord, followed by the liver, skeletal muscle, and pancreas (Jiralerspong S et al., 1997). FA is caused primarily by a pathological expansion of GAA triplet repeats located within intron 1 of the *FXN* gene (Campuzano V et al., 1996). In the general population, this region is polymorphic and typically contains fewer than 40 GAA repeats. In contrast, affected individuals harbor between 56 and 1700 repeats. Approximately 96% of FA patients are homozygous for this GAA expansion, whereas the remaining ~4% are compound heterozygotes, carrying an expansion on one allele and a point mutation on the other (Galea CA et al., 2016). Following the identification of the causative mutation, it was demonstrated that the expanded GAA tract induces transcriptional silencing of the *FXN* gene (Bidichandani SI et al., 1998). Consequently, FXN expression is markedly reduced, with residual protein levels in patients ranging from 10% to 30% of normal. The severity of clinical manifestations correlates directly with the number of GAA repeats on the shorter expanded allele, while the age of disease onset shows an inverse correlation (Dürr A et al., 1996).

2.4 Molecular mechanisms of FA

Since the identification of the causative mutation in FA, the molecular mechanisms underlying *FXN* gene silencing have remained only partially elucidated. Nevertheless, considerable research efforts have been devoted to uncovering the epigenetic and structural events responsible for the transcriptional repression of the gene (Gottesfeld JM, 2019). Extensive biochemical analyses have demonstrated that the expanded GAA·TTC repeat tract within intron 1 of *FXN* can adopt non-canonical DNA conformations. *In vitro* studies using plasmids harboring long GAA·TTC repeats revealed the formation of triplex (H-DNA) structures, consisting of two purine (R) GAA strands and one pyrimidine (Y) TTC strand, flanked by a single-stranded pyrimidine-rich region. These RRY configurations exhibit a strong propensity to form “sticky DNA” conformations that can impede the

progression of the transcription machinery, thereby inhibiting gene expression (Sakamoto N et al., 1999). Alternative mechanisms of transcriptional repression have also been proposed. One hypothesis involves the formation of DNA–RNA hybrid structures (R-loops). Gromak and colleagues demonstrated that *FXN* alleles in FA patients exhibit a high accumulation of R-loops, suggesting that their formation could represent an early event triggering heterochromatin assembly and subsequent transcriptional silencing (Groh M et al., 2014). In parallel, Bidichandani's group proposed a distinct RNA-mediated mechanism involving the antisense transcript FAST-1 (FXN Antisense Transcript 1). This transcript overlaps the CTCF (CCCTC-binding factor) insulator site within the *FXN* locus, potentially interfering with CTCF binding and promoting heterochromatin formation. Overexpression of FAST-1 resulted in reduced *FXN* expression, supporting this model, although the upstream mechanisms responsible for the increased FAST-1 levels observed in FA remain unclear (De Biase I et al., 2009). It is now widely accepted that heterochromatin formation plays a central role in *FXN* silencing and FA pathogenesis. Early evidence from Festenstein and colleagues demonstrated that the expanded *FXN* locus exhibits hallmark features of heterochromatin, including increased histone 3 lysine 9 di- and tri-methylation (H3K9me2/3), histone 3 lysine 27 tri-methylation (H3K27me3), and histone hypoacetylation (Saveliev A et al., 2003). DNA methylation has also been implicated in this repressive epigenetic landscape. Rodden and co-workers identified a Friedreich's ataxia–specific differentially methylated region (FA-DMR) within intron 1, characterized by approximately 90% methylation in FA samples compared with <10% in controls. This hypermethylation pattern was consistently observed across multiple patient-derived cell types and correlated strongly with reduced FXN transcription and earlier disease onset (Rodden LN et al., 2021). In general, DNA methylation acts as a signal for the recruitment of transcriptional repressor complexes through methyl-CpG binding proteins, which recruit histone deacetylases (HDACs). HDAC-mediated histone deacetylation of lysine residues on histone tails facilitates subsequent histone methylation by histone methyltransferases (HMTs), primarily at H3K9 and H3K27. These modifications promote the binding of heterochromatin protein 1 (HP1) to H3K9me2/3 and Polycomb group proteins to H3K27me3, leading to chromatin condensation and stable transcriptional silencing of the *FXN* locus (Chan PK et al., 2013; Soragni E et al., 2015) (Figure 4).

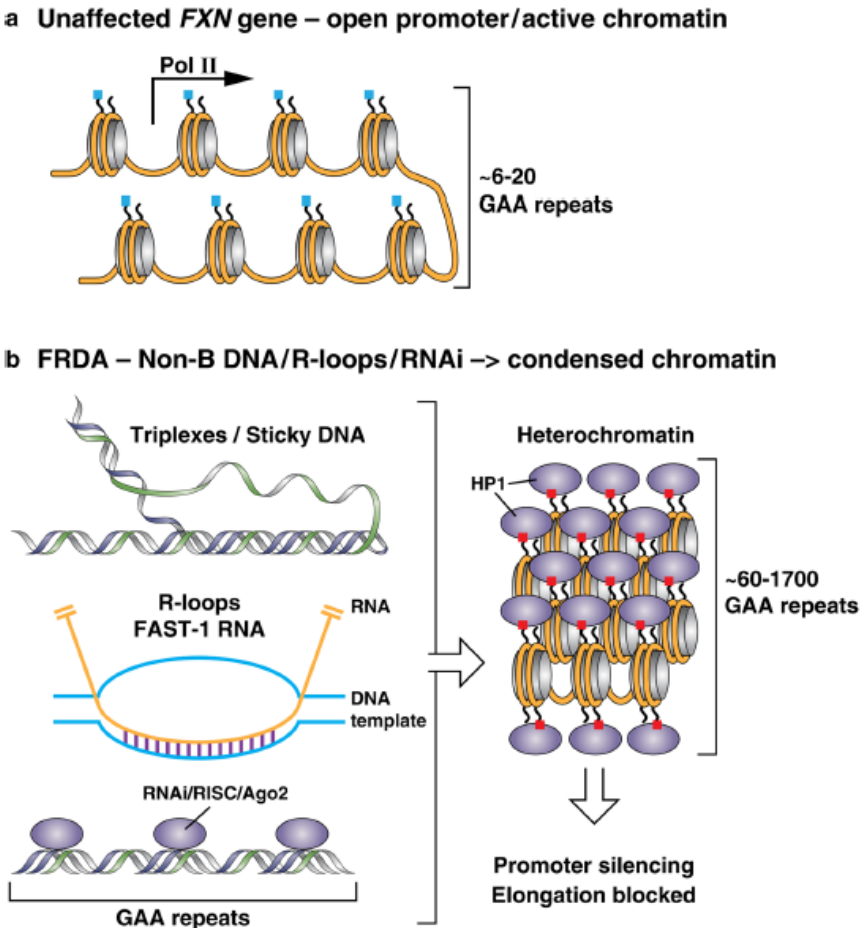

Figure 4. FA molecular mechanisms. (A) In cells from unaffected individuals, the *FXN* gene, characterized by short GAA·TTC repeat sequences, is organized within open, transcriptionally active chromatin. (B) In contrast, in cells from individuals with Friedreich's ataxia (FA), the *FXN* gene is embedded in compact heterochromatin. Several mechanisms have been proposed to explain how expanded GAA·TTC repeats induce heterochromatin formation. These include the formation of unusual DNA structures such as triplex DNA or sticky DNA; the presence of R-loops that recruit silencing complexes; short RNA transcripts that guide RNA interference machinery to the site; and an antisense transcript known as *FAST-1*, which interferes with the chromatin boundary protein CTCF, promoting heterochromatin spread. Collectively, these mechanisms can result in silencing of the *FXN* promoter and impede transcription elongation through the repeat region (from Gottesfeld JM, 2019).

2.3 Frataxin protein: function and dysfunction

The *FXN* gene encodes Frataxin, a 210-amino acid protein with a molecular mass of approximately 23 kDa. Translation of the *FXN* mRNA initially produces a cytosolic precursor protein, which is subsequently imported into mitochondria via an N-terminal mitochondrial targeting sequence. Upon translocation, the precursor undergoes an unusual two-step proteolytic processing by mitochondrial processing peptidase (MPP), leading to the formation of the mature protein (Condò I et al., 2007; Koutnikova H et al., 1998). In the first step, the full-length precursor is cleaved into an 18 kDa intermediate form, which is then further processed into the mature 14 kDa protein. The mature FXN

adopts a compact α/β fold comprising a twisted, six-stranded antiparallel β-sheet flanked by two α-helices (α1 and α2). Negatively charged residues located on the helical surface coordinate iron binding, whereas the uncharged residues of the β-sheet are thought to mediate protein–protein interactions (Monfort S et al., 2022). In addition to the canonical mitochondrial isoform, a minor fraction of FXN exists in extra-mitochondrial locations, specifically in the cytoplasm and nucleus, arising from alternative splicing or alternative translation initiation events (Condò I et al., 2006; Pianese L et al., 2002). These isoforms appear to enhance cellular fitness, as demonstrated by improved mitochondrial respiration and survival in cells expressing them (Agrò M, Díaz-Nido J, 2020; Condò I et al., 2006), although their precise biochemical roles remain to be clarified. To date, at least three FXN isoforms (types I–III) have been identified, resulting from alternative splicing. Type I (FXN^{81-210}) represents the canonical mitochondrial isoform, consisting of 130 amino acids with a molecular weight of approximately 14.2 kDa. Type II (FXN^{78-210}) contains 135 residues (14.9 kDa), while type III (FXN^{42-210}) comprises 164 residues (18.2 kDa). FXN II and FXN III localize predominantly to the cytosol and nucleus, respectively, and display tissue-specific expression patterns, FXN II is enriched in the nervous system, whereas FXN III is highly expressed in the heart (Guo L et al., 2018; Xia H et al., 2012). The primary role of FXN is in the biosynthesis of iron–sulfur clusters (ISCs), essential cofactors for numerous mitochondrial and cytosolic enzymes. Although its exact molecular function has long been debated, recent evidence suggests that FXN does not serve as an iron-storage or -chaperone protein, as initially proposed. Instead, FXN acts as a regulatory component that enhances ISC biogenesis by accelerating persulfide transfer from the cysteine desulfurase NFS1 to the scaffold protein ISCU (Bridwell-Rabb J et al., 2014; Gervason S et al., 2019; Parent A et al., 2015). The core mitochondrial ISC biosynthetic complex comprises five proteins: NFS1, FXN, ISCU, ISD11, and the acyl-carrier protein (ACP) (Fox NG et al., 2019). The process initiates with sulfur extraction from cysteine, catalyzed by NFS1, generating alanine and a cysteine-bound persulfide intermediate (Lill R, Mühlenhoff U, 2005). Sulfur is subsequently transferred from NFS1 to ISCU, facilitated by electron transfer from FDX2/FDXR, which reduces the persulfide to sulfide. FXN accelerates this sulfur transfer step (Gervason S et al., 2019; Parent A et al., 2015), thereby enhancing the overall rate of ISCs formation. Although ISCs synthesis can occur in the absence of FXN, the process becomes markedly inefficient, insufficient to meet cellular ISCs demands. Consequently, FA patients, who retain only minimal amounts of FXN, exhibit reduced ISCs production and the associated metabolic dysfunctions that compromise cellular homeostasis (Monfort S et al., 2022). Once [2Fe–2S] clusters are assembled on ISCU, they are transferred to glutaredoxin 5 (GLRX5) with the assistance of the chaperones HSC20 and HSPA9, and subsequently incorporated into recipient apo-proteins. These include mitochondrial aconitase, respiratory chain complexes I, II, and III of the electron transport chain (ETC), and, more recently, METTL17, a mitoribosomal assembly factor containing an ISC-binding pocket (Ast T et al., 2024). Additional proteins utilize [2Fe–2S] clusters as precursors to form [4Fe–4S] clusters on ISCA

scaffolds. Furthermore, the ISC assembly machinery produces a sulfur-containing compound, termed “compound X,” which is exported to the cytosol to support the cytosolic iron–sulfur cluster assembly (CIA) pathway responsible for extra-mitochondrial ISC formation (Monfort S et al., 2022) (Figure 5). *FXN* expression itself is tightly regulated by various transcription factors, indicating its potential role in modulating ISC biogenesis in response to cellular conditions (Guccini I et al., 2011; Yandim C et al., 2013). Among these regulators is NRF2, a key mediator of the antioxidant response (Sahdeo S et al., 2014). Activation of the NRF2–FXN axis during oxidative stress may promote ISC synthesis to replace Fe–S proteins damaged by reactive oxygen species (ROS) (D’Autréaux B, Toledano MB, 2007). Additionally, *FXN* expression is upregulated under hypoxic conditions through activation by HIF-1α and HIF-2α (Guccini I et al., 2011). This induction likely supports mitochondrial bioenergetics under low oxygen tension, consistent with observations that *FXN*-deficient human cells can partially restore proliferation under hypoxia, correlating with recovery of ISCs levels (Ast T et al., 2019). Moreover, ISCs synthesis appears to increase in response to intracellular iron availability via FXN-dependent regulation, suggesting a feedback mechanism that balances iron utilization and prevents mitochondrial iron overload (Monfort S et al., 2022). Given FXN’s central role in ISCs production, reduced protein levels have profound effects on mitochondrial and cellular metabolism, contributing to the neurodegeneration characteristic of FA. Deficiency in ISCs disrupts the activity of Fe–S–dependent enzymes, including those of the respiratory chain, leading to oxidative stress and dysregulation of mitochondrial iron homeostasis. As a compensatory response, iron import into mitochondria increases in an attempt to sustain ISC synthesis; however, the lack of functional FXN leads to pathological iron accumulation and oxidation. This, in turn, promotes excessive production of ROS, triggering oxidative stress, lipid peroxidation, and ultimately cell death (Cook A, Giunti P, 2017). ROS accumulation is a hallmark of FA pathophysiology. It arises primarily through two mechanisms. First, impaired electron flow through ETC complexes, due to defective ISCs–containing enzymes, results in electron leakage and the formation of superoxide and other ROS species. Second, elevated mitochondrial iron levels promote the generation of redox-active iron aggregates that catalyze ROS production. Under physiological conditions, hydrogen peroxide (H_2O_2) is detoxified by glutathione peroxidase in the presence of reduced glutathione (GSH). However, in FA mitochondria, the high oxidative burden leads to excessive GSH consumption, impairing H_2O_2 detoxification (Paupe V et al., 2009). The resulting accumulation of H_2O_2 fuels Fenton reactions, in which ferrous iron (Fe^{2+}) reacts with H_2O_2 to produce highly reactive hydroxyl radicals (•OH). These radicals are extremely cytotoxic, inflicting irreversible oxidative damage to proteins, lipids, and nucleic acids (Cook A, Giunti P, 2017).

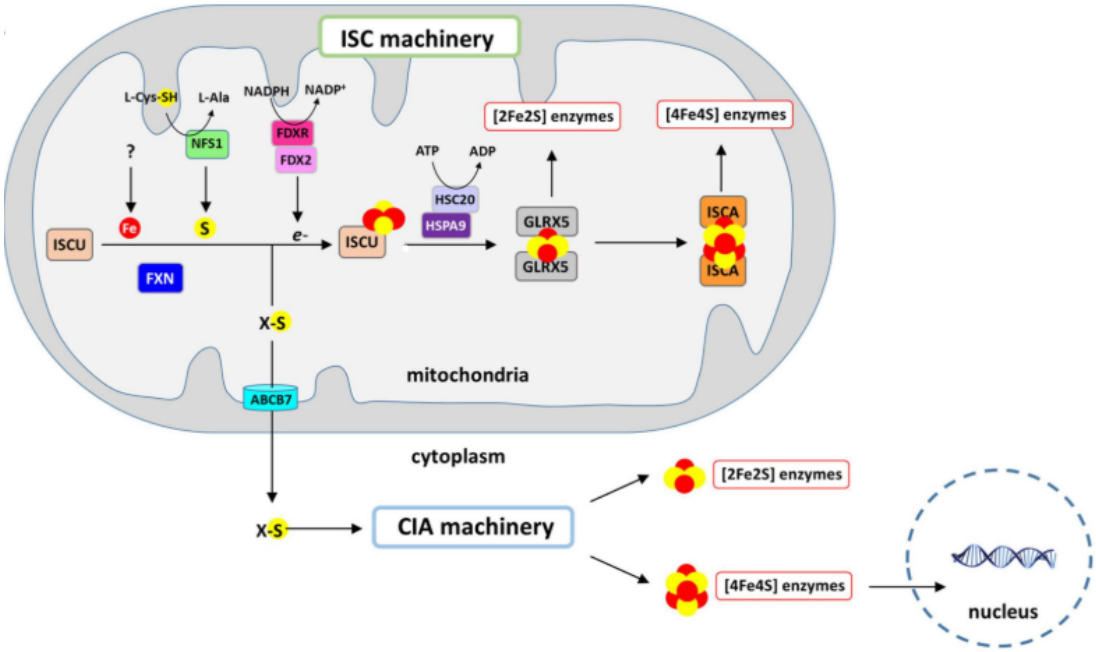

Figure 5. Iron-sulphur clusters (ISCs) biosynthesis machinery. Mitochondrial Fe-S cluster biosynthesis is initiated by the ISC machinery, which includes the scaffold protein ISCU, where [2Fe2S] clusters are assembled; the cysteine desulfurase NFS1, which donates sulfur as a cysteine-bound persulfide; and FDX2/FDXR, which reduces the persulfide to sulfide. FXN facilitates sulfide transferring from NFS1 to ISCU and so [2Fe2S] cluster formation. The resulting cluster is transferred to GLRX5 with the aid of the ATP-dependent chaperones HSC20 and HSPA9 and subsequently delivered to recipient apo-proteins. Conversion of [2Fe2S] to [4Fe4S] clusters is mediated by the ISCA proteins. In addition, the ISC machinery synthesizes a sulfur-containing compound (compound X) that is exported via the ABCB7 transporter to the cytosolic iron-sulfur cluster assembly (CIA) system. The CIA machinery then assembles [4Fe4S] clusters and incorporates them into cytoplasmic and nuclear protein targets (adapted from Monfort S et al., 2022).

2.5 Animal models of FA

The generation of a mouse model that faithfully reproduces the genetic basis of FA has been particularly challenging due to the nature of the mutation, an unstable GAA repeat expansion. Nevertheless, over the years, several FA mouse models have been successfully developed, each with specific advantages and limitations. Collectively, these models have enabled detailed investigation of different aspects of the disease, ranging from its molecular pathogenesis to the preclinical evaluation of novel therapeutic strategies. Given the essential role of FXN during embryonic development, complete *Fxn* knockout results in embryonic lethality at approximately embryonic day 6.5 (Cossée M et al., 2000). To circumvent this limitation, conditional knockout (cKO) models employing the Cre–LoxP recombination system have been generated to induce *Fxn* depletion in a tissue-specific manner. Considering the multisystemic nature of FA, both neuronal and non-neuronal cKO mouse models have been established (Perdomini M et al., 2013). One of the most studied models is the Muscle creatine kinase (Mck) cKO mouse, in which Cre recombinase

expression is driven by the *Mck* promoter, leading to selective Fxn depletion in cardiac and skeletal muscle. This model replicates the cardiomyopathy observed in FA patients and reproduces key molecular hallmarks of the disease, including decreased activity of ISCs enzymes and mitochondrial iron accumulation, which appear before overt cardiac symptoms. Importantly, the *Mck*-cKO mouse was the first FA model used to evaluate gene therapy approaches. Intravenous administration of an adeno-associated viral vector expressing human FXN (AAVrh10.CAG-hFXN-HA) prevented the onset of cardiomyopathy when delivered pre-symptomatically and reversed both molecular and cardiac phenotypes when administered after symptom onset (Perdomini M et al., 2014). A complementary neuronal model, the Parvalbumin cKO (*Pvalb*-cKO) mouse, employs Cre recombinase under the control of the Parvalbumin gene promoter to selectively delete FXN in proprioceptive neurons of the DRGs, Purkinje cells in the cerebellar cortex, and large neurons of the Dentate Nucleus. This model reproduces the sensory and cerebellar ataxia characteristic of FA, including progressive motor coordination deficits. Treatment with AAV-CAG-hFXN-HA at both pre-symptomatic and post-symptomatic stages resulted in a rapid and complete recovery of sensory neuropathy (Piguet F et al., 2018). Although cKO mouse models are powerful tools for studying FA pathogenesis and therapeutic interventions, they do not fully recapitulate the genetics of the disease. Unlike FA patients, who retain residual *FXN* expression, cKO mice exhibit complete loss of the protein in targeted tissues, which produces a more severe phenotype. To address this limitation, mouse models carrying missense mutations identified in FA patients, specifically G130V and I154F, have been developed (Fil D et al., 202072023; Medina-Carbonero M et al., 2022). These models exhibit globally reduced FXN expression while avoiding total deficiency. Although they do not perfectly reproduce the FA genotype, since the mutations are homozygous point mutations, whereas FA patients are typically compound heterozygotes with one expanded and one missense allele, they provide valuable insights into the pathogenic mechanisms of specific FXN variants. The G130V mutation, one of the most frequent in compound heterozygous FA patients, disrupts the processing of the intermediate FXN form to its mature form, resulting in accumulation of the intermediate species. It remains unclear whether this intermediate retains partial activity in ISCs biogenesis or is slowly converted into the mature form, possibly explaining the milder phenotype of such patients. Both *FXN* $^{G127V/G127V}$ and the *FXN* $^{I151F/I151F}$ mice display reduced FXN levels in the cerebral cortex, cerebellum, spinal cord, and heart, with the latter model also showing decreased expression in liver, pancreas, and skeletal muscle. These mice are smaller than controls and exhibit mild motor impairments, along with reduced activity of ISCs–containing enzymes, particularly the *FXN* $^{I151F/I151F}$ line (Fil D et al., 2020, 2023; Medina-Carbonero M et al., 2022). Another important model is the inducible FA knockdown (FAkd) mouse, developed using a doxycycline-inducible shRNA targeting *Fxn*. This model does not carry a GAA expansion but instead harbors an inducible shRNA cassette inserted into the Rosa26 locus. Upon doxycycline administration, *Fxn* expression is reduced, leading to motor deficits, cardiomyopathy, and mitochondrial abnormalities in cardiomyocytes and DRG

neurons. Notably, the severity of symptoms correlates with doxycycline dosage, and partial recovery is observed upon its withdrawal. This model allows temporal control of Fxn depletion, facilitating the study of disease progression dynamics and the identification of potential therapeutic windows. It also circumvents the embryonic lethality associated with constitutive *Fxn* deletion while maintaining low residual *Fxn* expression (Chandran V et al., 2017). Mouse models carrying GAA repeat expansions have also been generated. The first of such models, the KIKO mouse, was established in 2002 and combines one allele containing a 230-GAAs insertion (knock-in, KI) with a second allele bearing an exon 4 deletion (knockout, KO). Fxn levels in this model are reduced to 25–36% of normal, and the mice display mild neuromotor deficits, including reduced muscle strength and gait abnormalities that emerge around eight months of age. In addition, humanized transgenic mouse models have been created by introducing human *FXN* gene containing the pathogenic expansion via yeast artificial chromosomes (YACs). These hemizygous mice carry the human FXN transgene with the GAAs expansion and are homozygous null for the murine *FXN* gene. The first of these, the YG8R model, carries two human FXN transgenes with 90 and 190 GAA repeats, while the later YG8sR line contains alleles with 250–300 repeats (Al-Mahdawi S et al., 2006; Anjomani Virmouni S et al., 2014, 2015). Although these models display only mild phenotypes without overt ataxia, they provide valuable systems to investigate the epigenetic and transcriptional mechanisms underlying FXN silencing. More recently, a novel YAC-based model, YG8-800, was generated from the YG8sR line. This mouse harbors more than 800 GAA repeats and exhibits progressive locomotor and balance impairments between 11 and 20 weeks of age, along with cardiac hypertrophy from 26 weeks onward (Gérard C et al., 2023; Kalef-Ezra E et al., 2023).

2.6 Cellular models of FA

Significant progress has been made in the development of cellular models to study FA over recent years, largely driven by the advent of induced pluripotent stem cell (iPSC) technology. The first FA-derived iPSC lines, generated in 2010, retained silencing of the *FXN* gene and exhibited GAA repeat instability across passages (Ku S et al., 2010). Since then, FA-iPSCs have been differentiated into various cell types, including neurons and cardiomyocytes, which recapitulate key phenotypic features associated with FXN deficiency. The continuous improvement and expansion of differentiation protocols have enabled the use of iPSCs to model FA-related phenotypes and to investigate the molecular mechanisms underlying the disease (Hick A et al., 2013; Lee YK et al., 2014). In FA, specific neuronal populations within both the central and peripheral nervous systems are primarily affected. In particular, there is a pronounced degeneration of large sensory neurons, especially proprioceptive neurons, within the DRGs. As DRGs are complex and heterogeneous structures composed of multiple neuronal subtypes and glial cells, many differentiation protocols

have aimed to generate mixed cultures of sensory neurons. More recently, a refined protocol was developed to produce iPSC-derived primary sensory neuron cultures enriched up to 50% for proprioceptive neurons (Dionisi C et al., 2020). These proprioceptive neurons exhibited reduced survival compared to control cells and reproduced the characteristic epigenetic alterations observed in FA patients. Furthermore, transcriptomic and proteomic analyses revealed defects in cytoskeletal organization, neurite outgrowth, and synaptic plasticity (Dionisi C et al., 2023). Recent advancements in iPSC technology have also facilitated the generation of DRG-like organoids. The protocol established by Mazzara and colleagues (2020) enables the formation of three-dimensional, spatially organized structures containing the three major sensory neuron subtypes, mechanoreceptors, nociceptors, and proprioceptors, thus closely mimicking the in vivo DRG environment. DRG organoids derived from FA iPSCs displayed reduced neuronal survival, as well as abnormal axonal and mitochondrial morphology. Notably, these pathological phenotypes were fully rescued upon complete removal of FXN intron 1 containing the GAA repeat expansion, but only partially rescued when the repeat tract alone was excised. These findings suggest that deletion of the GAAs expansion alone may not suffice to reverse the epigenetic silencing of the *FXN* gene characteristic of FA (Mazzara PG et al., 2020). Beyond neuronal models, cardiomyocytes represent another key cell population affected in FA. iPSC-derived cardiomyocytes generated from FA patients exhibit FXN deficiency-induced mitochondrial dysfunction, characterized by impaired oxidative phosphorylation (OXPHOS) and abnormal iron accumulation. Additionally, these cardiomyocytes display hallmarks of hypertrophic cardiac stress, calcium signaling impairment, and lipid droplet accumulation, which may contribute to ferroptotic cell death (Hick A et al., 2013).

3. Existing and developing therapies for FA

In 2023, Omaveloxolone (commercial name Skyclarys™) became the first drug approved by the FDA for the treatment of FA in adults and adolescents aged 16 years and older. EMA subsequently granted its approval in 2024. Developed by Reata Pharmaceuticals, Omaveloxolone exerts its therapeutic effect through activation of the nuclear factor (erythroid-derived 2)-like 2 (NRF2) signaling pathway.

Multiple studies have demonstrated that FXN deficiency leads to increased oxidative stress and mitochondrial dysfunction, which are further aggravated by impaired NRF2 signaling. NRF2 is a key transcription factor that promotes the expression of antioxidant genes, suppresses proinflammatory gene expression, and facilitates the synthesis of co-substrates required for mitochondrial ATP production (Reisman SA et al., 2019). In FA, NRF2 fails to properly translocate to the nucleus in response to oxidative stress, resulting in downregulation of its target genes (Paupe V et al., 2009). Consequently, the cellular capacity to counteract oxidative stress is significantly reduced, further exacerbated by defective energy metabolism. Omaveloxolone restores NRF2 pathway activity by

inhibiting the ubiquitination and subsequent proteasomal degradation of NRF2, thereby maintaining physiological levels of the transcription factor. This allows NRF2 to activate its detoxifying downstream targets, ultimately re-establishing redox homeostasis and cellular function (Abeti R et al., 2018). Omaveloxolone, together with other compounds currently being evaluated in ongoing clinical trials, primarily acts to mitigate secondary consequences of FXN deficiency, leading to symptomatic improvement. The hope is that these effects may also contribute to slowing the progression of FA-associated neurodegeneration. However, despite the availability of standardized clinical assessment tools such as the International Ataxia Rating Scale (ICARS), the Friedreich's Ataxia Rating Scale (FARS), and the Scale for the Assessment and Rating of Ataxia (SARA), as well as the use of emerging biomarkers, evaluating treatment efficacy on neurological dysfunction remains challenging (Bürk K et al., 2013). For this reason, many clinical studies have focused on cardiac outcomes, which are more readily quantifiable, although neurological manifestations are ultimately more impactful on patients' quality of life. Current therapeutic strategies under investigation include compounds that attenuate oxidative stress and improve mitochondrial function, agents that modulate FXN-dependent metabolic pathways, and novel gene editing and gene therapy approaches aimed at correcting the primary molecular defect (Scott V et al., 2024).

3.1 Compounds to improve mitochondrial function

- **Vatiquinone** (PTC-743);

Vatiquinone, previously known as PTC-743 and developed by PTC Therapeutics, is postulated to improve mitochondrial and cellular function by targeting 15-lipooxygenase, a regulator of inflammation, oxidative stress and ferroptosis. MOVE-FA is a randomised, parallel-arm, double-blind, placebo-controlled trial that enrolled 146 children and young adults with FRDA (aged 7–21 years) conducted over 72 weeks, followed by a 24-week open label extension phase. Phase 3 was concluded in 2024 and now PTC announced that the FDA has accepted for filing the New Drug Application (NDA) for vatiquinone for the treatment of children and adults living with FA. The vatiquinone NDA is based on data from the placebo-controlled MOVE-FA study as well as results from two long-term studies including pediatric and adult FA patients. The company stated that data from these three studies demonstrate significant, durable and clinically meaningful evidence of slowing disease progression on key aspects of disease. In addition, these studies demonstrate that vatiquinone is safe and well tolerated in all age groups studied (curefa.org).

- **Elamipretide**;

Elamipretide (also known as ELAM, SS-31, Bendavia, MTP-131) is a peptide, developed by Stealth Therapeutics, which targets the inner mitochondrial membrane where it binds reversibly to

cardiolipin. It is reported to modulate mitochondrial function specifically by improving electron transport chain function and ATP production and reducing the formation of pathogenic ROS (Edzeamey FJ et al. 2024; Pharaoh G et al., 2023). It has been evaluated in a clinical trial in primary mitochondrial myopathy (86). A phase 1/2 clinical trial (ELViS-FA) is currently on-going to evaluate the effect of high dose (40‑60 mg) versus low dose (20‑30 mg) Elamipretide on visual acuity in 18 individuals with FRDA compared with baseline at 52 weeks (curefa.org).

3.2 Compounds to increase Frataxin levels

- **Nomlabofusp**;

Nomlabofusp (previously CTI-1601) is a novel recombinant fusion protein designed to deliver FXN to the mitochondria (Clayton R et al., 2024). Nomlabofusp is composed of a cell-penetrant peptide (CPP) and the complete human FXN protein fused to a mitochondrial targeting sequence, to facilitate the delivery of mature FXN to the mitochondria. In May 2021, Larimar Therapeutics shared top-line data from the Phase 1 placebo controlled single and multiple ascending dose (SAD and MAD) studies. Nomlabofusp was generally well tolerated at doses up to 100 mg administered daily for 13 days. In the 50 mg and 100 mg dose groups, treatment resulted in more than a two-fold increase in FXN levels in blood, buccal cells, and skin, which is in the range typically seen in in asymptomatic heterozygous carriers. The safety and pharmacokinetic data met the criteria for moving forward. This became the first time a FXN replacement therapeutic approach has been tested in people with FA. Top-line Phase 2 dose exploration results, released in February 2024, confirmed dose-dependent FXN increases in skin. In March 2025, the FDA indicated it is open to considering FXN concentration as a reasonably likely surrogate endpoint (RLSE). FDA recommended focusing on skin FXN levels over buccal cells due to more consistent sampling and lower variability and acknowledged that recent data support a relationship between increased skin FXN and key tissues affected in FA, including the heart, dorsal root ganglia, and skeletal muscle (curefa.org).

- **DT-216** (GeneTAC™);

DT-216 was developed by Design Therapeutics using a platform known as GeneTAC™ (gene-targeted chimera small molecules) (Khorkova O et al., 2024). The DNA binding component of this small molecule targets the site of the GAA repeat expansion, that interferes with *FXN* transcription, while the linked ligand component of the molecule facilitates transcription thus increasing the *FXN* gene expression, bypassing the triplet expansion. In August 2023, Design Therapeutics announced results from a phase 1 MAD study. They claimed that the treatment with DT-216 produced a statistically significant and dose-related increase in *FXN* mRNA levels in skeletal muscle biopsies. Based on concerns about on-going injection site safety compound, Design Therapeutics announced

on 17 March 2024, a new drug product, DT-216P2, designed to address these issues. The company has initiated dosing in a Phase 1 clinical trial in healthy volunteers in Australia to evaluate the safety and pharmacokinetics (PK) of single ascending doses of DT-216P2 via multiple routes of administration (intravenous infusion, subcutaneous infusion and subcutaneous injection) (curefa.org).

- **Dimethyl Fumarate;**

Dimethyl fumarate (DMF) is an anti-inflammatory and neuro-protective compound currently approved in Europe, Australia and the USA for treatment of remitting and relapsing multiple sclerosis. The potential of DMF to increase FXN protein levels in lymphocytes from individuals with FA was identified in a screening protocol for repurposed drugs (Sahdeo S et al., 2014). Two complementary actions for DMF were proposed: to increase FXN expression and, thus, protein levels and to induce NRF2, thus, enhancing antioxidant defenses. In this regard, Jasoliya and colleagues demonstrated that FXN expression was increased by 85% in multiple sclerosis patients, showing the great potentiality of this compound in enhancing FXN expression also in FA (Jasoliya MJ et al., 2017). Based on these promising results, a Phase 2 double-blind, randomised, placebo-controlled trial has begun to test the efficacy, safety and tolerability of DMF (curefa.org).

3.3 Gene editing and gene therapy approaches

Gene therapy represents a promising alternative to pharmacological approaches for the treatment of FA and other inherited disorders. This strategy aims to correct or replace the defective gene responsible for the disease, thereby addressing its root cause rather than merely alleviating symptoms. If successful, gene therapy could offer a transformative, one-time intervention, contrasting with the lifelong administration of symptomatic drugs, and thus provides considerable hope for individuals affected by currently incurable rare diseases. FA constitutes an especially suitable candidate for gene therapy, as the *FXN* gene is relatively small and can be readily packaged into an adeno-associated viral (AAV) vector, the preferred vehicle for gene delivery in this context. Moreover, since the disease phenotype manifests only when the pathogenic GAA repeat expansion is present in a homozygous state, restoration of approximately 50% of normal frataxin levels is expected to be sufficient to achieve a complete phenotypic rescue. Consequently, even modest expression levels of *FXN* may exert significant therapeutic benefit (Delatycki and Bidichandani, 2019). The first demonstration of the efficacy of gene delivery in FA was obtained in the conditional FXN knockout mouse models affecting cardiac and skeletal muscle (*Mck*-cKO). Systemic delivery of human FXN via an AAVrh10 vector successfully prevented the onset of cardiomyopathy when administered before symptom development and fully reversed cardiac pathology when delivered after disease onset (Perdomini M et al., 2014). Similarly, delivery of FXN through an AAV9 vector to

a parvalbumin-conditional FXN knockout mouse model (*Pvalb*-cKO), recapitulating the neuropathophysiological features of FA, resulted in a complete reversal of sensory ataxia (Piguet F et al., 2018). Despite these encouraging results, several challenges remain to be addressed before clinical translation. These include the risk of *FXN* overexpression leading to cellular toxicity, and the potential development of immune responses against the exogenously delivered FXN protein, which may hinder both initial administration and subsequent re-administration of AAV-based therapies (Sivakumar A, Cherqui S, 2022). In parallel, gene editing approaches have been explored as an alternative means of restoring FXN expression. In FA, gene editing strategies focus on excising the expanded GAA repeat within intron 1 of the *FXN* gene. Preclinical studies employing zinc finger nucleases (ZFNs) and CRISPR–Cas9 systems have demonstrated that targeted removal of the repeat expansion leads to reactivation of *FXN* expression (Li Y et al., 2015; Ouellet DL et al., 2017). However, the clinical application of these techniques is currently limited by challenges such as suboptimal editing efficiency and the risk of off-target genomic modifications (Sivakumar A, Cherqui S, 2022).

3.3.1 On-going gene therapy clinical trials

- Phase 1A study of gene therapy for FA cardiomyopathy (AAVrh.10hFXN, Weill Medical College of Cornell University)

As said above, the first demonstration of successful gene transfer and FA cardiac phenotype rescue was observed with a one-time intravenous administration of 10^{11} genome copies of AAVrh.10-hFXN, an AAV serotype rh10 gene transfer vector expressing human FXN, in the cardiac-specific cKO mouse model (Salami CO et al., 2020). Based on these studies, in 2022 the Weill medical college of Cornell university started the first gene therapy clinical trial for FA on humans. The trial consisted of an intravenous administration of a single dose of AAVrh.10hFXN, serotype rh.10 AAV gene transfer vector expressing the cDNA coding for human FXN in addition to immunosuppression therapy with prednisone for a total of 14 weeks. Outcomes will be measured for 5 years after administration (curefa.org).

- Phase 1/2 study of gene therapy for FA cardiomyopathy (LX2006, LEXEO)

Following this phase 1A trial, in 2022, LEXEO initiated an open-label, dose-escalation Phase 1/2 clinical trial (SUNRISE-FA) of LX2006 in patients with FA cardiomyopathy. The trial involved the single intravenous administration of one of three doses (low, mid and high) of LX2006 (AAVrh.10hFXN) to an estimated cohort of n=9. The gene therapy was designed to deliver the human *FXN* gene to cardiac cells over a 52-week period. In July 2024, Lexeo shared interim clinical data from the SUNRISE-FA Phase 1/2 clinical trial for the treatment of Friedreich ataxia cardiomyopathy (NCT05445323) and the Weill Cornell Medicine investigator-initiated Phase 1A trial (NCT05302271)

(from 8 participants with > 6-months of follow-up). They reported an amelioration of some cardiac parameters, including a reduction of the left ventricular mass index, generally increased in FA patients. In addition, LX2006 was well tolerated with no treatment-related serious adverse events to date. In July 2025, LEXEO announced that the FA program has received Breakthrough Therapy designation from the FDA for LX2006 based on interim clinical data from Phase 1/2 trials showing clinically meaningful improvements in cardiac biomarkers and functional measures (curefa.org).

4. Genome editing platforms

4.1 CRISPR-Cas9

Genome editing represents one of the most significant advancements in molecular biology, since it allows the targeted modification of the genome of living organisms. In the last years, this field has been completely revolutionized by the advent of CRISPR-Cas9 technology (Doudna JA., Charpentier E, 2014). In 2007, prokaryotic CRISPR-Cas system was shown to function as adaptive genome defense mechanism that recognizes and eliminate foreign nucleic acids associated with viruses and other mobile genetic elements (Barrangou R et al. 2007). In this system, fragments of the invader DNA are acquired and stored in repetitive arrays, that are subsequently transcribed and processed, producing CRISPR RNAs (crRNAs). crRNAs function as molecular guides that lead Cas proteins to recognize invading nucleic acids and target them for destruction. In 2012, it was demonstrated that Cas9 proteins destroyed the foreign DNA by cleaving it, thanks to their endonuclease activity (Gasiunas G et al., 2012). The specificity of this system was given by a dual-RNA guide structure composed by crRNA and trans-activating RNA (tracrRNA). For biotechnological purposes, CRISPR-Cas9 system was further simplified by integrating the two RNA components into a single guide RNA (sgRNA), providing a programmable and ready-to-use platform for Cas9 targeting a specific genomic site (Jinek M et al., 2012). With the approval of the first CRISPR-based therapy against sickle cell disease and beta-thalassemia, in 2023, CRISPR-Cas9 is now entering in its translational era. Cas9 functions as an active nuclease when complexed with either a dual RNA system composed of crRNA and tracrRNA, or with a single-guide RNA (sgRNA). Once guided to its target locus, Cas9 induces site-specific double-strand breaks (DSBs) in the DNA. Target specificity is achieved by modifying the 20-nucleotide sequence at the 5′ end of the sgRNA to enable complementary base pairing with the desired genomic target. Additionally, efficient binding and cleavage require the presence of a protospacer adjacent motif (PAM) on the non-target DNA strand, located immediately downstream of the target sequence. Following target recognition, Cas9 introduces a DSB approximately three nucleotides upstream of the PAM. This cleavage results in either blunt-ended DSBs or DSBs with a single-nucleotide 5′ overhang. The DSB formation is mediated by two distinct nuclease domains within Cas9: the HNH domain, which cleaves the target strand (TS), and the RuvC domain, which acts on the non-target strand (NTS). Inactivation of one

on the two domains generates a Cas9 nickase, capable of producing single-strand breaks. When both nuclease domains are inactivated, Cas9 functions as an RNA-guided DNA-binding protein, called dead Cas9 (dCas9), which can be employed as a platform for tethering effector proteins to specific genomic loci (Jinek M et al., 2012). Traditional genome editing strategies typically rely on the generation of site-specific DSBs followed by cellular DNA repair mechanisms. DSBs introduced by Cas9 are primarily repaired via endogenous end-joining pathways; namely, non-homologous end joining (NHEJ) and microhomology-mediated end joining (MMEJ), which are generally error-prone. These pathways are predominant in mammalian cells and involve the direct ligation of broken DNA ends. Prior to ligation, processing of DNA extremities may result in the loss or addition of nucleotides, leading to small insertions or deletions. This mutagenic repair process is widely used to disrupt protein-coding genes, enabling functional gene knockouts or the deletion of defined genomic regions through the simultaneous induction of two DSBs. Alternatively, precise genomic modifications can be achieved via homology-directed repair (HDR), a high-fidelity repair pathway that uses a homologous DNA sequence as a template to guide repair. By supplying an exogenous repair template containing the desired modifications, HDR can be exploited to introduce specific point mutations, insertions, or deletions at the target site. However, HDR activity is largely restricted to proliferating cells, as it requires DNA repair proteins that are predominantly expressed during the S and G2 phases of the cell cycle (Jinek M et al., 2012). Despite its broad utility, CRISPR-Cas9 system presents several limitations, which must be carefully considered in the context of both *in vitro* and *in vivo* applications. One of the main issues of this technology arises from the intrinsic properties of natural CRISPR-Cas systems, which exhibit a degree of tolerance to mismatches between the guide RNA and the target DNA sequence. This feature is thought to reflect an evolutionary adaptation that enables the bacterial immune system to cope with the rapid mutation rates of invading phages. However, in the context of genome editing, such mismatch tolerance is undesirable, as it increases the risk of off-target activity, where partially complementary genomic sites may be accidentally recognized and cleaved, leading to unwanted genetic modifications alongside the desired on-target edits. Off-target editing remains a major concern for therapeutic applications and for this many efforts have been spent to develop robust and sensitive methods for the prediction and detection of off-target edits and to improve the specificity of CRISPR genome editors by molecular engineering (Pacesa M et al., 2024). Besides, the DNA-binding mechanism of CRISPR nucleases restricts their targeting capability to genomic loci adjacent to a PAM. This requirement imposes limitations, particularly in genomic regions with high adenine/thymine (A/T) content, which are often poorly accessible to widely used nucleases such as Streptococcus pyogenes Cas9 (SpCas9), that works through an NGG PAM. To avoid these PAM-related constraints, a number of engineered Cas9 variants with altered or relaxed PAM specificities have been developed in recent years. While these variants significantly broaden the landscape of targetable genomic sites, they often sacrifice targeting fidelity (Pacesa M et al., 2024). In addition, the efficient and selective delivery of gene

editing components remains one of the most significant challenges. Ensuring safe, precise, and effective delivery of CRISPR elements to the desired cells or tissues is a critical prerequisite for achieving therapeutic benefit. Among current delivery strategies, viral vectors are the most commonly employed for *in vivo* administration. Recombinant adenoviruses, lentiviruses, and adeno-associated viruses (AAVs) can be engineered to carry genome editing cargo in place of viral genes. Of these, AAVs are the most widely used due to their favorable characteristics, including low immunogenicity, high transduction efficiency, and broad cell tropism. However, a significant limitation of AAV vectors lies in their restricted packaging capacity, which is approximately 4.7 kilobases. This poses a challenge for the delivery of full-length SpCas9 (approximately 4.2 kb) together with its corresponding sgRNA (~100 nucleotides) within a single AAV construct, unless highly compact regulatory elements are employed. To address this issue, research efforts have increasingly focused on the identification and adaptation of smaller Cas9 orthologs and more compact members of the Cas12 family, which are more compatible with the size constraints of AAV vectors. Moreover, the immunogenicity of CRISPR components and their associated delivery systems remains a significant concern for *in vivo* therapeutic applications. Host immune responses may be triggered against both the nuclease and the vector, potentially limiting the safety and efficacy of gene editing treatments, especially in the context of repeated or systemic delivery (Pacesa M et al., 2024).

4.2 Zinc finger nucleases

Another system that could be employed for genome editing is represented by zinc fingers nucleases (ZFNs), which were exploited before the CRISPR-Cas9 technology. These nucleases present two separate domains: the DNA-binding domain and the DNA-cleavage domain. The DNA-binding domain is composed of a set of Cys_2His_2 zinc fingers (ZFs) in which each unit of about 30 aminoacids binds a single atom of zinc. The crystal structure analysis showed that each finger contacts 3 base pairs (bp) of DNA in a modular fashion (Pavletich NB, Pabo CO, 1991). This means that, by assembling specific ZFs, many different DNA sequences can be targeted. The cleavage domain is composed of the restriction enzyme FokI. FokI must dimerize to cut DNA (Bitinaite J et al., 1998), therefore the best way to achieve cleavage is to design two sets of fingers directed to neighboring sequences and fuse each to a monomeric nuclease domain. In this way, when both sets of ZFs bind to their target sequence the dimerization can happen and so the DNA cutting. Several studies have demonstrated that the optimal configuration includes a short linker between the two domains and spacers of 5-6 bp between binding sites (Bibikova M et al., 2001). The requirement for dimerization is a great advantage for this genome editing tool because it makes cleavage much more specific, since it happens only when the two proteins have an adequate specificity for their target sites. Once generated the DSB, as happens for the CRISPR-Cas9 system, it can be repaired by NHEJ or HR, according to the final goal of DNA editing.

5. Transcriptional activators

5.1 CRISPR-mediated transcriptional regulation

Starting from CRISPR-Cas9 system, multiple tools have been developed in the last years. Qi and colleagues in 2013 created a mutant Cas9, with D10A and H840A mutations within the RuvC and HNH nuclease domains, which is defective in nucleolytic activity but is still able to perform RNA-dependent DNA-binding (Qi LS et al., 2013). This was called “dead” Cas9 (dCas9) and it started to be employed as a shuttle-protein to deliver catalytically active domains to specific DNA target loci. This allowed to perform specific epigenetic regulation of gene expression in different ways, according to the exploited effector domain. Generally, transcription activators or repressors, epigenetic remodeling factors and nucleolytic domains from other nucleases can be fused to the dCas9. dCas9 fused to activators or repressors, respectively indicated as CRISPRa and CRISPRi, can be divided in first- and second-generation systems that will be explained in the following chapters. The main advantage represented by this tool is that it controls gene expression without interfering with DNA, moreover, its effect can be reversible.

5.1.1 First-generation CRISPRa systems

First-generation CRISPRa systems consist of two elements: dCas9 fused to a transactivator domain and a sgRNA. For transactivating purposes, the sgRNAs employed generally target upstream or proximal promoter regions. The first CRISPRa developed were composed of dCas9 fused to VP64, p300 or p65. VP64 is a tetramer of VP16, a well characterized transcription activator from the herpes simplex virus. Then, different oligomers of VP16 (VP48, VP160 and VP192) have been used as activators and it was observed that the efficiency of activation was directly proportional to the size of the oligomer, although it was also dependent on the biological context. p65, on the other hand, which is the activation domain of NF-kappa B factor, can also contribute to transcription initiation. It has turned out to be less effective than VP64 and it has rarely been used on its own, however it had become part of another powerful activating system called VPR (Chavez A et al., 2015). The VPR is formed by activation domains VP64-p65-Rta, linked by short linkers and fused in tandem to the dCas9 (Figure 6). Lastly, p300 is the catalytic core of human acetyltransferase and it works through acetylation of histone H3 lysine 27, which leads to activation of both proximal and distant gene enhancers. Moreover, it can contribute to chromatin remodeling. Methylation is another important biological process that has an impact on gene transcription, indeed, hypermethylation of promoters leads to silencing of the gene, whereas hypomethylation is an indicator of a potentially active promoter. For this reason, dCas9 has been fused with demethylating domains too. An example is represented by dCas9-TET1. TET oxidizes the methyl group of the cytosine, leading to base excision repair and thus reducing DNA methylation levels. In the light of this, Liu and colleagues (2016) chose

dCas9-TET1 as a demethylation effector to increase *BDNF* expression levels in neurons (Liu XS et al., 2016). Beyond directly inducing gene expression enhancement, demethylation can also favor transactivation events, for example by allowing chromatin relaxation. Although first generation systems, except VPR, are significantly less efficient than second generation systems, they have one important advantage, the smaller size of the transgene, which is more preferable if the capacity of the vector is limited.

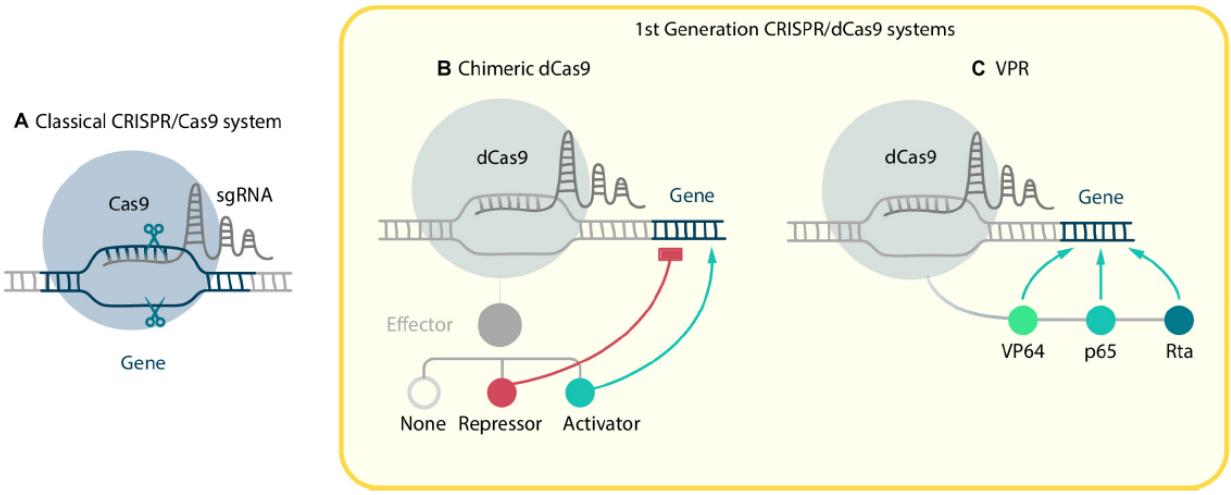

Figure 6. First-generation CRISPR/dCas9 systems. The first-generation CRISPR/dCas9 systems are composed of two key elements: dCas9 fused to an effector domain and the guiding sgRNA. These systems allow for targeted control of gene expression. (B) In one approach, chimeric dCas9 can be used alone to physically obstruct RNA polymerase, thereby blocking transcriptional elongation. Alternatively, when fused to regulatory effector domains, dCas9 can act as a tool to either repress or activate gene expression. (C) Another configuration, known as VPR, enhances transcriptional activation by fusing dCas9 to a tripartite activator composed of VP64, p65, and Rta domains, resulting in a strong upregulation of target gene expression (From Shakirova KM et al., 2020).

5.1.2 Second-generation CRISPRa systems

Second generation systems consist of three components: dCas9, sgRNA, and effectors, multiple copies of which are recruited by special domains on the dCas9 or sgRNA.

The first steps toward the development of second-generation systems were made when it was observed that the crystal structure of the dCas9:gRNA:DNA complex has the tetraloop and stem-loop 2 of the sgRNA protruding outside of the Cas9-sgRNA complex (Nishimasu H et al., 2014). This highlighted the possibility of exploiting this structure to add there protein-interacting RNA aptamers that could facilitate the recruitment of effectors domains to the Cas9 protein. The pioneer system is called Scaffold as it is based on scaffold RNA (scRNA), formed by introducing hairpin aptamer domain to the 3' of the sgRNA (Zalatan JG et al., 2015). In this way, aptamer-specific proteins, fused with effectors, can bind to those sequences and so modify gene expression. For the recruitment of

different effectors to the target site, different aptamers are necessary. Thus, a single scRNA molecule encodes both information about the target DNA sequence and the effectors to recruit in order to execute a precise regulatory function in that locus. scRNA-mediated VP64 recruitment showed a greater expression activation than the one observed with dCas9-VP64 fusion protein (Zalatan JG et al., 2015). However, the insertion of more copies of aptamers in the scRNA can have a negative effect on its own expression, resulting in a diminished number of effectors recruited. Therefore, an evolution of this system was developed: the Casilio system. It relies on the combination of CRISPR-Cas9 and the Pumilio RNA-binding protein. Pumilio has an RNA-binding domain (PUF), that recognizes a specific 8-mer RNA sequence called PUF-binding site (PBS). Therefore, in total the system is composed of dCas9, sgRNA with PBSs and PUF domains fused with the effector. In this case, the advantage of this upgrade is that its linear architecture doesn't interfere with the sgRNA transcription, resulting more efficient than Scaffold CRISPRa (Shakirova KM et al., 2020).

Another second-generation CRISPRa system is represented by dCas9-SAM, which is composed of three major components: chimeric dCas9-VP64, sgRNA with synthetic aptamers for MS2 recruitment and a chimeric MS2-p65-HSF1 activation helper protein. This chimeric transactivator complex can be recruited to both the tetraloop and the stem-loop of the hairpin aptamer, which binds dimerized MS2 bacteriophage coat proteins (Konermann S et al., 2014). Considering that antibodies can bind to short peptide sequences with high affinity and specificity, a dCas9 decorated with peptide epitopes has been created. Besides, such "designed" epitopes are different from naturally occurring peptides in the cell, eliminating possible off-target binding. This concept is at the basis of the SunTag system. It consists of the dCas9 fused with multiple copies of GCN4 peptide (this particular multi-peptide tag was called SunTag), an antibody single-chain variable fragment (scFv) fused with the activation domains (for ex. VP64, p65-HSF1or p300), and the sgRNA. GCN4(n) recruits n molecules of the chimeric scFv-activator protein to the target site, allowing significant amplification of the transactivation signal. Lastly, among the second-generation systems we have to consider the Three-component repurposed technology for enhanced expression (TREE), which recruits effectors via RNA aptamers and protein tags. It consists of dCas9-VP64, sgRNA with two MS2 aptamers, SunTag fused with MS2 protein, and scFv-effector. In the TREE system the effectors are connected with the scFv antibodies that bind to the GCN4 epitope as they do in SunTag systems, this results in a higher accumulation of effector molecules around the target site (Tanenbaum ME et al., 2014) (Figure 7).

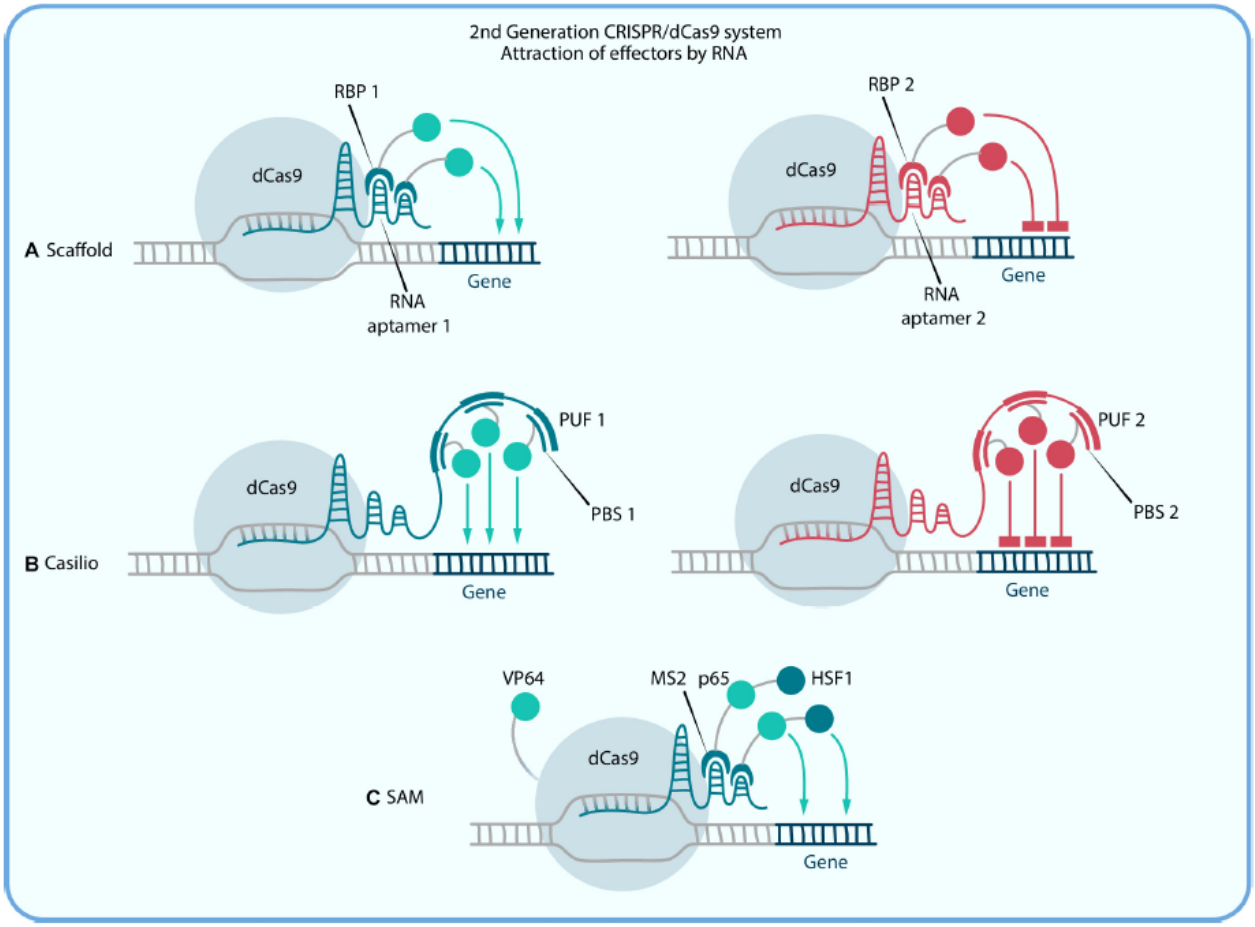

Figure 7. Second-generation CRISPR/dCas9 systems. (A) Scaffold and (B) Casilio systems utilize engineered RNA elements to enable the simultaneous recruitment of multiple effectors to distinct sgRNAs. In the Scaffold system, RNA aptamers are embedded within the sgRNA to recruit specific RNA-binding proteins (RBPs), which in turn bring in effector proteins. Similarly, the Casilio system incorporates PUF-binding sites (PBS) into the sgRNA, allowing PUF proteins fused to effectors to bind selectively and guide functional outputs. (C) In the SAM (Synergistic Activation Mediator) system, the RNA-binding protein MS2 is fused to two transcriptional activators, p65 and HSF1, while dCas9 is separately fused to another activator, VP64. This combination enhances gene activation by assembling a potent multi-component activator complex at the target site (from Shakirova KM et al., 2020).

5.2 Zinc finger proteins-based transcriptional regulators

As previously discussed, zinc finger proteins are able to target specific DNA sequences according to their aminoacids composition. This feature made them suitable for the generation of artificial modulators of gene expression, in an analogous way to CRISPR/Cas9 (described in the previous paragraph). In 1998, the first synthetic transcriptional activators and repressors were created by fusing ZF proteins to the VP64 domain and to the Krüppel-associated box (KRAB) repression domain, respectively. Then, it was demonstrated that these molecules were able to induce up- or down-regulation of ERBB2 and ERBB3 genes in human cells (Beerli RR et al., 1998). Subsequently,

these synthetic repressors were exploited to inhibit the transcription and replication of HIV-1. The inhibitory ZFs, targeting the HIV promoter, were able to induce a decrease of HIV replication in primary cells up to 100-fold (Segal DJ et al., 2004). Moreover, ZF activators (ZFAs) were developed to increase the γ-globin gene expression, as a potential therapeutical approach for sickle cell disease and β-thalassemia. In particular, it was shown that, targeting *γ-globin* promoter, the gene was up-regulated in primary human hematopoietic stem cells and *in vivo* in a transgenic mouse model (Costa FC et al., 2012). Besides, ZF technology was used to discover genes involved in important cellular phenotypes, such as cancer progression and drug resistance. A library of 84 million unique six-fingers ZFs variants was designed to recognize random 18 bp sequences through combinatorial assembly of individual ZF domains. When fused to the VP64 domain and administered to the human cells by retroviruses, it was found that each protein could find one or more targets in the genome and regulate adjacent genes. By selecting cells in which specific cell surface markers were upregulated, zinc finger proteins that targeted the promoters of those gene products were isolated (Blancafort P et al., 2005). Lastly, ZFs can be exploited to modulate gene expression by manipulating the epigenetic state of a gene. For this reason, they can also be fused to DNA methyltransferase domain to control methylation or de-methylation of specific DNA regions.

In a work by Cherif and colleagues (2018), similarly to ZFAs, Platinum TALE (plTALE) proteins targeting the regulatory region of the *FXN* gene, fused with a transcriptional activator (TA) such as VP64 or P300, were used to increase the expression of that gene. Many effectors, $plTALE_{VP64}$, $plTALE_{p300}$, and $plTALE_{SunTag}$, targeting 14 sequences of the *FXN* gene promoter or intron 1 were produced. This permitted selection of 3 $plTALE_{VP64s}$ and 2 $plTALE_{SunTag}$ that increased *FXN* gene expression by up to 19-fold in different FA primary fibroblasts. Adeno-associated viruses were used to deliver the best effectors to the YG8R mouse model to validate their efficiencies *in vivo*. The obtained results showed that these selected $plTALE_{VP64s}$ or $plTALE_{SunTag}$ induced transcriptional activity of the endogenous *FXN* gene as well as expression of the FXN protein in YG8R mouse heart by 10-fold and in skeletal muscles by up to 35-fold. The aconitase activity was positively modulated by the frataxin level in mitochondria, and it was, thus, increased *in vitro* and *in vivo* by the increased *FXN* expression (Cherif K et al., 2018).

Aim of the thesis

The central aim of this PhD thesis is to develop and comprehensively evaluate targeted epigenetic strategies capable of reactivating the endogenous Frataxin (*FXN*) gene in Friedreich's ataxia (FA), a neurodegenerative disorder caused by epigenetic silencing due to GAA·TTC trinucleotide repeat expansions within the first intron of the gene. The research seeks to establish an effective means of reversing this silencing and restoring *FXN* expression in disease-relevant cell types.

To achieve this, the study focuses on two distinct transcriptional activation platforms: a CRISPR-based activation (CRISPRa) system utilizing a catalytically inactive Cas9 (dCas9) fused to a VP160 activation domain and guided by multiple sgRNAs targeting the *FXN* promoter, and a zinc-finger activators (ZFAs) system composed of custom-engineered zinc-finger proteins fused to a VP64 activation domain. Both systems are evaluated for their capacity to induce *FXN* transcription in patient-derived fibroblasts and induced pluripotent stem cells (iPSC)-derived neural progenitor cells, cortical neurons, and sensory neurons, representing the primarily degenerating neurons in the disease. The thesis aims to determine the relative efficacy, reliability, and therapeutic potential of these activation systems by assessing their ability to restore *FXN* expression and correct downstream disease-associated molecular pathways. In doing so, the work seeks to advance the understanding of targeted chromatin reactivation as a therapeutic approach and to identify the most promising gene activation strategy for future translational applications in FA.

CHAPTER 2

Unpublished work

Transcriptional activators rescue Frataxin expression and downstream pathways in Friedreich's ataxia diseased cell types

Melacini Elena [1,2,3], Rossi Margherita [1], Di Pizio Agostina [1,3], Moscato Giosuè [1,3], Muggeo Sharon [1,3], Luoni Mirko[1,3], Giannelli Serena Gea[1], Broccoli Vania [1,3].

1. Stem Cells and Neurogenesis Unit, Division of Neuroscience, San Raffaele Scientific Institute, Milan, 20132, Italy;
2. University of Milano Bicocca (Unimib), Milan, 20126, Italy;
3. National Research Council (CNR), Institute of Neuroscience, Milan, 20900, Italy.

Abstract

Friedreich's ataxia (FA) is an autosomal recessive neurodegenerative disorder caused by the epigenetic silencing of the Frataxin (*FXN*) gene, resulting from the pathological expansion of GAA·TTC trinucleotide repeats in its first intron. Given the strong correlation between *FXN* silencing and repressive chromatin states, we explored targeted epigenetic reactivation strategies using engineered transcriptional activators. We employed the CRISPR activation (CRISPRa) system based on a lentiviral vector encoding dCas9 fused to the potent VP160 activation domain, along with multiple sgRNAs targeting *FXN* promoter. This system successfully restored *FXN* expression in primary fibroblasts, iPSC-derived neural progenitor cells (NPCs), cortical neurons, and sensory neurons derived from a mildly affected patient (PTS, 330/300 GAA repeats) and a more severely affected patient (PTL, 530/1000 GAA repeats). Rescue of disease-associated pathways was also observed, upon CRISPRa treatment. Additionally, we tested zinc-finger activators (ZFAs), consisting of zinc-finger proteins targeting FXN promoter and fused to the VP64 activation domain. Given their compact size and human origin, ZFAs offer great promise for translational applications. Notably, we showed that a specific combination of three ZFAs effectively reactivated gene expression in PTS-derived fibroblasts, NPCs and sensory neurons. However, ZFAs were not effective on PTL-derived cells. Overall, our findings demonstrated that targeted epigenetic reactivation of the endogenous *FXN* gene holds strong therapeutic potential. Remarkably, our comparative analysis of CRISPRa and ZFAs highlighted CRISPRa as the most powerful and reliable tool for restoring endogenous *FXN* expression in the context of FA.

Introduction

Friedreich's ataxia (FA) is the most common recessive hereditary ataxia with 1 over 40000 people affected in the Caucasian population (Koeppen AH, 2011; Pandolfo M, 2009). FA primary symptoms are limbs and gait ataxia, while additional neurological features include dysarthria, absent reflexes and loss of vibration and proprioceptive sensing (Corben LA, 2010). FA predominantly affects sensory neurons in the dorsal root ganglia, mainly the proprioceptive ones, as well as the Dentate Nucleus in the cerebellum and the corticospinal tracts (Harding IH, 2020). Beyond its neurological manifestations, FA is considered a multisystemic disorder, most notably associated with cardiomyopathy, the leading cause of mortality, and diabetes. Up to now, only one symptomatic treatment was approved by FDA (2023) and EMA (2024): Omaveloxolone (Lynch DR et al., 2021; 2023). It acts on downstream pathways, activating the NRF2 transcription factor that binds to antioxidant response elements in the DNA to activate genes protecting cells from oxidative damage (Abeti R et al., 2018). Indeed, increased production of reactive oxygen species (ROS) is one of the hallmarks of FA pathophysiology. Nevertheless, no curative treatment for the disease exists (Keita M et al, 2022). FA is caused by a GAA triplet expansion in the first intron of the Frataxin (*FXN*) gene, a 95 kilobases gene located on chromosome 9 (Campunzano V et al., 1996). The region bearing the GAA repeats is normally polymorphic, with up to 40 repeats in healthy people, while in patients the number is comprised between 56 and 1700 repeats. Approximately 96% of the patients are homozygous for the GAAs expansion on both alleles, the remaining 4% are compound heterozygous for the expansion on one allele and a point mutation on the other one (Galea CA et al., 2016). The GAA triplet expansion causes *FXN* gene silencing (Bidichandani SI et al., 1998). Notably, patients display between 10% to 30% of residual FXN amount and the severity of the disease is directly proportional to the number of GAA repeats on the allele with the shorter expansion, while the age of onset is inversely proportional to it (Durr A et al., 1996). It is widely accepted that heterochromatin formation is a key event in FA pathogenesis. Several studies reported increased levels of histones modifications like histone 3 lysine 9 di- and tri-methylation (H3K9me2/3), histone 3 lysine 27 tri-methylation (H3K27me3) and histones hypoacetylation, in the *FXN* gene carrying the expanded GAA triplet region (Al-Mahdawi S et al., 2008; Herman D et al., 2006; Rai M et al., 2008; Saveliev A et al., 2003). Methylation also plays an important role in *FXN* silencing. Indeed, Rodden and colleagues showed the existence of a FA-specific region of hypermethylation in intron 1 as a novel epigenetic signature. The hypermethylation of this differentially methylated region (FA-DMR) was observed in a variety of patient-derived cells and it significantly correlated with *FXN* transcriptional deficiency and age of onset (Rodden LN et al., 2021). Moreover, the GAA triplets region displayed a tendency to acquire unusual "sticky" DNA structures and R-loops, that block the gene transcription (Sakamoto N et al., 1999; Gerhardt J et al., 2016; Groh M et al., 2014). FXN is a small mitochondrial protein involved in iron-sulphur cluster (ISCs) biogenesis (Bridwell-Rabb J et al., 2014; Parent A et al., 2015;

Gervason S et al., 2019; Lill R et al., 2012). Therefore, its absence results in defective functionality of ISCs-harboring proteins, such as complexes I, II and III of the electron transport chain, with consequent impaired oxidative phosphorylation and abnormal ATP production. Besides, unexploited electrons interact with free oxygen molecules, producing ROS (Paupe V et al., 2009; Vaubel RA, Isaya G, 2013). Overall, reduced levels of FXN in FA lead to widespread mitochondrial dysfunction, compromising both the functionality and integrity of the mitochondria and, more broadly, disrupting the cell's antioxidant defense mechanisms (Cook A, Giunti P., 2017; Jasoliya MJ et al., 2017). Because of the nature of FA mutation, an unstable GAA expansion, the generation of a mouse model that recapitulates the genetics of the disease has been challenging. Some models bearing the mutated human gene have been generated, exploiting BAC or YAC technology that allows the insertion of the exogenous gene with the simultaneous knock-out of the murine ortholog (Al-Mahdawi S et al., 2006; Anjomani Virmouni S et al., 2014/2015). However, most of the mouse models obtained over the years display only mild phenotypes that are not always sufficient for the research aims. Until now, most therapeutic approaches under investigation have centered on delivering exogenous *FXN* through gene therapy (Chang JC et al., 2024; Perdomini M et al., 2014; Piguet F et al., 2018; Salami CO et al., 2020) or, as Omaveloxolone, mitigating cellular phenotypes resulting from FXN deficiency (Abeti R et al., 2018; Lynch DR et al., 2023, 2024). Nevertheless, on one hand, gene therapy faces several challenges, including delivery difficulties, immune responses, risk of uncontrolled or harmful gene expression, high costs, long-term safety concerns, and complex ethical and regulatory issues (Colella P et al., 2017). Symptomatic therapies, on the other hand, fail to provide a definitive solution. In this study, we propose a novel strategy aimed at reactivating the endogenous *FXN* gene to restore its expression in patient-derived cells. Specifically, our objective was to re-establish physiological FXN levels in cell types affected by the disease. To this end, we exploited induced pluripotent stem cells (iPSCs) derived from FA patients and differentiated them into disease-relevant cell types, including sensory neurons, which are among the most severely affected (Codazzi F et al., 2016; Hick A et al.,2012; Ku S et al., 2010; Liu J et al., 2011). We explored two gene activation strategies: CRISPR activation (CRISPRa) (Shakirova MK et al., 2020) and zinc finger activators (ZFAs) (Beerli RR et al., 1998; Blancafort P et al., 2005; Costa FC et al., 2012; Segal DJ et al., 2004). Overall, we demonstrated that it is possible to achieve *FXN* gene reactivation by employing tools that boost its expression, overcoming GAA repeat expansion, without the need to intervene with nucleases to correct the genetic defect, which represents a more invasive system. Furthermore, our results demonstrate that this approach can restore *FXN* expression to physiological levels, thereby minimizing the toxic effects associated with *FXN* overexpression (Belbellaa B et al., 2020) and providing a promising alternative to traditional gene therapy strategies.

Results

CRISPRa-mediated reactivation of *FXN* gene in FA-derived primary fibroblasts

To evaluate the efficacy of the CRISPR activation (CRISPRa) technology within the genetic context of Friedreich's ataxia (FA), we employed a lentiviral vector encoding a dead Cas9 (dCas9) fused to the potent VP160 activation domain, along with multiple single-guide RNAs (sgRNAs) targeting *FXN* promoter (sgP1, sgP2, sgP3) (Fig. 1A; Supplementary table 1). The promoter region was chosen for its open chromatin and active transcription features identified through integrative analysis of publicly available datasets of RNA Pol II, H3K4me3, and ATAC-seq data from primary fibroblasts (Fig. S1A). Firstly, we performed a screening to identify the most potent sgRNA in primary fibroblasts derived from FA patients. Specifically, fibroblast lines were obtained from two FA patients (referred to as PTS and PTL) (Mazzara PG et al., 2020), exhibiting distinct levels of disease severity, as well as from a healthy donor, in order to determine whether *FXN* gene locus was epigenetically modifiable. The PTS patient, carrying 330/300 GAA repeats, developed late-onset disease at age 32 and, at age 52, presented with mild dysarthria, horizontal nystagmus, mild dysmetria, involuntary tremor, ataxic gait, and no signs of cardiomyopathy. In contrast, the PTL patient, with 530/1000 GAA repeats, exhibited early-onset symptoms at age 13 and, by age 36, had developed pronounced scoliosis, saccadic slowing, moderate dysarthria, complete loss of ambulation, lower limb plegia, distal weakness in both upper and lower limbs, proximal strength preservation in the upper limbs, and apallesthesia in the lower extremities. Fibroblasts from all three individuals were transduced with lentiviral vectors encoding dCas9-VP160 along with individual or combinations of sgRNAs. Ten days post-transduction, *FXN* mRNA levels were quantified by RT-qPCR. As expected, a correlation was observed between GAA repeats length and the degree of *FXN* transcriptional repression, with both FA-derived fibroblast lines displaying reduced transcript and protein levels compared to the healthy control (CTRL), which harbored a normal number of GAA repeats (Fig. 1C–D; Fig.1E–F). Among the sgRNAs tested, sgP2 emerged as the most effective in inducing *FXN* expression, both when used alone and in combination with sgP1 and sgP3 (Fig. 1B–D). These transcriptional findings were further validated at the protein level by Western blot analysis, which confirmed a complete restoration of FXN amounts in both PTS and PTL fibroblasts (Fig. 1E–F). Additional CRISPRa constructs, including dCas9-VPR (Chavez A et al., 2015), dCas9-TET1 (Liu XS et al., 2016), and dCas12a-NFZ (Tycko J et al., 2025), were also evaluated under identical conditions. However, none achieved activation levels comparable to those obtained with dCas9-VP160 (Fig. S2A-F), underscoring the superior efficacy of this activation system in inducing the silenced *FXN* locus in the context of expanded GAA repeats. Therefore, dCas9-VP160 was selected as CRISPRa effector for the subsequent experiments.

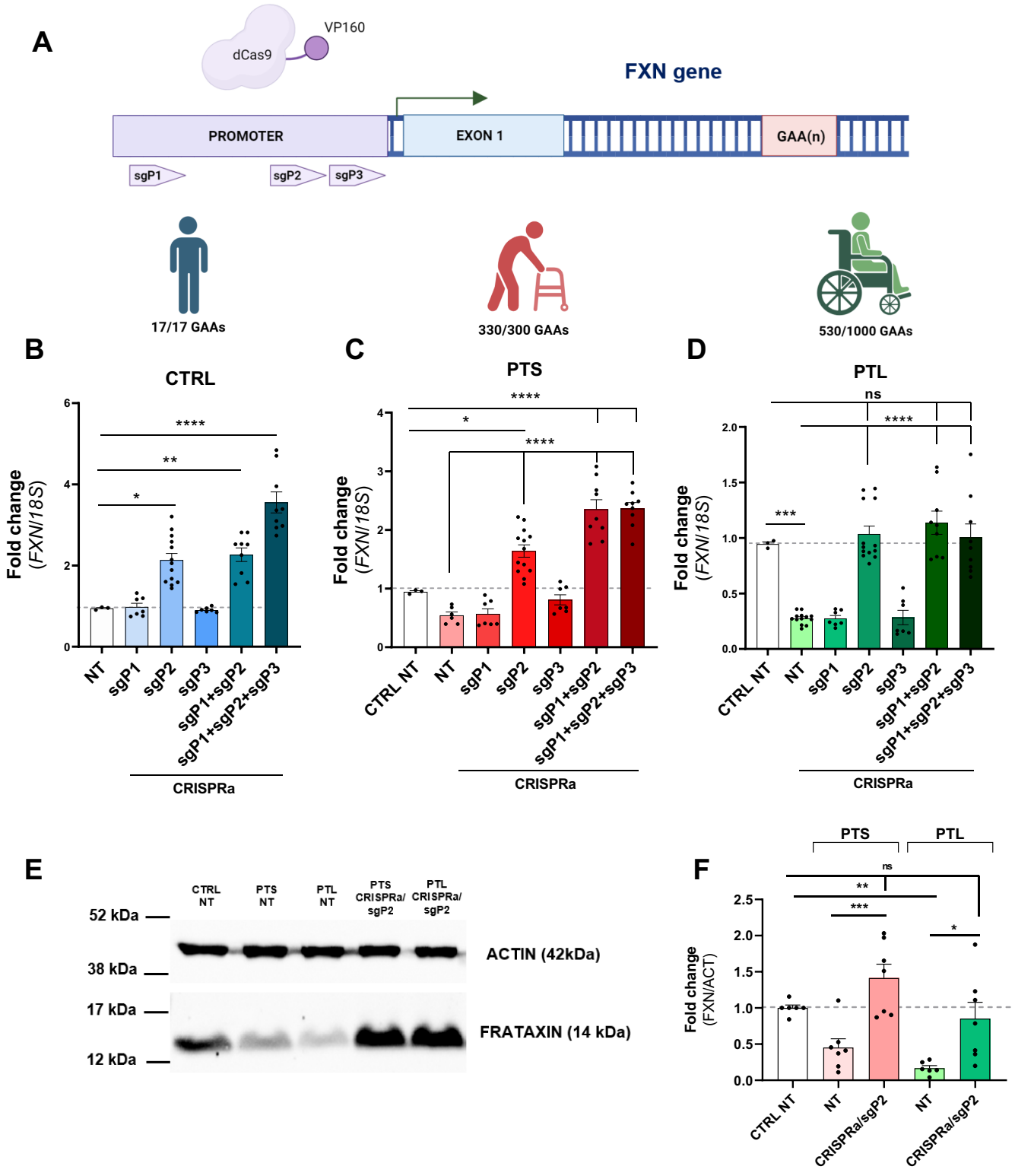
A
dCas9
VP160
FXN gene
PROMOTER
EXON 1
GAA(n)
sgP1
sgP2
sgP3
17/17 GAAs
330/300 GAAs
530/1000 GAAs
B
CTRL
Fold change (FXN/18S)
NT
sgP1
sgP2
sgP3
sgP1+sgP2
sgP1+sgP2+sgP3
CRISPRa
C
PTS
CTRL NT
D
PTL
ns
E
CTRL NT
PTS NT
PTL NT
PTS CRISPRa/ sgP2
PTL CRISPRa/ sgP2
52 kDa
38 kDa
17 kDa
12 kDa
ACTIN (42kDa)
FRATAXIN (14 kDa)
F
Fold change (FXN/ACT)
CRISPRa/sgP2

Figure 1. CRISPRa sgRNAs screening in FA patients-derived primary fibroblasts. A. Schematic representation of the transcriptional activation approach using the dCas9-VP160 in combination with different sgRNAs targeting *FXN* gene promoter. **B-D**. *FXN* gene expression levels relative to 18S, normalized to the untreated healthy control (white), in primary fibroblasts from the healthy control (CTRL), the milder patient PTS (330/300 GAAs) and the more severe patient PTL (530/1000 GAAs) treated with dCas9-VP160 in combination with individual or pooled sgRNAs (sgP1, sgP2 and sgP3) to screen for the most effective ones. **E**. Western blot analysis of FXN protein levels in fibroblasts from healthy control and patients either untreated or upon CRISPRa lentiviral transduction. B-ACTIN was used as loading control. **F**. Western Blot densitometric quantification of FXN protein in fibroblasts by ImageJ software, normalized to the untreated healthy control (white). **B-D, F**. Statistical analysis One-way ANOVA, with multiple comparison analysis by Dunnett's test. n≥3. * p<0,05. ** p<0,02. *** p<0,001. **** p<0,0001. ns: not significant. All data are mean±SEM. Statistical analyses were conducted by comparing all experimental groups with one another.

CRISPRa-mediated reactivation of *FXN* gene in iPSCs-derived neuronal cell types

FA is a neurodegenerative disorder predominantly impacting sensory neurons in the dorsal root ganglia (DRGs) and neurons within the deep cerebellar nuclei, as mentioned above. To assess the potential therapeutic effects of CRISPRa, we implemented this system in cell types primarily affected by the disease. As previously described, induced pluripotent stem cells (iPSCs) were generated by reprogramming fibroblast lines derived from the two FA patients (PTS and PTL). The cell lines from both patients were stabilized and selected based on their expression of key pluripotency markers and their ability to differentiate into multiple lineages (Mazzara PG et al., 2020). iPSCs from the control and the two patients' lines were then differentiated into neural progenitor cells (NPCs) using an optimized protocol adapted from Marchetto et al., 2010. This protocol involves the initial formation of embryoid bodies, which are plated at day 10 (DIV10) to facilitate neural rosettes formation and terminal differentiation into NPCs (Fig. 2A). To confirm their identity, NPCs were stained for SOX2, PAX6 and NESTIN markers (Fig. S3A-C). Subsequently, NPCs derived from the control, PTS and PTL lines were transduced with the CRISPRa/sgP2 system. Ten days post-transduction, FXN protein levels were analyzed by Western blot. CRISPRa treatment resulted in increased FXN amounts across all cell lines, with the extent of rescue correlating with disease severity. Notably, NPCs derived from the PTL patient exhibited only a partial restoration of FXN levels (Fig. 2B-C). Additionally, NPCs were differentiated into cortical neurons (Banfi F et al., 2023) (Fig. 2D). At DIV30, mature neurons (TUJ1+/MAP2+) (Fig. S4A) were transduced with the CRISPRa/sgP2 system. FXN protein levels, assessed ten days post-transduction, revealed a robust upregulation across all cell lines, achieving full restoration to physiological levels (Fig. 2E-F). Given that FA primarily affects sensory neurons in the DRGs, we also differentiated NPCs into sensory neurons using an optimized protocol based on Mazzara et al., 2020 (Fig. 2G). The obtained DIV30 sensory neurons (TUJ1+/PV+) (Fig. S5A) were treated with the CRISPRa/sgP2 system. FXN protein levels, evaluated ten days after transduction, demonstrated successful restoration to a near-physiological range (Fig. 2H-I). Variability in *FXN* upregulation across experimental groups and cellular models may be influenced by differences in lentiviral transduction efficiency. Although fibroblasts, NPCs and neurons are

generally transduced efficiently by lentiviral vectors, transduction efficiency can still vary depending on cell type and cellular state, leading to heterogeneous transgene expression. Consequently, differences in observed FXN levels may partially reflect variability in viral uptake or expression rather than intrinsic differences between experimental conditions, and this technical variability should be considered when interpreting comparisons across groups and models. Overall, these results demonstrated that, despite the presence of epigenetic repressive markers characterizing the mutated *FXN* gene, the CRISPRa-mediated *FXN* reactivation strategy in disease-relevant neuronal subtypes revealed both feasible and effective.

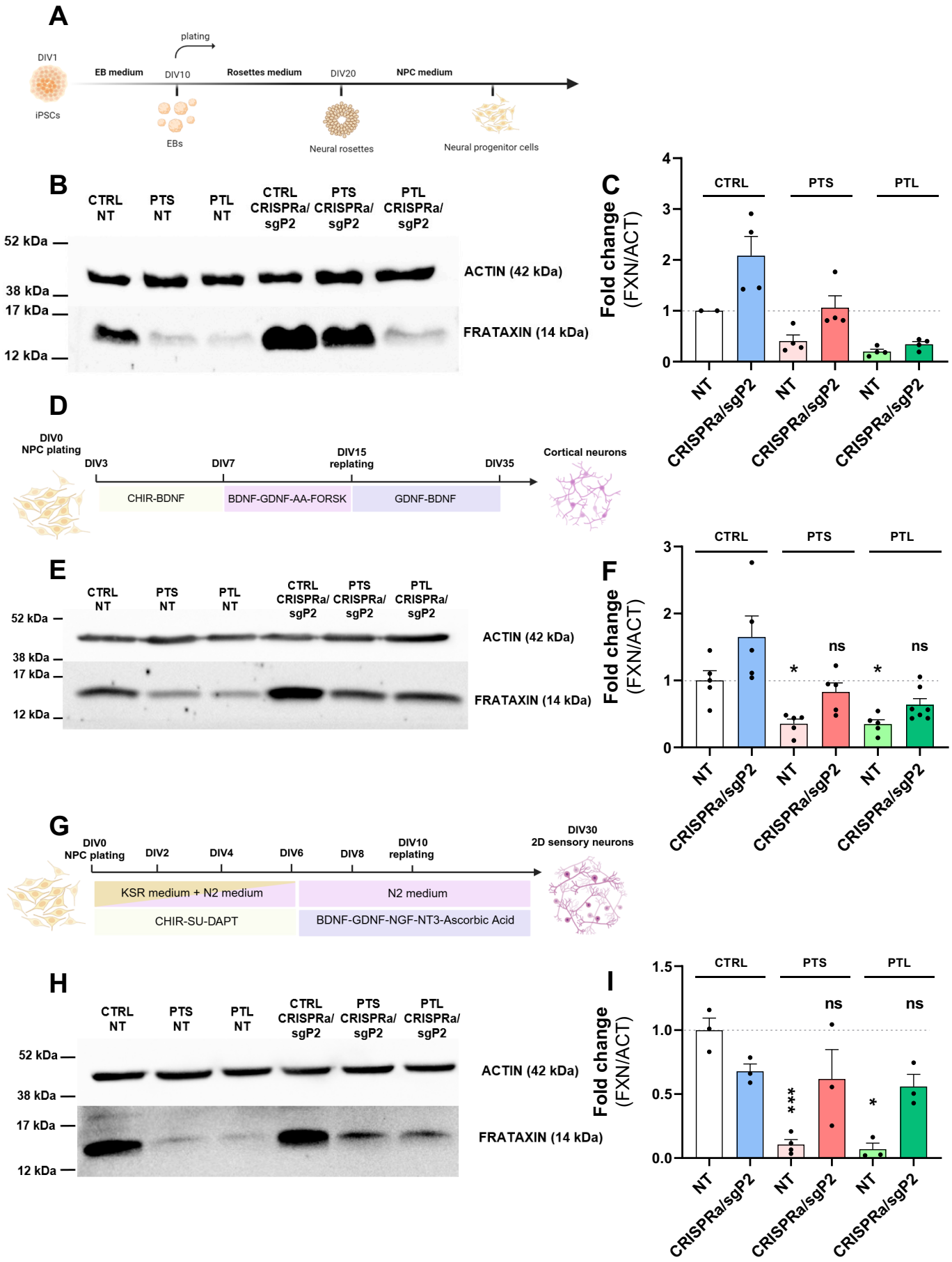
A
plating
DIV1
EB medium
DIV10
Rosettes medium
DIV20
NPC medium
iPSCs
EBs
Neural rosettes
Neural progenitor cells
B
CTRL NT
PTS NT
PTL NT
CTRL CRISPRa/ sgP2
PTS CRISPRa/ sgP2
PTL CRISPRa/ sgP2
52 kDa
38 kDa
17 kDa
12 kDa
ACTIN (42 kDa)
FRATAXIN (14 kDa)
C
Fold change (FXN/ACT)
CTRL
PTS
PTL
NT
CRISPRa/sgP2
D
DIV0 NPC plating
DIV3
DIV7
DIV15 replating
DIV35
Cortical neurons
CHIR-BDNF
BDNF-GDNF-AA-FORSK
GDNF-BDNF
E
F
ns
*
G
DIV0 NPC plating
DIV2
DIV4
DIV6
DIV8
DIV10 replating
DIV30 2D sensory neurons
KSR medium + N2 medium
N2 medium
CHIR-SU-DAPT
BDNF-GDNF-NGF-NT3-Ascorbic Acid
H
I
***

Figure 2. CRISPRa technology for *FXN* gene reactivation in multiple iPSCs-derived cell types. **A**. Protocol for iPSCs differentiation into neural progenitor cells (NPCs) (adapted from Marchetto MC et al., 2010). **B**. Western blot analysis of FXN protein levels in NPCs from healthy control and patients either untreated or upon CRISPRa lentiviral transduction. B-ACTIN was used as loading control. **C**. Western Blot densitometric quantification of FXN protein in NPCs by ImageJ software, normalized to the untreated healthy control (white). **D**. Protocol for NPCs differentiation into cortical neurons (adapted from Banfi F et al., 2021). **E**. Western blot analysis of FXN protein levels in cortical neurons at DIV40 from healthy control and patients either untreated or upon CRISPRa lentiviral transduction. B-ACTIN was used as loading control. **F**. Western Blot densitometric quantification of FXN protein in cortical neurons at DIV40 by ImageJ software, normalized to the untreated healthy control (white). **G**. Protocol for NPCs differentiation into sensory neurons (adapted from Mazzara PG et al., 2020). **H**. Western blot analysis of FXN protein levels in sensory neurons at DIV40 from healthy control and patients either untreated or upon CRISPRa lentiviral transduction. B-ACTIN was used as loading control. **I**. Western Blot densitometric quantification of FXN protein in sensory neurons by ImageJ software, normalized to the untreated healthy control (white). **C, F, I.** Statistical analysis One-way ANOVA, with multiple comparison analysis by Dunnett's test. n≥3. **** p<0,0001. All data are mean±SEM. Statistical analyses were conducted by comparing all experimental groups with the healthy control (white).

RNA-sequencing on NPCs for transcriptomic and off-target genes analysis

Given the pivotal role of *FXN* in mitochondrial metabolism and the severe consequences associated with its deficiency, our study focused on evaluating the effects of CRISPRa-mediated *FXN* activation on molecular pathways known to be disrupted in FA. Specifically, to gain insights into how *FXN* reactivation influenced the cellular transcriptional landscape, we performed genome-wide RNA sequencing (RNA-seq) on PTS-derived NPCs treated with CRISPRa (VP160) or untreated (CTRL) (Fig.3A). Correlation heatmaps and principal component analysis (PCA) (Fig. S6A–B) revealed distinct clustering between treated and control samples, demonstrating high intra-group consistency. Differential gene expression analysis between the CRISPRa-treated and untreated conditions identified 332 upregulated and 494 downregulated genes, highlighting significant transcriptional differences (Fig. S6C–D). To further elucidate the impact of CRISPRa on FXN-related pathways, we focused our analysis on genes involved in iron–sulfur clusters (ISCs) biogenesis and reactive oxygen species (ROS) detoxification. In CRISPRa-treated NPCs, *FXN* expression increased approximately fivefold, accompanied by elevated expression of genes associated with ISCs biosynthesis, assembly, and transfer to recipient proteins (*ISCU*, *NUBP1*, *NUBP2*, *BOLA3*, *SLC25A37*) (Fig.3B). These findings suggest that *FXN* restoration acts as a positive regulatory signal promoting mitochondrial ISCs synthesis and enhancing transcription of components within this pathway. Consistently, genes encoding ISCs-containing proteins, such as *ACO1*, were also upregulated. Additionally, genes involved in ROS detoxification (*GLRX3*, *GLRX5*, *SOD1*, *SOD3*, *TXN*, *TXNRD1*, *SRXN1*, *GPX1*, *GPX3*, *NQO1*) displayed increased expression, indicating activation of cellular mechanisms aimed at restoring redox homeostasis (Fig.3B). Importantly, gene set enrichment (GSEA) analysis revealed significant dysregulation of pathways associated with neural commitment, neuronal fate specification, and neural differentiation in VP160-treated samples compared with controls (Fig. S6E). While these changes may have biological relevance and indicate that VP160

influences developmental and neurogenic programs, they may represent an unintended effect in the context of therapeutic application. Notably, because the ultimate therapeutic goal is to target post-mitotic neurons rather than progenitor or differentiating populations, this apparent obstacle is expected to be mitigated in fully differentiated neuronal models, where developmental pathways are largely inactive. Remarkably, NPCs were selected for this analysis rather than neurons, in which *FXN* upregulation was more variable, because *FXN* induction in NPCs was robust, allowing us to push the system and obtain clearer insights into the transcriptional consequences of CRISPRa application. Given the potential for off-target effects associated with the CRISPRa system, particularly due to the possible non-specific binding of the sgP2 sgRNA, the CRISPOR online tool was used to predict potential off-target genes. This analysis identified a set of candidate genes with sequences differing from sgP2 by three or four mismatches, all located in intergenic or intronic regions, thus making off-target activity unlikely (Supplementary Table 5). To experimentally assess this, we cross-referenced the predicted off-target genes with our RNA-seq dataset. The majority showed no significant expression changes following CRISPRa/sgP2 treatment, supporting the specificity of sgP2-mediated *FXN* activation (Fig. 3C). Interestingly, *IGF2BP2* emerged as the only gene displaying significant upregulation in RNA-seq data. However, validation by RT-qPCR, performed on the same RNA samples, did not confirm this increase, emphasizing the importance of cross-methodological verification. In addition to the predicted off-target effects associated with potential sgRNA aspecificity, we extended our analysis to include genes located in close genomic proximity to the *FXN* locus on chromosome 9. The majority of these neighboring genes did not exhibit significant transcriptional changes following CRISPRa induction, indicating a high degree of locus specificity. Notably, only two genes, *PIP5K1B* and *APBA1*, located approximately 330 kb upstream and 392 kb downstream of FXN respectively, showed a statistically significant upregulation (Fig. 3D). Interestingly, previous studies have reported cis-silencing of *PIP5K1B* in lymphocytes and primary fibroblasts derived from Friedreich's ataxia (FA) patients (Bayot et al., 2013). In light of this evidence, the observed increase in *PIP5K1B* expression is likely a downstream consequence of *FXN* reactivation rather than an off-target effect of CRISPRa, supporting the notion that restoration of *FXN* expression rescues molecular pathways disrupted by FXN protein deficiency. Overall, these findings demonstrate that the CRISPRa system effectively reactivated *FXN* expression without inducing notable off-target transcriptional effects and without unintended epigenome editing (Fig. S6F).

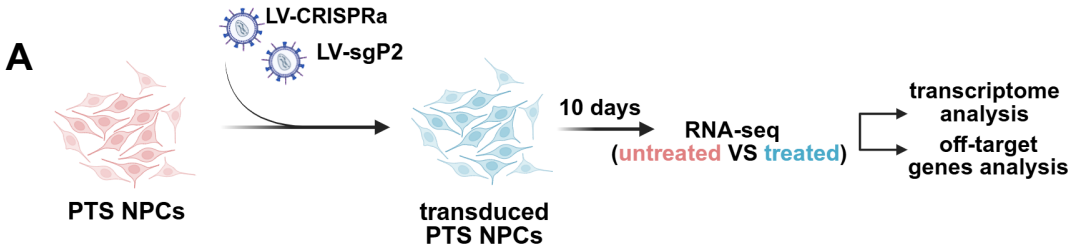
A
LV-CRISPRa
LV-sgP2
PTS NPCs
transduced PTS NPCs
10 days
RNA-seq
(untreated VS treated)
transcriptome analysis
off-target genes analysis

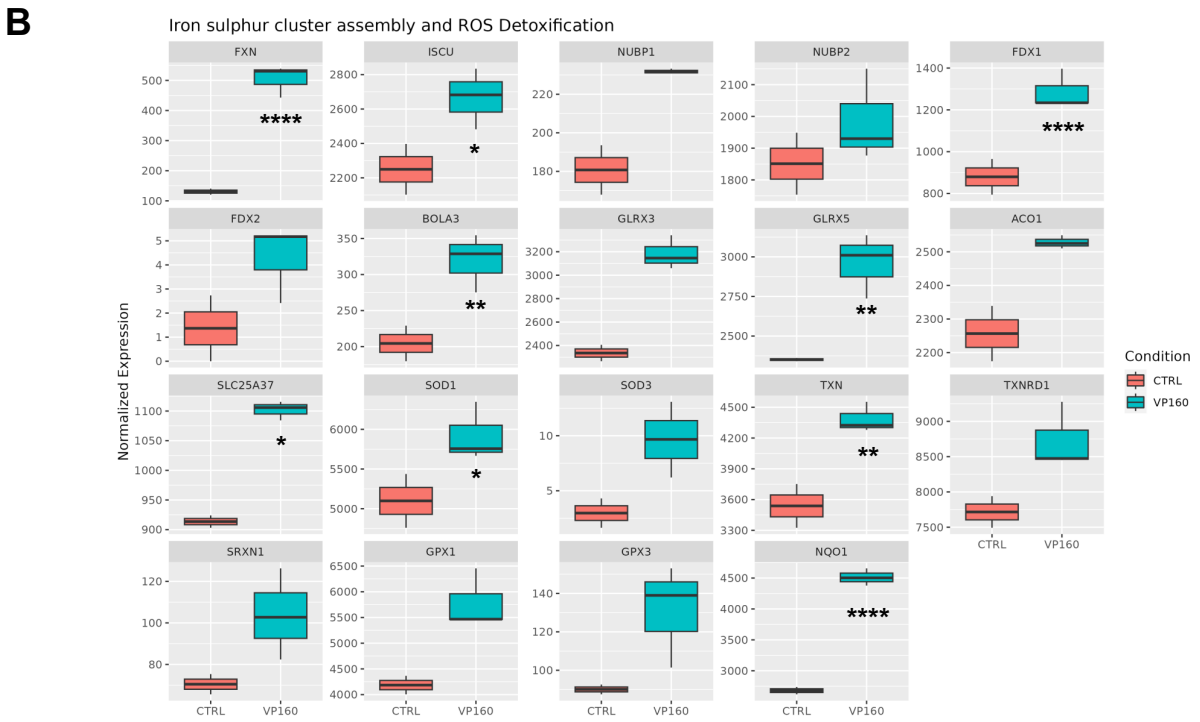
B
Iron sulphur cluster assembly and ROS Detoxification
FXN
ISCU
NUBP1
NUBP2
FDX1
FDX2
BOLA3
GLRX3
GLRX5
ACO1
SLC25A37
SOD1
SOD3
TXN
TXNRD1
SRXN1
GPX1
GPX3
NQO1
Normalized Expression
CTRL
VP160
Condition

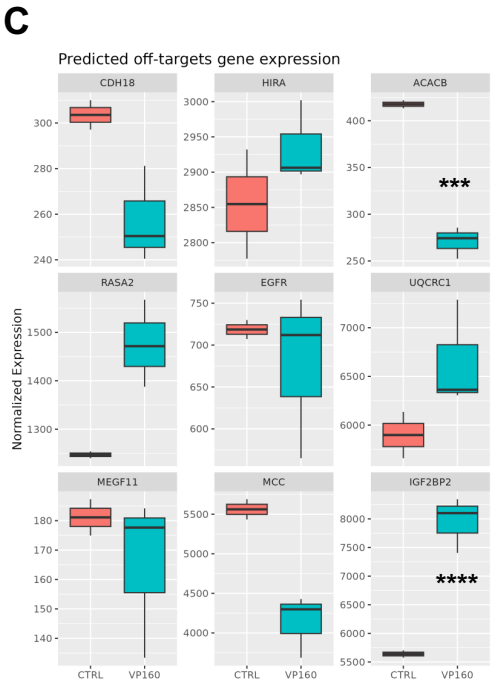
C
Predicted off-targets gene expression
CDH18
HIRA
ACACB
RASA2
EGFR
UQCRC1
MEGF11
MCC
IGF2BP2
Normalized Expression
CTRL
VP160

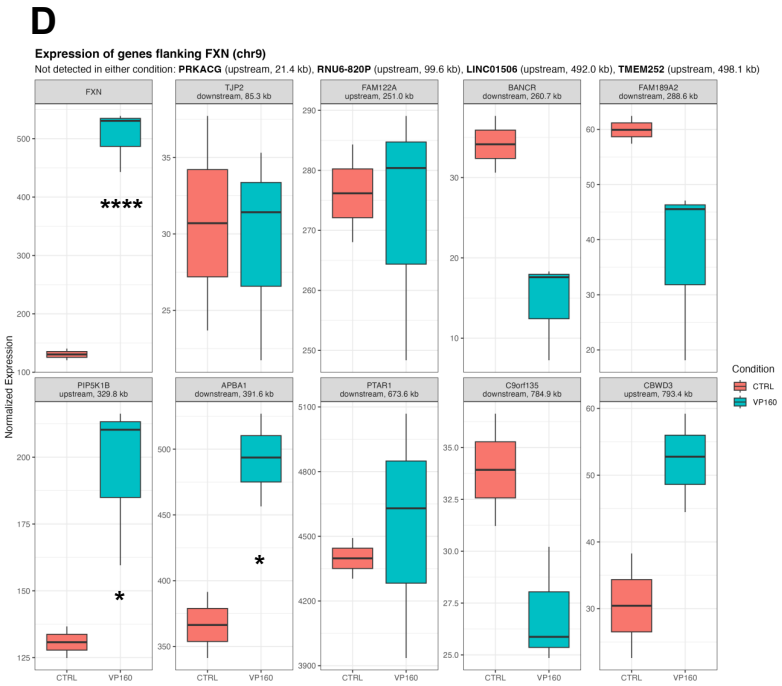
D
Expression of genes flanking FXN (chr9)
Not detected in either condition: PRKACG (upstream, 21.4 kb), RNU6-820P (upstream, 99.6 kb), LINC01506 (upstream, 492.0 kb), TMEM252 (upstream, 498.1 kb)
FXN
TJP2 downstream, 85.3 kb
FAM122A upstream, 251.0 kb
BANCR downstream, 260.7 kb
FAM189A2 downstream, 288.6 kb
PIP5K1B upstream, 329.8 kb
APBA1 downstream, 391.6 kb
PTAR1 downstream, 673.6 kb
C9orf135 downstream, 784.9 kb
CBWD3 upstream, 793.4 kb
Normalized Expression
CTRL
VP160
Condition

Figure 3. RNA sequencing on PTS patient NPCs for transcriptomic and off-target genes analysis. A. Schematic overview of the workflow: PTS patient-derived NPCs, either untreated or CRISPRa treated, were subjected to RNA-seq to perform a detailed transcriptomic analysis of the molecular pathways predominantly affected in FA and to assess the potential upregulation of the predicted off-target genes (by CRISPOR software). **B**. Normalized expression of genes involved in Fe-S clusters biosynthesis, assembly and transfer to the recipient proteins (*FXN, ISCU, NUBP1, NUBP2, BOLA3, SLC25A37*), genes involved in ROS detoxifying processes (*GLRX3/5, SOD1, SOD3, TXN, TXNRD1, SRXN1, GPX1, GPX3, NQO1*), genes of Fe-S containing proteins (*ACO1*), in untreated (CTRL, pink) vs treated NPCs (VP160, light blue). **C**. Normalized expression of the off-target genes predicted by CRISPOR software in untreated (CTRL, pink) vs treated NPCs (VP160, light blue). **D**. Normalized expression of the genes in close genomic proximity to the *FXN* locus on chromosome 9 in untreated (CTRL, pink) vs treated NPCs (VP160, light blue).

CRISPRa treatment rescues redox homeostasis in iPSCs-derived cortical neurons

In FA toxic accumulation of ROS plays a central role in disease pathophysiology. Loss of FXN disrupts ISCs biosynthesis, resulting in the defective activity of ISCs-dependent proteins. Several subunits of the electron transport chain require ISCs to properly function, therefore their activity is impaired in FA. This leads to electron leakage and free electrons react with oxygen producing superoxide anions and other ROS. Moreover, unused iron further exacerbates this condition generating hydroxyl radicals, via Fenton reaction. ROS have a detrimental effect on cellular homeostasis that culminates in cell death. Notably, as mentioned above, the only available and approved drug for FA (Omaveloxolone) works by inducing the expression of antioxidant defense genes, through NRF2 transcription factor activation, reducing oxidative stress. Studies reported that Omaveloxolone significantly improved patients' neurological symptoms in the long term, without major side effects (Gunther K et al., 2025). Thus, to verify the potential therapeutic effect of the CRISPRa approach, ROS levels were measured in iPSCs-derived cortical neurons. To do so, we exploited the dye $DCFH_2$-DA that upon presence of hydroperoxides is oxidized to form the fluorescent compound DCF, measurable via live imaging (Fig. 4A). Therefore, DIV40 iPSCs-derived cortical neurons, untreated or treated with CRISPRa, were incubated with $DCFH_2$-DA and co-labeled with CD-56 neuronal marker in order to visualize cell bodies and protrusions (Fig. 4B). The obtained results, based on mean fluorescence intensity measured in ≥180 cells per condition, displayed a complete rescue of the redox homeostasis in both PTS and PTL cortical neurons, upon CRISPRa treatment. Indeed, ROS levels were restored to basal physiological amounts recorded in the untreated control neurons (Fig. 4B-D). Collectively, these findings support the therapeutic potential of CRISPRa-mediated *FXN* reactivation in recapitulating the beneficial antioxidant effects of Omaveloxolone observed in patients.

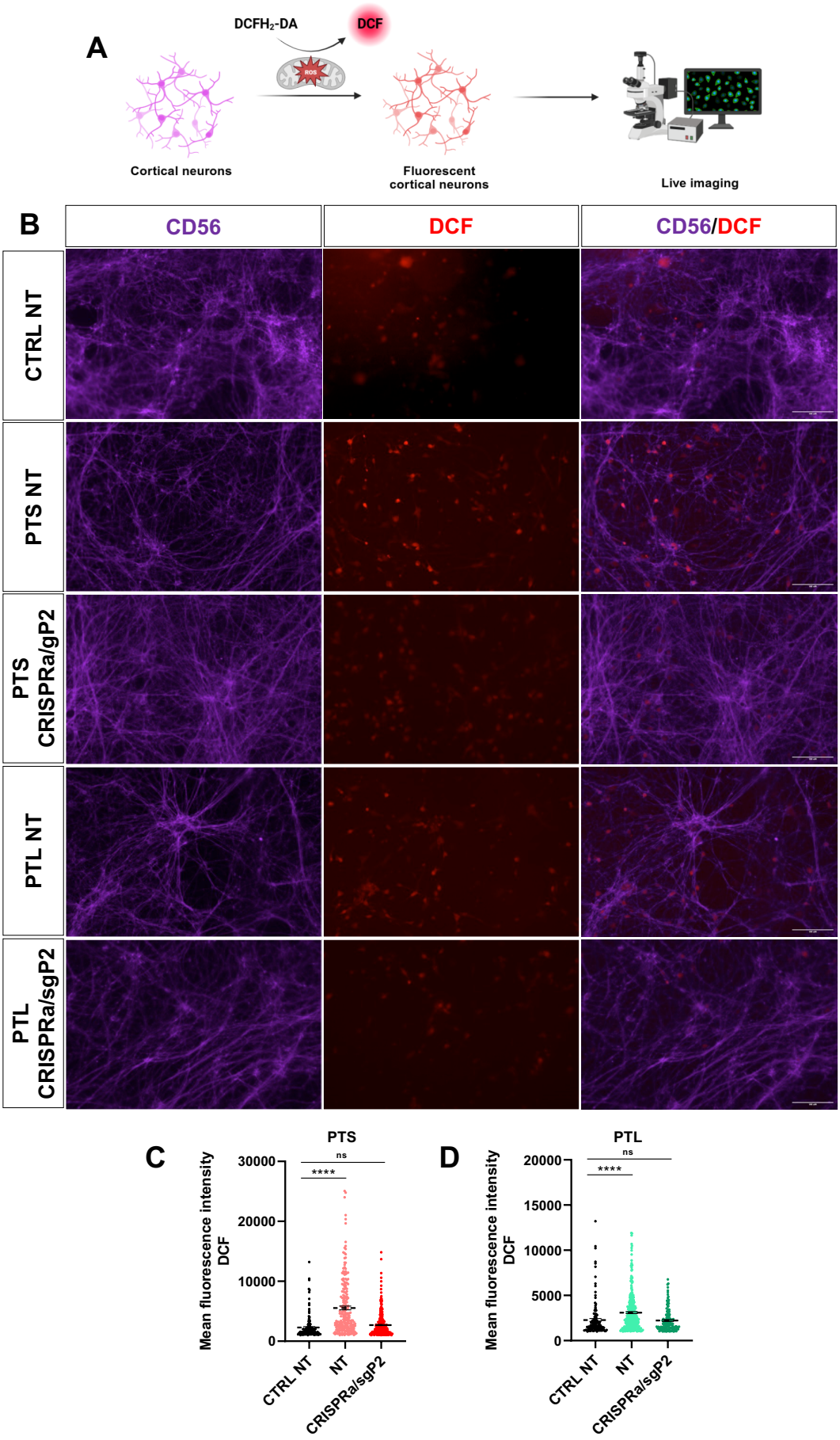
A
DCFH2-DA
DCF
ROS
Cortical neurons
Fluorescent cortical neurons
Live imaging
B
CD56
DCF
CD56/DCF
CTRL NT
PTS NT
PTS CRISPRa/gP2
PTL NT
PTL CRISPRa/sgP2
C
PTS
Mean fluorescence intensity DCF
30000
20000
10000
0
ns
****
CTRL NT
NT
CRISPRa/sgP2
D
PTL
Mean fluorescence intensity DCF
20000
15000
10000
5000
0
ns
****
CTRL NT
NT
CRISPRa/sgP2

Figure 4. ROS levels analysis in iPSCs-derived cortical neurons. A. Scheme of the experimental procedure for ROS detection in cell culture. Cellular peroxide levels were assessed using the dye $DCFH_2$-DA, which is oxidized by hydroperoxides to form the fluorescent compound DCF. Fluorescence is then measured by live imaging. **B**. ROS levels were measured in iPSCs-derived cortical neurons at DIV40 from healthy control, PTS and PTL patients with or without CRISPRa treatment. DCF signal (red) was paired with the CD56 staining (purple), to visualize the neurons bodies and processes. Scale bar 100 uM. **C, D**. ROS levels quantification as mean fluorescence intensity of DCF in ≥180 cells in healthy control, PTS and PTL patients, either untreated or CRISPRa treated. Statistical analysis by One-way ANOVA, with multiple comparison analysis by Dunnett's test **** p<0,0001. ns: not significant. All data are mean±SEM. Statistical analyses were conducted by comparing all experimental groups with the healthy control (black).

ISCs-harboring proteins levels are increased upon CRISPRa treatment

Iron-sulphur clusters (ISCs) are essential inorganic cofactors necessary for the correct functioning of many proteins, at the basis of fundamental life processes. Despite the diverse functions in which ISCs are involved, they are mainly known for their role in electron transport chain (ETC). Electrons donated by both NADH and FADH2 are transferred through numerous ISCs found in Complexes I, II and III of the ETC, with molecular oxygen serving as the terminal electron acceptor, forming water (Fig. 5A). A study by Ast et al. (2024) demonstrated that nearly all ISCs-containing proteins were depleted in FXN-deficient cells. Building on this, we investigated the protein levels of ETC subunits in iPSC-derived sensory neurons from both control and PTL patient at DIV40, ten days after CRISPRa treatment. Our findings revealed a significant increase in the complex I subunit (NDUF8B) levels in PTL neurons treated with CRISPRa compared to their untreated counterpart (Fig. 5B, F). In contrast, subunits of complexes II and III, which also contain ISCs, showed only a trend toward increased levels, without reaching statistical significance (Fig. 5B, C-E, G). Nevertheless, according to a recent study by Doni and colleagues, complex I is the main one that physically interacts with FXN. Moreover, they proved that ISCs belonging to complex I are significantly reduced relative to the control, pointing out a specific susceptibility of this complex to FXN decrease. Their results display a structural and functional interplay between complex I and FXN and highlight the potential for developing FA therapies specifically targeting this component of the ETC (Doni D et al., 2023). To further test our hypothesis, we analyzed the levels of METTL17, a recently identified ISC-containing protein involved in mitochondrial ribosome assembly. This protein was reported to be post-transcriptionally depleted in FXN-deficient cells and when overexpressed it restored the bioenergetic defects given by FXN absence (Ast T et al., 2024). Specifically, we examined iPSCs-derived cortical neurons from control, PTS, and PTL patients at DIV40, ten days following CRISPRa transduction. Interestingly, METTL17 levels were directly proportional to FXN levels (Fig. 5H-I), consistent with ISCs deficiency impairing the stability or maturation of target proteins, as previously reported (Ast T et al., 2024). Indeed, neurons derived from PTS and PTL patients exhibited significantly reduced METTL17 levels, which were restored upon *FXN* reactivation via CRISPRa

(Fig. 5H-I). These findings indirectly support the capacity of CRISPRa to restore ISCs biogenesis and thereby re-establish critical metabolic pathways essential for neuronal functionality and viability.

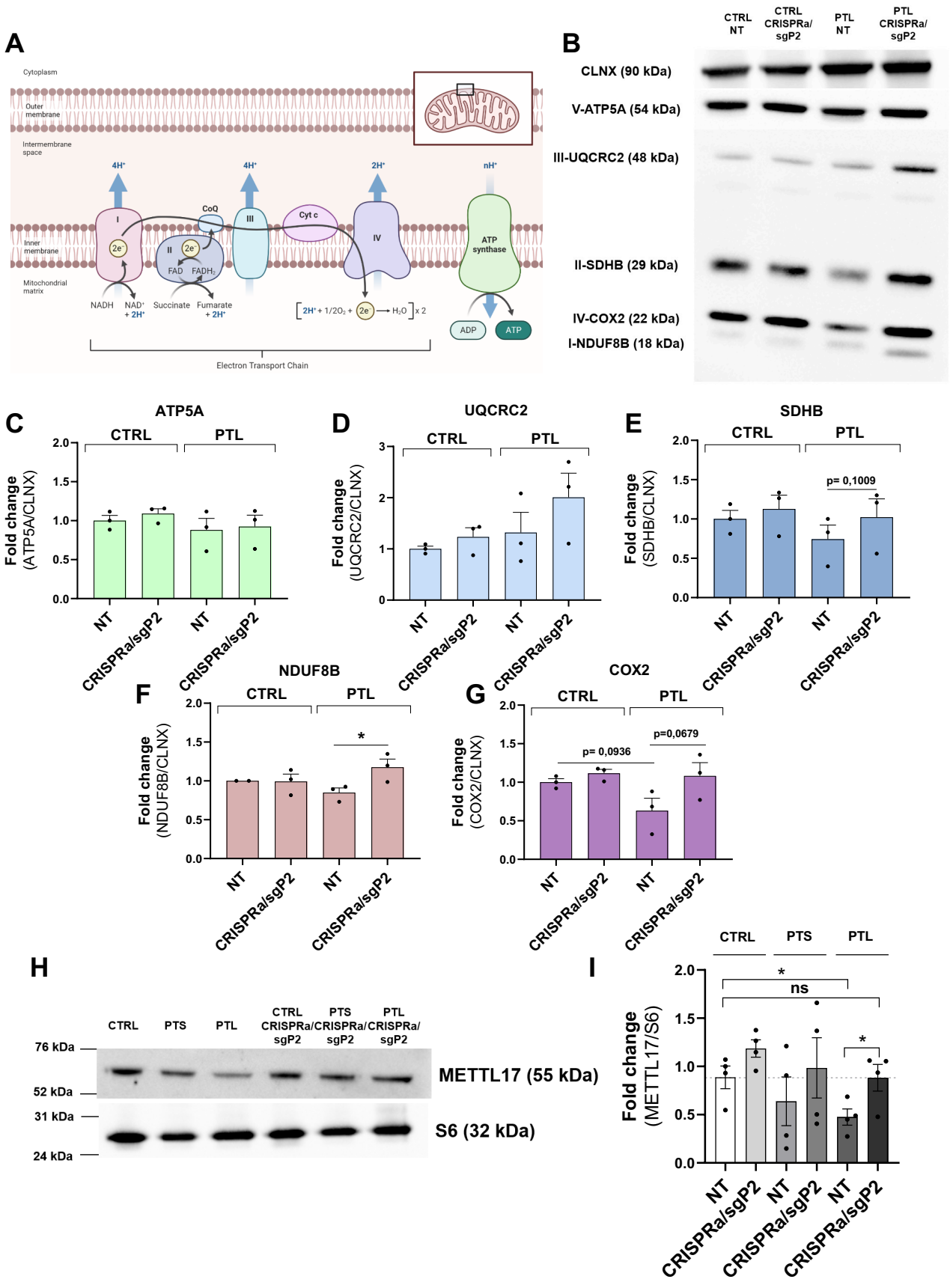

Figure 5. ISCs-containing proteins levels are increased upon CRISPRa treatment in iPSCs-derived neurons. A. Schematic representation of respiratory complexes involved in the electron transport chain and, thus, in ATP production on the mitochondria membrane. **B**. Western blot analysis of respiratory complex subunits, including ISCs-containing proteins NDUFB8, SDHB, and UQCRC2, was performed on whole-cell extracts from healthy control and PTL iPSC-derived sensory neurons at DIV40. CALNEXIN was used as loading control. **C-G.** Western Blot densitometric quantification of respiratory complexes subunits in healthy control and PTL iPSCs-derived sensory neurons at DIV40 by ImageJ software, normalized to the untreated healthy control. Statistical analysis by paired t-test. n=3. * p<0,05. All data are mean±SEM. **H**. Western blot analysis of ISCs-harboring protein METTL17, a conserved mitoribosome assembly factor, in whole-cell extract from healthy control and PTL iPSCs-derived cortical neurons at DIV40. S6, a component of the 40S ribosomal subunit, was used as loading control. **I**. Western blot densitometric quantification of METTL17 protein in healthy control and FA iPSCs-derived cortical neurons at DIV40 by ImageJ software, normalized to the untreated healthy control (white). Statistical analysis by paired t-test. n=4. * p<0,05. ns: not significant. All data are mean±SEM. Statistical analyses in fig.5C-G were conducted by comparing untreated with treated healthy control and untreated with treated PTL patient. Statistical analyses in fig.5I were conducted by comparing all experimental groups with one another.

CRISPRa in cortical neurons from FA YG8sR mouse model

Following the assessment of CRISPRa system efficacy in human cells, we sought to evaluate its performance in the YG8sR FA mouse model. The YG8sR mouse is a transgenic, humanized model that carries a single copy of the human *FXN* (*hFXN*) gene with an expanded GAA repeat tract (250–300 repeats) on a yeast artificial chromosome (YAC) and lacks endogenous murine *FXN* (*mFXN*) expression (Anjomani Virmouni S et al., 2015). To this end, primary cortical neurons were isolated from E17.5 YG8sR embryos and cultured *in vitro*. Cells were transduced with the CRISPRa system using individual or combined sgRNAs (sgP1, sgP2, and sgP3). After ten days of treatment, hFXN protein levels were quantified via Western blot analysis (Fig. S7A). Unexpectedly, none of the tested CRISPRa conditions, including the previously reported effective sgP2, resulted in increased hFXN protein amounts (Fig. S7B-C). To investigate this lack of response, we analyzed basal FXN levels in brain and cerebellum tissues from 3 and 15 months old YG8sR mice in comparison to wild-type controls. Strikingly, we observed that baseline hFXN protein levels in YG8sR tissues ($hFXN^{+}/mFXN^{-/-}$) were markedly higher than the corresponding basal mFXN levels in wild-type mice ($mFXN^{+/+}$) (Fig. S7D-G). These findings suggested that the neuronal system under study may already exhibit near-maximal human *FXN* expression, potentially limiting the capacity for further upregulation by the CRISPRa system.

Zinc fingers activators (ZFAs) increase FXN levels in multiple FA-derived cell types

Following the demonstration of CRISPRa-mediated *FXN* gene reactivation and acknowledging the potential limitations associated with its clinical translation, we sought a more translatable alternative. To this end, we investigated the use of zinc-finger activators (ZFAs) as a surrogate approach. Due to their relatively small size, ZFAs are compatible with adeno-associated virus (AAV) vectors,

preferred tools for *in vivo* delivery, and, being derived from human proteins, they are expected to elicit a lower immunogenic response. ZFAs consist of engineered DNA-binding zinc finger arrays fused to transcriptional activation domains, enabling targeted upregulation of gene expression. With technical assistance from Merck, we designed a panel of ZFAs targeting the FXN promoter, focusing specifically on the region also targeted by sgP2, which had proven effective in the CRISPRa context (Fig. 1B-D). A pool of five ZFAs (ZF84, ZF145, ZF168, ZF172, ZF187) was selected based on predicted off-target profiles (ZFAs with ≤3 mismatches were excluded) and non-overlapping binding sites (Fig. 6A, Supplementary table 2). Each ZFA was fused to either a VP64 or VP160 activation domain to assess whether the strength of the activation domain influenced *FXN* induction levels. Lentiviral vectors encoding individual ZFAs, with a V5 tag, nuclear localization signal (NLS), and under the control of the EF1α promoter, were constructed for expression studies (Fig. 6B–C). To evaluate the efficacy of these ZFAs, we performed a screening in primary fibroblasts derived from control, PTS, and PTL patients. Cells were transduced with individual or pooled ZFAs, and *FXN* mRNA levels were measured by RT-qPCR ten days post-transduction. Among the tested conditions, the combination of ZF145, ZF172, and ZF187 yielded the highest *FXN* induction, regardless of whether the VP64 or VP160 activation domain was used. Remarkably, increased *FXN* gene expression following triple ZFA transduction was observed only in fibroblasts from the milder PTS patient, with no detectable effect in fibroblasts from the more severely affected PTL patient (Fig. 6D-E). Protein analysis corroborated the mRNA findings, revealing FXN restoration exclusively in PTS-derived fibroblasts (Fig. 6F-G). Given that the extent of FXN induction was comparable between the VP64- and VP160-based ZFAs, we selected the VP64 constructs for subsequent experiments. A recent study by Chen et al. (2024) demonstrated that the intrinsically disordered region of the FUS protein (FUS-IDR) can enhance transcriptional activation when used as a supplemental activation domain. Based on these findings, we generated a chimeric construct by fusing FUS-IDR to ZFA145, the best performing when used alone (Fig. 6D), in combination with the VP64 domain (Fig. S8A), aiming to assess whether this dual activation strategy could enhance *FXN* expression, making it possible to employ a single ZFA instead of three. However, protein analysis revealed no significant increase in FXN levels (Fig. S8B–C). To further assess the efficacy of the ZFAs system, we applied it to iPSC-derived neuronal cell types from the PTS patient, following the same strategy used in the CRISPRa experiments. FXN protein levels were first evaluated in neural progenitor cells (NPCs) derived from control and PTS iPSCs (Fig. 6H). Due to significant cell death associated with triple lentiviral transduction, protein analysis was performed four days post-treatment. The results showed that ZFAs efficiently restored FXN levels in PTS-derived NPCs to physiological levels (Fig. 6I-J). We then extended our analysis to sensory neurons differentiated from PTS NPCs and analyzed them at DIV30 (Fig. 6L). Again, due to high levels of cell mortality upon triple ZFAs transduction, FXN levels were assessed four days post-treatment. Western blot analysis revealed a significant increase of FXN protein amounts in ZFAs-treated sensory neurons, confirming the efficacy of the ZFAs approach

in a disease-relevant neuronal cell type (Fig. 6M-N). Our findings establish ZFAs as a novel tool for the restoration of endogenous *FXN* expression. However, additional studies on cell lines from other patients are required to establish their applicability on a large-scale basis.

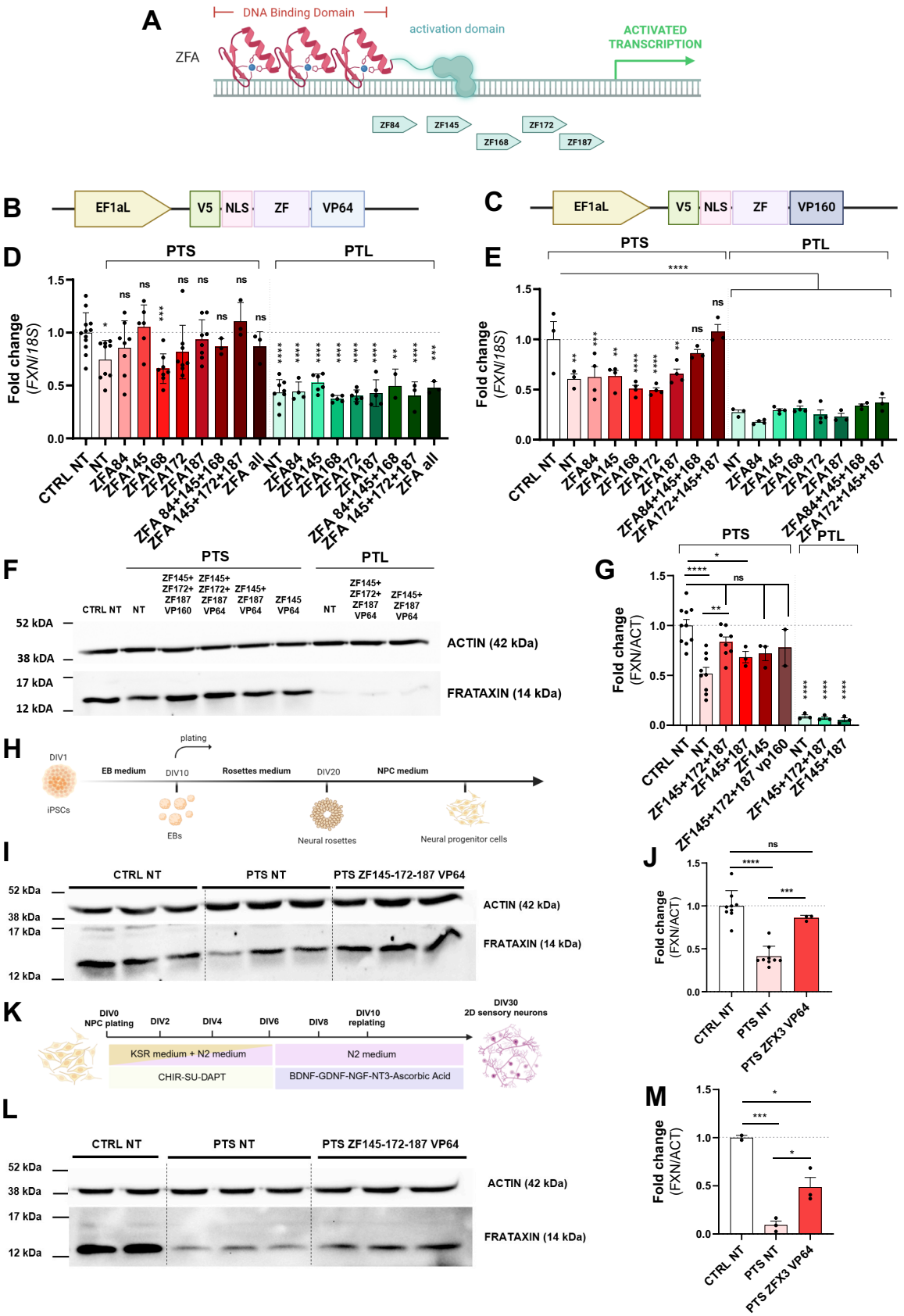

Figure 6. Zinc-fingers activators (ZFAs) for *FXN* gene reactivation in multiple FA cell types. A. Cartoon showing the screened ZFAs (ZF84, ZF145, ZF168, ZF172, ZF187) targeting *FXN* gene promoter and boosting gene expression. **B, C**. Schematic illustration of the lentiviral constructs encoding zinc-finger proteins fused to the two tested activation domains, VP64 and VP160. The constructs expression is driven by the EF1a promoter and they include a nuclear localization signal (NLS) and a V5 epitope tag. **D, E**. *FXN* gene expression levels relative to 18S, normalized to the untreated healthy control (white), were assessed to identify the most effective ZFA or combination of ZFAs (with VP64 or VP160 activation domains) in primary fibroblasts from PTS (330/300 GAAs) and PTL (530/1000 GAAs) patients. **F**. Western blot analysis of FXN protein levels in PTS and PTL patients-derived primary fibroblasts upon treatment with selected ZFAs from the previous screening. B-ACTIN was used as loading control. **G**. Western bot densitometric quantification of FXN protein in healthy control and FA-derived primary fibroblasts by ImageJ software, normalized to the untreated healthy control (white). **H**. Protocol for iPSCs differentiation into neural progenitor cells (NPCs) (adapted from Marchetto MC et al., 2010). **I**. Western blot analysis of FXN protein levels in iPSCs-derived NPCs from healthy control and PTS patient, upon treatment with ZF145, ZF172 and ZF187 combination. B-ACTIN was used as loading control. **J**. Western blot densitometric analysis of FXN protein levels in iPSCs-derived NPCs from healthy control and PTS patient, upon treatment with ZF145, ZF172 and ZF187 combination, by ImageJ software. **K**. Protocol for NPCs differentiation into sensory neurons at DIV40 (adapted from Mazzara PG et al., 2020). **L**. Western blot analysis of FXN protein levels in iPSCs-derived sensory neurons at DIV30 from healthy control and PTS patient, upon treatment with ZF145, ZF172 and ZF187 combination. B-ACTIN was used as loading control. **M**. Western blot densitometric analysis of FXN protein levels in iPSCs-derived sensory neurons from healthy control and PTS patient at DIV30 upon treatment with ZF145, ZF172 and ZF187 combination, by ImageJ software. **C, E, G, I, K**. Statistical analysis by One-way ANOVA, with multiple comparison analysis by Dunnett's test. $n \geq 3$. * $p<0,05$. ** $p<0,02$. *** $p<0,001$. **** $p<0,0001$. ns: not significant. All data are mean±SEM. All data are mean±SEM. Statistical analyses were conducted by comparing all experimental groups with one another.

Discussion

In this study, we propose novel approaches for *FXN* gene reactivation as potential therapeutic strategies for Friedreich's ataxia (FA). FA is a neurodegenerative disorder that affects 1 over 40000 individuals (Koeppen AH, 2011; Pandolfo M, 2009). Patients primarily display limbs and gait ataxia with additional neurological features including dysarthria, absent reflexes and loss of vibration and proprioceptive sensing (Corben LA, 2010). This is due to the loss of sensory neurons in the dorsal root ganglia (DRGs), mainly the proprioceptive ones, as well as the degeneration of the Dentate Nucleus in the cerebellum and the corticospinal tracts (Harding IH, 2020). FA is caused by a pathogenic expansion of the GAA triplet in the intron 1 of the *FXN* gene, resulting in its silencing (Campunzano V et al., 1996). Among the different approaches explored in the field (Li Y et al., 2015; Matuszek Z et al., 2025; Mazzara PG et al., 2020; Ouellet DL et al., 2017; Perdomini M et al., 2014; Piguet F et al., 2018) transcriptional reactivation of the *FXN* gene offers a major advantage by enhancing endogenous *FXN* expression, while circumventing the need for genome-editing interventions targeting the expanded GAA repeats. Here, we conducted a comparative study between two approaches, CRISPR activation (CRISPRa) and zinc finger activators (ZFAs), on cells derived from two FA patients: a mildly affected individual (PTS, 330/300 GAA repeats) and a severely affected individual (PTL, 530/1000 GAA repeats).

Starting from the CRISPRa approach, we employed a catalytically inactive Cas9 (dCas9) fused to the potent transcriptional activation domain VP160, in combination with multiple sgRNAs (sgP1, sgP2, sgP3) targeting *FXN* promoter. The promoter region was selected based on an integrative analysis of publicly available datasets, including RNA polymerase II occupancy, H3K4me3 enrichment, and ATAC-seq data from primary fibroblasts, which collectively highlighted this locus as a favorable target due to its accessible chromatin landscape (Fig. S1A). Indeed, multiple studies have shown that the *FXN* gene harboring the expanded GAA repeats exhibits increased levels of repressive histone modifications, including histone 3 lysine 9 di- and tri-methylation (H3K9me2/3), histone 3 lysine 27 tri-methylation (H3K27me3), as well as histone hypoacetylation, together with higher DNA methylation levels. All together these modifications participate in heterochromatin formation, that concomitantly with DNA secondary structures and DNA-RNA hybrid generation, cause *FXN* silencing (Saveliev A et al., 2003). Notably, the employed dCas9-VP160 in combination with the sgP2 guide proved effective in the restoration of FXN amounts in both PTS and PTL fibroblasts (Fig. 1B-F). In order to find the best CRISPRa tool, in addition to dCas9-VP160, we evaluated alternative CRISPRa constructs, including dCas9-VPR, dCas9-TET1, and dCas12a-NFZ, under the same experimental conditions. However, none achieved activation levels comparable to those obtained with dCas9-VP160 (Fig. S2A-F), underscoring the superior efficiency of this system in reactivating the silenced *FXN* locus in the presence of expanded GAA repeats. A similar transcriptional boosting approach was previously investigated by Cherif and colleagues (2018). In

their study, they provided the first evidence that the *FXN* gene can be reactivated in primary fibroblasts from patients, even in presence of long GAA repeats expansion. Indeed, they employed “platinum” TALEs (plTALEs) fused to activator domains to target the *FXN* promoter or intron 1. Their *in vitro* results showed that some of these plTALE-VP64s or plTALE-SunTag constructs substantially increased *FXN* mRNA and FXN protein levels. Besides, they showed that delivery of these effectors via AAV9 in FA YG8R mouse model (Al-Mahdawi S et al., 2004) determined a significant increase of *FXN* mRNA and FXN protein levels in muscle and heart, but not in the brain that turned out to be hard to target (Cherif K et al., 2018). However, despite these striking results, they did not explore the system in a human disease-relevant context and, since FA mainly affects DRGs, spinal cord and cerebellum, evidence of gene reactivation in neurons is crucial. Therefore, our primary objective was to investigate the use of transcriptional activators in patients-derived neuronal cultures to assess their impact on the cell types more susceptible to degeneration during FA progression. Our results showed that CRISPRa-mediated activation induced a robust increase in FXN protein levels across several disease-relevant neural cell types derived from FA induced pluripotent stem cells (iPSCs). *FXN* re-expression was successfully achieved in iPSC-derived neural progenitor cells (NPCs), cortical neurons, and sensory neurons, the neuronal population most severely affected in FA. Notably, FXN protein restoration was achieved in cells from both PTS and PTL patients, regardless of the length of their GAA repeat expansions, highlighting the capacity of CRISPRa to overcome the transcriptional silencing imposed by even extensive GAA repeat tracts (Fig. 2A-I). The only exception was a partial recovery observed in NPCs from the PTL patient, suggesting that heterochromatin compaction may restrict gene reactivation in certain cell types, particularly under more severe disease conditions (Fig. 2C). Once assessed the effectiveness of the CRISPRa/sgP2 tool, we investigated potential off-target effects. Importantly, no significant unintended transcriptional changes were observed among the potential off-target genes predicted by CRISPOR software and among the genes in close genomic proximity to the *FXN* locus, supporting the specificity of the sgP2-mediated activation (Fig. 3C-D). Remarkably, *FXN* reactivation was accompanied by the functional recovery of downstream pathways known to be impaired in FA. Specifically, we observed normalization of cellular redox homeostasis, as indicated by the upregulation of detoxifying genes (Fig. 3B) and a concomitant reduction in reactive oxygen species (ROS) levels, which, as expected, were elevated in untreated FA-derived cortical neurons (Fig. 4B–D). Given the established role of FXN in iron–sulfur cluster (ISC) biosynthesis, we investigated whether CRISPRa-mediated FXN restoration could rescue also this defective process. Transcriptomic analysis revealed the upregulation of genes encoding components involved in ISCs assembly (Fig. 3B), suggesting that FXN reactivation promoted the re-establishment of this essential pathway. To indirectly assess ISCs abundance following CRISPRa treatment, we quantified ISC-containing proteins in both control and FA-derived neurons, as ISCs depletion is known to reduce the levels of these proteins. Notably, CRISPRa treatment restored their near-physiological levels, indicating a replenishment of the ISCs

pool (Fig. 5A-I). These results collectively support the potential of transcriptional activation strategies to rescue both *FXN* expression and associated cellular dysfunctions in FA human neuronal models, representing an advancement to the work of Cherif and colleagues (Cherif K et al., 2018). During the past years, other molecular approaches have been explored for *FXN* gene expression restoration. Several groups focused on GAA triplet expansion excision (Li Y et al., 2015; Mazzara PG et al., 2020; Ouellet DL et al., 2017). In this regard, we have previously shown in Broccoli's lab that *FXN* gene can be reactivated in iPSCs-derived DRG organoids (DRGOs) from patients with different GAA repeats lengths, by exciding the triplet expansion through CRISPR/Cas9 technology (Mazzara PG et al., 2020). Through this alternative approach, we demonstrated that targeted excision of the GAA repeats markedly alleviated molecular and cellular disease features in DRGOs. More specifically, we showed that removing only the expanded GAA tract proved less effective at reversing key pathological hallmarks, such as *FXN* re-expression, axonal outgrowth, and synaptic organization, compared to a larger deletion that removed nearly the entire *FXN* intron 1, where most of the epigenetic repressive marks are concentrated. Interestingly, an innovative approach was recently described by David Liu's group at Harvard university. Using adenine base editors (ABEs), they were able to introduce interruptions (A•T → G•C) in the GAA repeats stretch, mimicking some naturally occurring variants (e.g. GAG, GGA) found in some individuals, that are associated with reduced repeat instability. This strategy effectively enhanced *FXN* expression in fibroblasts derived from FA patients and reduced somatic repeat instability *in vivo* (Matuszek Z et al., 2025). The main disadvantage of the CRISPR/Cas9 or base editors approaches is that an intervention at the DNA level could cause unintended and irreversible genomic changes. For instance, it has been reported that Cas9 can induce strand breaks that are sometimes repaired incorrectly, resulting in insertions, deletions, or chromosomal rearrangements (Kalter N et al., 2025; Kosicki M et al., 2018; Xue C et al., 2021). Consequently, such approaches are highly invasive and challenging to implement in a clinical setting. Similarly, the dCas9-VP160 system also faces significant limitations in terms of translational and clinical applicability. One of the major challenges is its large molecular size, which exceeds the packaging capacity of AAV vectors, currently among the most widely used and clinically validated platforms for *in vivo* gene delivery. Consequently, direct delivery of the full-length dCas9-VP160 construct using a single AAV vector is not feasible. To address this limitation, several alternative strategies have been proposed to improve the clinical translatability of CRISPR-based transcriptional activation approaches. One such strategy involves dual-AAV (split-AAV) systems, in which the dCas9 component and transcriptional activation domains are distributed across two separate vectors and reconstituted into a functional complex following co-infection of target cells. Among these approaches, intein-mediated protein trans-splicing has emerged as a particularly promising solution. This method enables the delivery of large Cas9-based constructs as two inactive protein fragments, each fused to complementary split intein domains. Upon co-expression within the same cell, the intein domains associate and catalyze protein trans-splicing, resulting in the accurate

reconstitution of a full-length, functional Cas9 protein (Truong DJ et al., 2015; Zhi S et al., 2022). When applied to catalytically inactive Cas9 (dCas9)-based transcriptional activators, split-intein systems offer additional advantages by enabling modular assembly of dCas9 and regulatory effector domains. This modularity facilitates flexible vector design and the potential incorporation of alternative transcriptional regulators depending on the therapeutic context (Ma D et al., 2016). Nevertheless, for all dual-AAV approaches, the efficiency of protein or mRNA reconstitution, the balance of fragment expression levels, and the temporal coordination of vector delivery remain critical parameters that require careful optimization to ensure robust and reproducible activity. An additional promising strategy involves the use of smaller Cas9 orthologs derived from alternative bacterial species, such as *Staphylococcus aureus* Cas9 (SaCas9), which possess reduced coding sequences compatible with AAV packaging limits. Although these orthologs are characterized by distinct PAM requirements and may exhibit reduced targeting flexibility, their compact size makes them attractive candidates for *in vivo* applications (Butterfield GL et al., 2025). In summary, while dCas9-VP160 represents a powerful tool for transcriptional modulation in experimental settings, future studies should focus on the development and evaluation of alternative vector architectures and compact CRISPR-based activator systems to achieve an optimal balance between transcriptional efficacy and delivery feasibility.

Since the final goal of our work was to find the best tool for translational purposes, we explored ZFAs as a clinically more translatable alternative to CRISPRa for *FXN* reactivation. ZFAs offer practical advantages, including their smaller size, allowing efficient packaging into AAV vectors, and their derivation from human proteins, which should reduce immunogenicity. By designing a panel of promoter-targeted ZFAs, we identified a triple combination (ZF145, ZF172, ZF187) that effectively boosted *FXN* expression in fibroblasts from PTS patient, but not in fibroblasts from the more severely affected PTL patient, suggesting that residual chromatin accessibility may influence efficacy of this approach. Importantly, the ZFAs strategy proved effective in iPSC-derived neuronal cells from the PTS patient, where FXN protein was restored to near-physiological levels in both NPCs and sensory neurons (Fig. 6A-M). These results validate ZFAs as a valuable platform for targeted *FXN* upregulation. However, considering that they were effective only in mildly affected patient-derived cells, in the next future we will assess in other patients' cell lines the efficacy of the system in order to understand if it could be applicable on a large-scale basis. Notably, ZF transcriptional regulators (repressors or activators) hold great potential for clinical applications. Indeed, Sangamo therapeutics is already applying this technology to several neurological disorders. For example, they developed and tested ZF-repressors (ZFRs) for Huntington's disease that bind to the expanded CAG repeats and repress the mutant *HTT* allele selectively. *In vitro* and *in vivo* experiments proved the efficacy of the system, with minimal off-target effects, representing a valuable option towards therapy (Zeitler B et al., 2019). Moreover, a currently on-going clinical trial (NCT06980948) is testing ZFRs for the treatment of small fiber neuropathy (clinicaltrials.gov; Sangamo.com).

Part of this work was focused on *in vivo* experiments with the CRISPRa system, in which we tested *FXN* gene reactivation in primary cortical neurons derived from E17.5 YG8sR pups. Unexpectedly, our treatment did not result in increased human FXN levels. This is likely because, according to our experiments, basal human FXN levels in YG8sR mice were already higher than murine Fxn in wild-type (WT) animals (Fig. S7), suggesting that the genetic context in this model may already be saturated and therefore unresponsive to further gene induction. Brain tissues from mice aged 3 and 15 months were analyzed to assess whether the age-dependent GAA repeat expansion reported in the literature resulted in a significant reduction of human *FXN* expression. However, human FXN levels remained higher than endogenous murine Fxn levels in WT animals, even at advanced age, indicating that GAA expansion did not lead to a marked repression of human *FXN* gene in this model. To date, this aspect has not been described in previous studies. Notably, Cherif et al. (2018) represent the only work in which an attempt was made to upregulate the human *FXN* gene in a comparable model (YG8R) using TALEN-based transcriptional activators. In that study, no significant increase in human FXN protein levels was detected in brain tissues. In the absence of alternative validated models, the only mouse line that could currently be considered for this purpose is the recently developed YG8JR model, an upgraded version of the YG8sR model employed in the present work. The YG8JR mouse carries more than 800 GAA repeats and has been reported to exhibit markedly reduced human FXN expression, together with earlier disease onset and more severe ataxic phenotypes compared with previously available models (Kalef-Ezra et al., 2023). These findings highlighted a persistent challenge in the field: the absence of animal models that accurately recapitulate the molecular and transcriptional features of FA, and that can reliably serve as platforms to evaluate strategies for *FXN* reactivation. *In vivo* studies are crucial for evaluating this kind of potential therapy, as they not only provide insights into biodistribution, histological outcomes, and behavioral effects, but also allow assessment of treatment durability, clarifying how long a single injection remains effective and identifying the optimal therapeutic window during disease progression.

A key advantage of the systems explored here, CRISPRa and ZFAs, is their ability to restore *FXN* expression at physiological levels, thereby avoiding the toxicity associated with *FXN* overexpression. This feature provides a potential advantage over conventional gene therapy, which until now has been considered the best alternative and the only definitive treatment option for FA. However, several *in vivo* studies have highlighted a major limitation of gene therapy: toxicity linked to uncontrolled *FXN* expression. Because gene therapy relies on delivering exogenous *FXN* copies via viral vectors, it is not possible to precisely control the number of viral genomes that reach different tissues. Given that commonly used AAV serotypes, such as AAV9, show high tropism for the heart and liver, transgene accumulation is particularly pronounced in these organs. Importantly, excessive FXN amounts in heart and liver has been shown to be toxic (Belbellaa B et al., 2018; Huichalaf C et al., 2022). In summary, in this study we describe and validate two novel molecular strategies for

reactivating the endogenous *FXN* gene. From our comparative analysis of CRISPRa and ZFAs, we demonstrate that CRISPRa represents the most powerful and efficient approach to restore endogenous *FXN* expression, achieving robust and physiological reactivation levels across multiple disease-relevant neuronal cell types in the context of FA. While further studies are required to fully characterize the most effective ZFAs, particularly by assessing potential off-target effects and validating their efficiency across additional patient-derived cell lines, our findings demonstrate the feasibility of the *FXN* reactivation approach and lay the groundwork for future clinical translation.

Material and methods

Cell cultures

Fibroblasts culture

FA patients and healthy donor fibroblasts were obtained from the Franco Taroni's lab at the IRCCS Carlo Besta Neurological Institute. All human skin fibroblast (HSF) cultures were maintained in DMEM medium (Dulbecco's Modified Eagle's Medium-high glucose, Sigma-Aldrich) containing 10% fetal bovine serum (FBS, Sigma-Aldrich), 1% Pen/Strept, 2 mM glutamine (Sigma-Aldrich), 1% nonessential amino acids (MEM NEAA, ThermoFisher Scientific), 1% sodium pyruvate solution (Sigma-Aldrich). The cultures were kept in a humidified atmosphere of 5% CO2 at 37 °C under atmospheric oxygen conditions.

Induced pluripotent stem cells (iPSCs) culture

iPSCs used in this study were derived from patients and healthy donor human skin fibroblasts as previously described (Mazzara PG et al., 2020). They were maintained in feeder-free conditions in a mTeSR™1 (Stem Cell Technologies 85850) medium supplemented with 1% Penicillin-Streptomycin (Sigma-Aldrich P0781 Stock 10,000 units penicillin and 10 mg streptomycin/mL). Cells were fed daily and passaged in cell clumps weekly using Accutase solution (Sigma-Aldrich) in 6-well culture plates coated with Matrigel® hESC-Qualified Matrix, LDEV-free (Corning 354277).

iPSCs differentiation into neural progenitor cells (NPCs)

Neural progenitor cells (NPCs) were derived from iPSCs following previously described protocols with appropriate optimizations (Marchetto MC et al., 2010). In brief, iPSCs were enzymatically dissociated into small clusters using Accutase (Sigma-Aldrich) and transferred to low-adhesion plates in mTeSR1 medium supplemented with 0.5× N-2 supplement (ThermoFisher Scientific), 1% penicillin-streptomycin (Sigma-Aldrich), 0.5 µg/mL human Noggin (PeproTech), 5 µM SB-431542 (Sigma-Aldrich), and 10 µM ROCK inhibitor Y-27632. The medium was refreshed every three days. After 10 days, the resulting embryoid bodies were transferred to Matrigel-coated plates (1:100 dilution, growth factor-reduced Matrigel, Corning) and cultured in DMEM/F12 (Sigma-Aldrich) supplemented with 1× N-2 supplement, 1% non-essential amino acids (MEM NEAA, ThermoFisher Scientific), and 1% penicillin-streptomycin. The medium was changed every other day. On day 10 post-plating, neural rosettes were manually collected and dissociated using Accutase, and the resulting NPCs (passage 0) were seeded onto Matrigel-coated flasks in NPC expansion medium consisting of DMEM/F12, 0.5× N-2 supplement, 0.5× B-27 supplement (ThermoFisher Scientific), 1% penicillin-streptomycin, and 20 ng/mL basic fibroblast growth factor (bFGF, ThermoFisher Scientific). NPCs were passaged twice weekly using Accutase.

NPC differentiation into post-mitotic cortical neurons

On day 0, when neural progenitor cell (NPC) cultures reached approximately 90% confluency, the medium was replaced with differentiation medium. This medium consisted of NPC medium lacking bFGF and was supplemented with 10 µM SU5402, 8 µM PD0325901, and 10 µM DAPT (all from Sigma-Aldrich). Fresh differentiation medium was applied daily on days 1 and 2. On day 3, cells were enzymatically dissociated into a single-cell suspension using Accutase (Sigma-Aldrich) for 20 minutes at 37 °C. Following centrifugation and cell counting, the cells were seeded at a density of 55,000 cells/cm² onto plates or coverslips pre-coated with poly-L-lysine (PLL, 100 µg/mL), laminin (2 µg/mL), and fibronectin (2 µg/mL) (all from Sigma-Aldrich). Cells were cultured in neuronal maturation medium supplemented with 10 µM ROCK inhibitor Y-27632 for the first 24 hours. The neuronal maturation medium was composed of Neurobasal A (ThermoFisher Scientific) supplemented with 1× B-27, 2 mM glutamine, 1% penicillin-streptomycin, 20 ng/mL BDNF (PeproTech), 100 nM ascorbic acid (Sigma-Aldrich), 1 µg/µL laminin, 10 µM DAPT, and 250 µM dbcAMP (Selleckchem). On the following day, the medium was replaced to remove the ROCK inhibitor, and thereafter, half of the culture medium was refreshed twice weekly with fresh neuronal maturation medium (Banfi F et al., 2023).

NPC differentiation into post-mitotic sensory neurons

Sensory neurons were derived from neural progenitor cells (NPCs) following previously described protocols with appropriate optimizations (Mazzara PG et al., 2020). On day 0, when NPCs cultures reached approximately 90% confluency, the medium was replaced with differentiation medium. From day 1 to day 6, CHIR99021 3 µM (Miltenyi 130-103-926); SU5402 3 µM (Merck SML0443) and DAPT 10 µM (Merck D5942) were added. During these days KSR medium was gradually switched to N2 medium (Neurobasal medium (Thermo 21103049); N2 (Thermo 17502-048); pen/strep; NEAA, and L-Glutamine 2 mM). On day 7 cells were enzymatically dissociated into a single-cell suspension using Accutase (Sigma-Aldrich) for 10 minutes at 37 °C. Following centrifugation and cell counting, the cells were seeded at a density of 55,000 cells/cm² onto plates or coverslips pre-coated with poly-L-lysine (PLL, 100 µg/mL), laminin (2 µg/mL), and fibronectin (2 µg/mL) (all from Sigma-Aldrich). Cells were cultured in neuronal maturation medium supplemented with 10 µM ROCK inhibitor Y-27632 for the first 24 hours. The maturation medium was changed to 100% N2 medium plus recombinant human Brain Derived Neurotrophic Factor 10 ng/ml (BDNF Peprotech 450-02); Glial-Derived Neurotrophic Factor 10 ng/ml (GDNF Peprotech 450-10); Nerve Growth factor 10 ng/ml (NGF Merck N6009); Neurotrophin-3 10 ng/ml (NT-3 Peprotech 450-03) and Ascorbic Acid 200 µM (AA Merck 49752). Half of the medium was replaced with fresh medium every 72 h until samples were collected for analysis or for up to 90 days.

Primary cortical neurons culture

Primary cultures of mouse embryonic cortical neurons were prepared from embryonic day 17.5 (E17.5) embryos YG8sR pregnant females. Each embryo's brain was processed separately, and a skin biopsy was used for genotyping. Briefly, after dissection, corteces were enzymatically digested with 0.025% trypsin (Gibco) in Hank's balanced salt solution (HBSS; Euroclone) for 20 min at 37°C.Then HBSS with trypsin was removed, and the corteces were washed with plating medium (neurobasal medium [Gibco] supplemented with 2% B27, 3.3 mM glucose, 1% glutamine, and penicillin/streptomycin) and mechanically dissociated with a P1000 pipette to obtain a homogeneous cell suspension. Cells were then plated on plates coated with poly-L-lysine (PLL; 0.1 mg/mL) and coverslips.

sgRNAs design and annealing

Sequences of the sgRNAs (see supplementary table 1) were designed using CRISPOR online tool (http://crispor.tefor.net/) and selected for predicted specificity score and on-target activity. The annealing process of the sgRNAs was performed by using 1µl of each Forward and Reverse primers (100µM), 1 µl of T4 PNK buffer 10X (NEB), 0.5 µl of T4 PNK (NEB M0201S) and 6.5 µl of ddH2O to reach a final volume of 10 µl. The phosphorylation and annealing process was done using the following thermocycler program: 30' at 37°C, 5' at 95°C, ramp with temperature decreasing 0.1°C/s and 1' at 25°C.

Vectors cloning

The annealed sgRNAs were cloned using BsmBI restriction enzyme into U6-filler-sgRNA scaffold cassette, originating from LentiCRISPR (Addgene #52961). This cassette was placed in a lentiviral backbone carrying blasticidin antibiotic resistance, under the control of Ef1a core promoter.
Ef1alpha-dCas9VP160-T2A-PuroR was generated from pAC94-pmax-dCas9VP160-2A-PuroR (Addgene plasmid 48226). The dCas9VP160-2A-PuroR cassette was cut with AgeI and inserted into the TetO-FUW vector digested with AgeI.
ZF-VP64 targeting *FXN* gene promoter were designed and selected according to specificity parameters by Merck company, who sent us pUC plasmids containing V5-NLS-ZF-VP64 sequences. These sequences were amplified by PCR and inserted into the Ef1alpha-GFP lentiviral vector through MluI and SalI digestion, to generate the lentiviral vector Ef1alpha-V5-NLS-ZF-VP64. Ef1alpha-V5-NLS-ZF-VP160 constructs were obtained by transferring the V5-NLS-ZF sequences into the Ef1alpha-dCas9-VP160-puro through BamHI digestion.

The construct Ef1alpha-V5-NLS-ZF145-VP64-NLS-FUS was obtained cloning the FUS domain, amplified by PCR from the pcDNA3.1-GFP-FUS plasmid (Addgene #183236), in the vector Ef1alpha-V5-NLS-ZF145-VP64 without stop codon, through SalI and EcorV digestion.

Lentiviral vectors production

Replication-deficient lentiviral vectors were generated using the HEK293 (Human Embryonic Kidney 293T) packaging cell line. A total of 7.5 million cells were plated on 150-mm dishes in Dulbecco's Modified Eagle Medium (DMEM) high glucose (Sigma-Aldrich) supplemented with 10% fetal bovine serum (FBS), 1% sodium pyruvate, 1% glutamine, and 1% penicillin-streptomycin (all from Sigma-Aldrich). Cells were allowed to adhere overnight before transfection. Approximately 2–3 hours prior to transfection, the culture medium was replaced with Iscove's Modified Eagle Medium (IMDM) containing 10% FBS, 1% non-essential amino acids (Gibco), 1% sodium pyruvate, 1% glutamine, and 1% penicillin-streptomycin, to synchronize the cell cycle. Transfection was performed using the calcium phosphate method with four plasmids: pREV encoding the lentiviral rev gene; pVSV-G encoding the viral surface glycoprotein responsible for vector tropism; pMDL encoding the viral gag and pol genes (capsid and polymerase proteins); and a transfer plasmid carrying the transgene of interest flanked by viral long terminal repeats (LTRs) that serve as the viral genome. For each 150-mm dish, a transfection mix was prepared by combining 1125 µL sterile water (S.A.L.F.) with 6.25 µg pREV, 9 µg pVSV-G, 12.5 µg pMDL, and 32 µg of the transfer plasmid. Subsequently, 125 µL of 2.5 M CaCl2 was added, and after 5 minutes of incubation, 1250 µL of HEPES-buffered saline (HBS: 0.285 M NaCl, 1.5 mM Na2HPO4, 1 M HEPES, pH 7.12) was added dropwise while vortexing gently. The mixture was then incubated at room temperature for 15 minutes before being added to the cells. Following overnight incubation at 37 °C with 5% CO2 and 20% O2, the medium was replaced with fresh IMDM. After 30 hours, the supernatant containing viral particles was collected, filtered through a 0.22 µm Stericup filter (Corning), and aliquoted into ultracentrifuge tubes (Beckman). Viral particles were concentrated by centrifugation at 20,000 rpm for 2 hours, after which the supernatant was carefully removed. The dry pellets were then resuspended in 80 µl of PBS, shook at 4°C for 30 minutes and stored at -80°C until use. Lentiviral titration was performed with Lentiviral qPCR Titration Kit (Abm LV900).

RNA extraction and quantitative real-time PCR (RT-qPCR)

Total RNA was extracted using the NucleoZOL reagent (Macherey-Nagel) following the manufacturer's instructions. Cells were prepared at a concentration of 5×10^6 cells/mL and lysed in 500 µL of NucleoZOL. The mixture was incubated for 5 minutes at room temperature to ensure complete dissociation of nucleoprotein complexes. Following lysis, 200 µL of nuclease-free water

(ddH_2O) was added, and the samples were vortexed vigorously for 15 seconds. The mixture was then incubated for an additional 5 minutes at room temperature, followed by centrifugation at 12,000 × g for 15 minutes. Subsequently, 500 µL of the resulting supernatant was transferred to a new tube and mixed with 500 µL of isopropanol. The samples were centrifuged again at 12,000 × g for 5 minutes at room temperature to precipitate the RNA. After discarding the supernatant, the RNA pellet was washed with 150 µL of 75% ethanol, followed by centrifugation at 8,000 × g for 5 minutes. The supernatant was then carefully removed, and the RNA pellet was air-dried before being resuspended in RNase-free water. The purified RNA was stored at −80°C until further use.

For qPCR, cDNA synthesis was obtained by reverse transcription of 1 µg RNA using the ImProm-II Reverse Transcription System (Promega), according to manufacturer's instructions. qPCR was performed in duplicate with custom-designed oligos using Titan HotTaq EvaGreen qPCR Mix 5x (BIOATLAS) in a final volume of 20 µl, 2 µl of cDNA, 9.8 µl of H2O, 3.2 µl of Titan Master Mix and 1 µl of a solution containing forward and reverse primers (5 µM). At the end of the reaction, the threshold cycle values recorded were visualized using the software "CFX Manager software" (Biorad). The analysis of the expression of the gene of interest was carried out by normalizing the values of the measured threshold cycles (Ct) on 18S ribosomal RNA gene. Once the value of ΔCt (Ct, FXN - Ct, 18S) was calculated, the fold change value (2(-ΔΔCt)) of the expression of *FXN* was determined with respect to the control (ΔΔCt = ΔCt, sample - ΔCt, control). RT-qPCR primers are listed in supplementary table 3.

RNA-sequencing and off-target genes analysis

RNA libraries were generated starting from 1 µg of total RNA extracted using NucleoZOL (Machery-Nagel). RNA quality was assessed by using a Tape Station instrument (Agilent). To avoid over-representation of 3'ends, only high-quality RNA with a RNA Integrity Number (RIN) ≥ 9 was used. RNA was processed according to the TruSeq Stranded mRNA Library Prep Kit protocol. The libraries were sequenced on an Illumina HiSeq 3000 with 150bp paired-end reads using Illumina TruSeq technology. Image processing and basecall was performed using the Illumina Real Time Analysis Software. Raw paired-end reads were quality checked with FastQC and trimmed by Trimmomatic 0.39 to remove adapters and trim low-quality bases, ensuring high-quality reads for downstream analysis. The trimmed reads were aligned to the human reference genome GRCh38/hg38 using STAR 2.5.3a. Gene-level quantification was performed using featureCounts v1.6.4 against the Gencode v31 basic annotation. Following alignment and quantification, downstream analyses were carried out in R. Differential gene expression analysis was conducted using DESeq2, which normalized the read counts and identified differentially expressed genes (DEGs). Genes with an absolute log2 fold change > 1 and an adjusted p-value < 0.05 were considered significant. Results were visualized through volcano plots to highlight DEGs across the different comparisons.

Exploratory data analysis included a Principal Component Analysis (PCA), performed on the 500 most highly variable genes to assess sample clustering and variability. Additional statistical visualizations, such as heatmaps and other graphical outputs, were generated in R.
Potential off-target genes targeted by the sgRNA sgP2 were identified through the online CRISPOR software (http://crispor.tefor.net). The predicted off-target genes are listed in the supplementary table 5.

Western blot

Fibroblasts, NPCs, neurons, and murine tissues were homogenized in RIPA buffer (50 mM Tris pH 7.5, 150 mM NaCl, 1 mM EDTA, SDS (0.1% for cells, 1% for tissues), 1% Triton X-100, Roche Complete EDTA-free Protease Inhibitor Cocktail, and Roche PhosSTOP EASYpack). Proteins were separated by SDS-PAGE (Sodium Dodecyl Sulphate – PolyAcrylamide Gel Electrophoresis), then incubated with primary antibodies overnight at 4 °C in a blocking solution containing 5% non-fat dry milk in PBS-Tween 0.1% (Sigma-Aldrich), as specified in the corresponding antibody datasheets (see supplementary table 4 for the full list of primary antibodies and their working dilutions). Band densitometry, relative to control samples, was quantified using Fiji software (v1.48i, NIH, USA) and normalized to the indicated housekeeping proteins in each Figure (β-ACTIN, S6 and CALNEXIN).

Immunostaining

Cells were fixed with ice-cold 4% paraformaldehyde (PFA) for 30 minutes at 4 °C, then washed three times with PBS. They were subsequently incubated at room temperature for 1 hour in a blocking solution containing 10% donkey serum (to prevent nonspecific binding) and 0.1% Triton X-100 to permeabilize the cell membrane. Following this, cells were incubated overnight at 4 °C with the primary antibodies. After three PBS washes, cells were incubated for 1 hour at room temperature in blocking solution containing DAPI (1:1000, Sigma-Aldrich) and Alexa Fluor-488, Alexa Fluor 647 or Alexa Fluor-546-conjugated anti-rabbit or anti-mouse secondary antibodies (1:1000, ThermoFisher Scientific). After another series of PBS washes (3×), cells were mounted using fluorescent mounting medium (Dako). Imaging was performed using a Nikon Eclipse 600 fluorescence microscope and Olympus FluoVIEW FV3000RS Confocal. See supplementary table 4 for the full list of primary antibodies and their working dilutions.

Reactive Oxygen Species (ROS) detection by DCF assay

Intracellular reactive oxygen species (ROS) levels were measured using the 2′,7′-dichlorofluorescin diacetate (DCFDA or H_2DCFDA) assay (Sigma-Aldrich), a cell-permeant fluorogenic dye that is oxidized to fluorescent 2′,7′-dichlorofluorescein (DCF) upon reaction with ROS. iPSCs-derived cortical neurons were seeded on PLL-coated glass coverslips in 24-well plates at an appropriate density to reach ~80% confluency at the time of the assay. On the day of the experiment, cells were washed once with pre-warmed phosphate-buffered saline (PBS) and incubated with 10 µM H_2DCFDA 20 minutes at 37 °C in the dark. To specifically label neuronal cell bodies and protrusions, cells were co-incubated with an anti-CD56 antibody conjugated to Alexa Fluor 647 (BD biosciences No 557711) for 20 minutes at 37 °C in the dark. After incubation, cells were gently washed with PBS to remove unbound antibody and excess dye. Finally, cells were incubated in fresh medium prior microscope live-imaging. Imaging was performed using a Nikon Eclipse 600 fluorescence microscope.

Quantification of intracellular ROS levels by DCF fluorescence

Intracellular ROS levels were quantified in neuronal cultures using DCF fluorescence imaging. Acquired images were analyzed using ImageJ software (NIH). Individual cells were identified based on nuclear staining using the Hoechst signal. Regions of interest (ROIs) corresponding to single cells were defined using the Hoechst channel, and these ROIs were then applied to the DCF fluorescence channel (546 nm) to measure fluorescence intensity, which is proportional to intracellular ROS levels. Background fluorescence was determined from cell-free regions and subtracted from all measurements. A fluorescence intensity threshold was subsequently applied to exclude background and nonspecific signal. The resulting background-corrected DCF fluorescence intensity for each individual cell was extracted and used for quantitative analysis. Single-cell DCF intensity values were plotted and analyzed to compare ROS levels between experimental conditions.

Zinc-fingers activators (ZFAs) design

Zinc-fingers activators (ZFAs) were designed by Merck company (Product Name: CompoZr™ Knockout Zinc Finger Nucleases). They identified the possible 18-bp sequences targetable by ZFAs on the *FXN* promoter region that we selected. ZFAs target sites were designed using an *in silico* design pipeline based on the reference genome sequence. An initial pool of candidate ZFAs target sequences was generated and subsequently subjected to genome-wide off-target analysis to assess binding specificity. Off-target searches were performed by aligning each candidate target sequence against the genome to identify potential off-target sites with up to three nucleotide mismatches. Designs exhibiting an excessive number of predicted off-target sites with ≤3 mismatches were

excluded from further analysis. Off-target burden was quantified by calculating the sum of mismatch scores across all identified off-target alignments for each candidate.

To avoid functional interference between ZFAs, additional positional constraints were applied, requiring that selected target regions did not overlap within the genomic locus of interest. Candidates failing to meet this non-overlapping criterion were removed.

Following this filtering process, nine ZFAs designs were retained for downstream experimental validation. Five of these designed ZFAs were employed in the present work. The target sequences of the selected ZFAs are listed in supplementary table 2. Supplementary information regarding the technical parameters used for ZFAs selection and the bioinformatic prediction of the off-target sites are available at the following link: https://drive.google.com/drive/folders/1W-sHI5A0njPZcqB88wnhxPpD7kybB_cG?usp=drive_link .

Statistical analysis

All data are represented as the mean calculated between different experiments and the variation between experiments is depicted as the mean ± standard error (SEM). For each experiment, “n” indicates the number of independent experiments. Analyses of significant differences between means were performed using Student’s t-test, one-way or two-ways ANOVA, depending on the number of groups and variables in each experiment. Data were then submitted to Tukey’s or Dunnett’s post hoc test using GraphPad Prism software. The null hypothesis was rejected when $P < 0.05$. In the graphs, “ns” indicates nonsignificant differences when $P > 0.05$, * indicates significant differences with $P < 0.05$, ** indicates significant differences with $P < 0.01$, *** indicates significant differences with $P < 0.001$ and **** indicates significant differences with $P < 0.0001$.

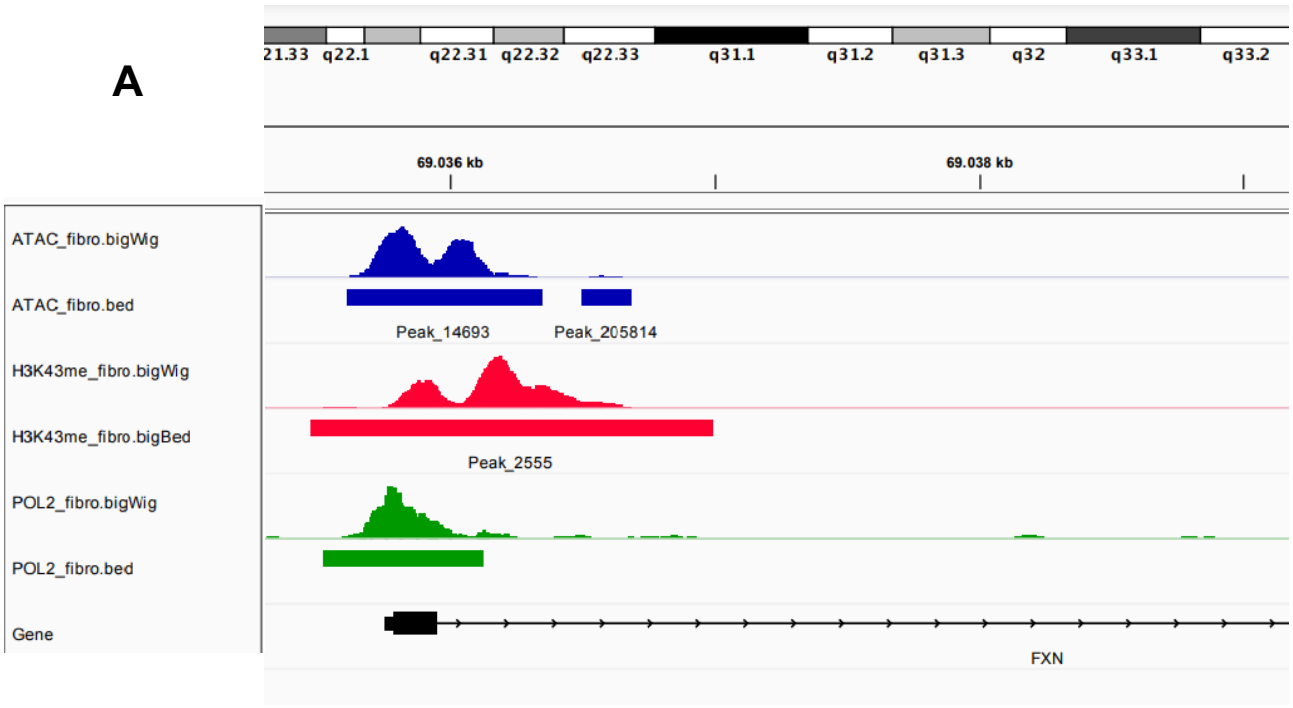

Figure S1. *FXN* gene chromatin accessibility analysis. A. Map of the most accessible chromatin regions within the *FXN* gene, based on integrated analysis of publicly available datasets on Pol II gene promoter occupancy, H3K4me3 enrichment, and ATAC-seq profiles from primary fibroblasts. The region adjacent to the transcription start site is identified as the most promising target for molecular interventions, owing to its relatively open chromatin conformation.

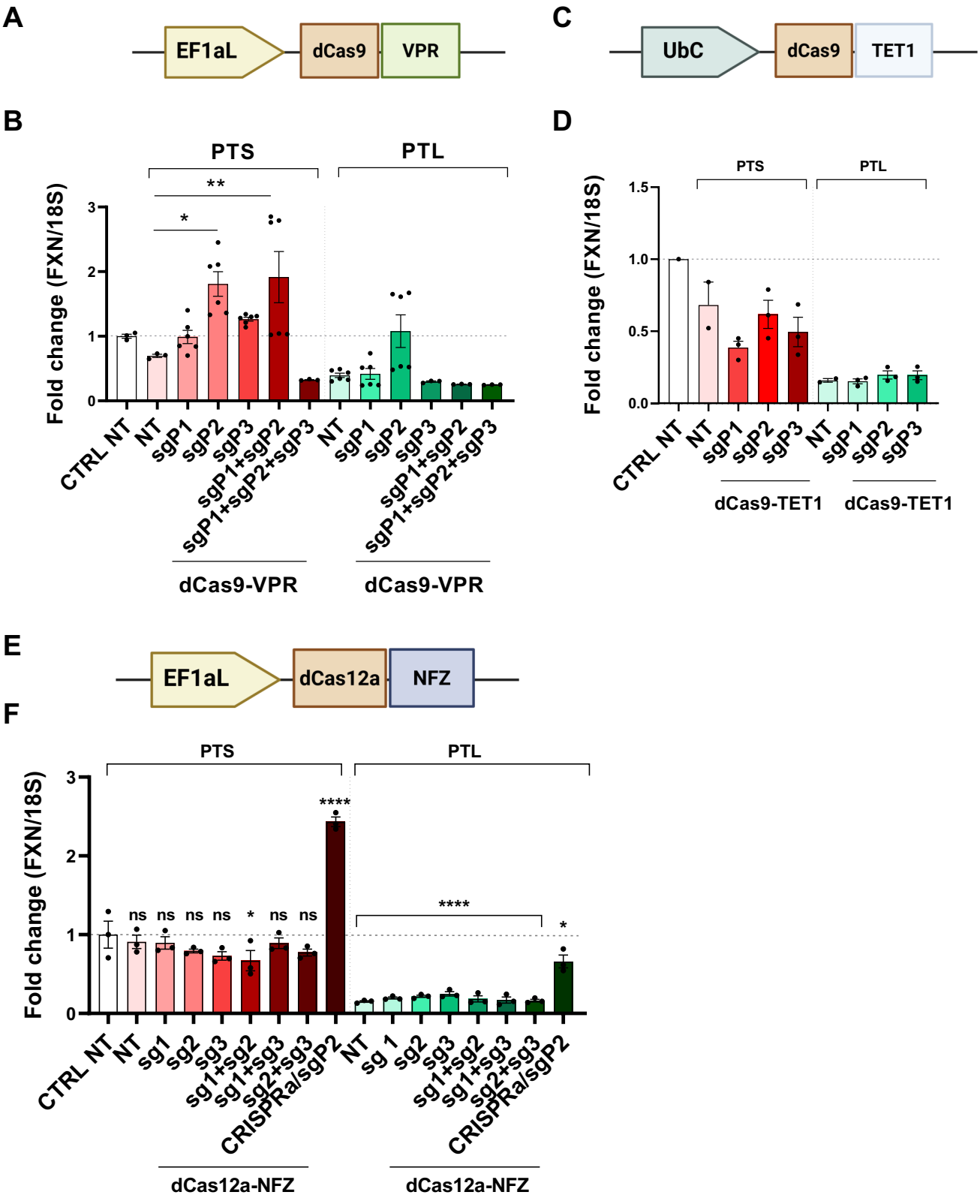
A
EF1aL
dCas9
VPR
C
UbC
dCas9
TET1
B
PTS
PTL
Fold change (FXN/18S)
CTRL NT
NT
sgP1
sgP2
sgP3
sgP1+sgP2
sgP1+sgP2+sgP3
dCas9-VPR
D
dCas9-TET1
E
EF1aL
dCas12a
NFZ
F
sg1
sg2
sg3
sg1+sg2
sg1+sg3
sg2+sg3
CRISPRa/sgP2
dCas12a-NFZ

Figure S2. Test of alternative epigene**tic regulators for FXN reactivation. A.** Schematic illustration of the lentiviral construct coding for dCas9 fused with the activation domain VPR, under the control of the EF1a promoter. **B**. *FXN* gene expression levels relative to 18S, normalized to the untreated healthy control (white), in primary fibroblasts from the healthy control (CTRL), the milder patient PTS and the more severe patient PTL treated with dCas9-VPR in combination with individual or pooled sgRNAs (sgP1, sgP2 and sgP3) to screen for the most effective ones. **C**. Schematic illustration of the lentiviral construct coding for dCas9 fused with the demethylating domain TET1, under the control of the UbC promoter. **D**. *FXN* gene expression levels relative to 18S, normalized to the untreated healthy control (white), in primary fibroblasts from the healthy control (CTRL), the milder patient PTS and the mosre severe patient PTL treated with dCas9-TET1 in combination with individual sgRNAs (sgP1, sgP2 and sgP3) to screen for the most effective ones. **E**. Schematic illustration of the lentiviral construct coding for dCas12a fused with the activation domain NFZ, under the control of the EF1a promoter. **F**. *FXN* gene expression levels relative to 18S, normalized to the untreated healthy control (white), in primary fibroblasts from the healthy control (CTRL), the milder patient PTS and the more severe patient PTL treated with dCas12a-NFZ in combination with individual or pooled sgRNAs (sg1, sg2 and sg3) to screen for the most effective ones. The condition with CRISPRa/sgP2 was used as positive control of FXN reactivation. **B, D, F**. Statistical analysis One-way ANOVA, with multiple comparison analysis by Dunnett's test. * p<0,05. ** p<0,02. **** p<0,0001. ns: not significant. All data are mean±SEM. All data are mean±SEM. Statistical analyses were conducted by comparing all experimental groups with one another. In figure S2F the statistical significance is referred to the untreated healthy control (white).

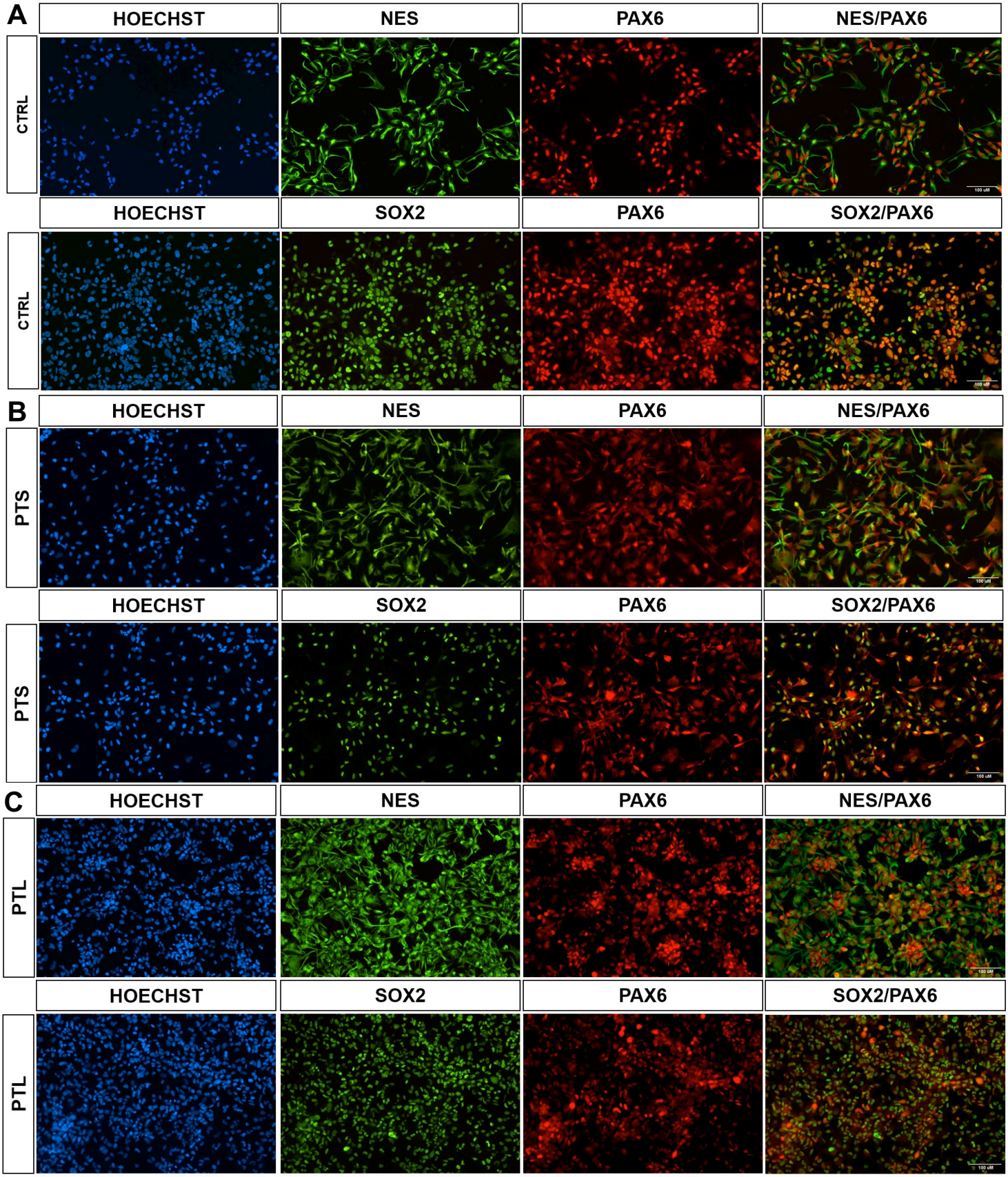

Figure S3. Characterization of iPSCs-derived NPCs and neurons from healthy control, PTS and PTL patients. A-C. Immunofluorescence on iPSCs-derived NPCs from healthy control, PTS and PTL patients stained for NESTIN, SOX2 (green) and PAX6 (red) markers. Scale bar 100 um.

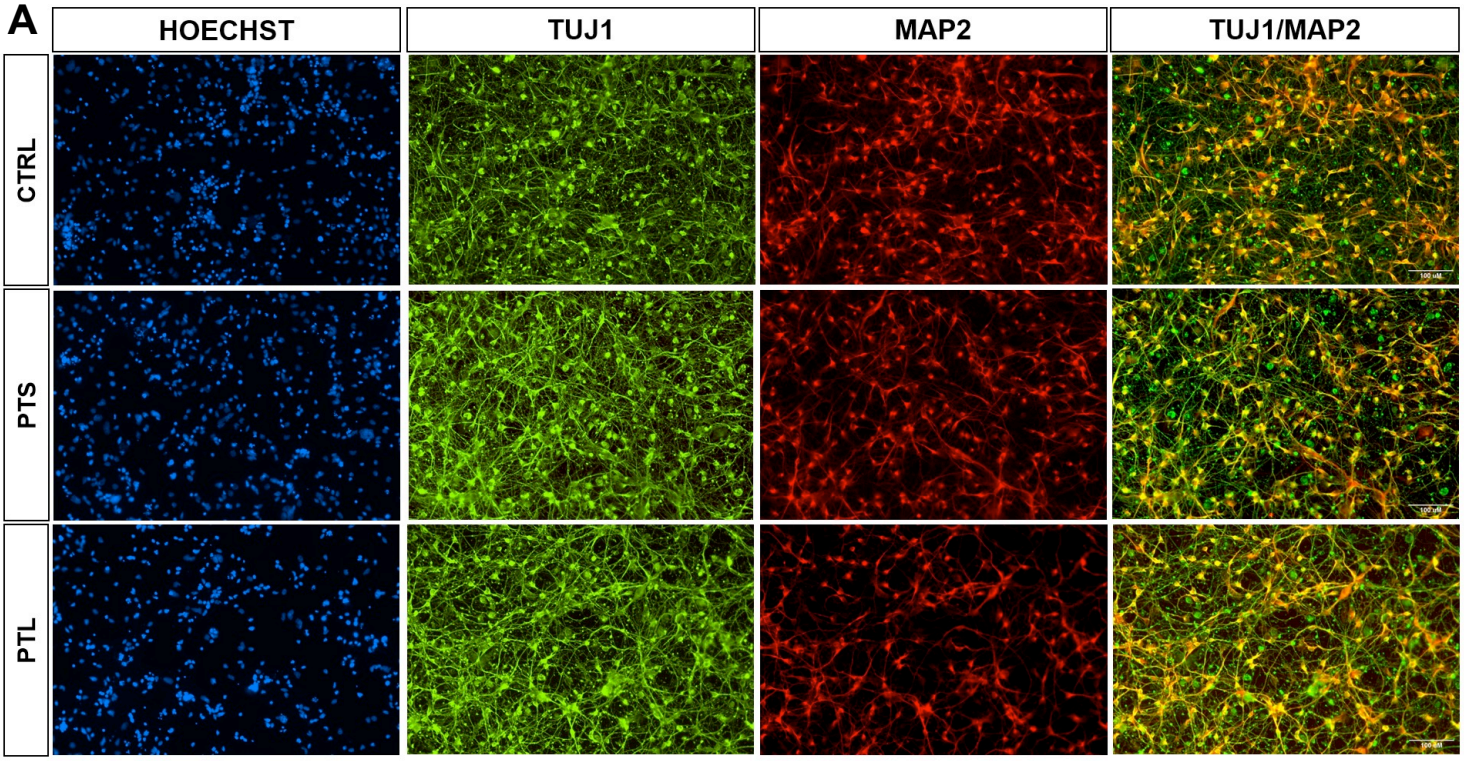

Figure S4. Characterization of iPSCs-derived cortical neurons from healthy control, PTS and PTL patients. A. Immunofluorescence on iPSCs-derived cortical neurons at DIV40 from healthy control, PTS and PTL patients stained for TUBULIN β3 (green) and MAP2 (red) markers. Scale bar 100 um.

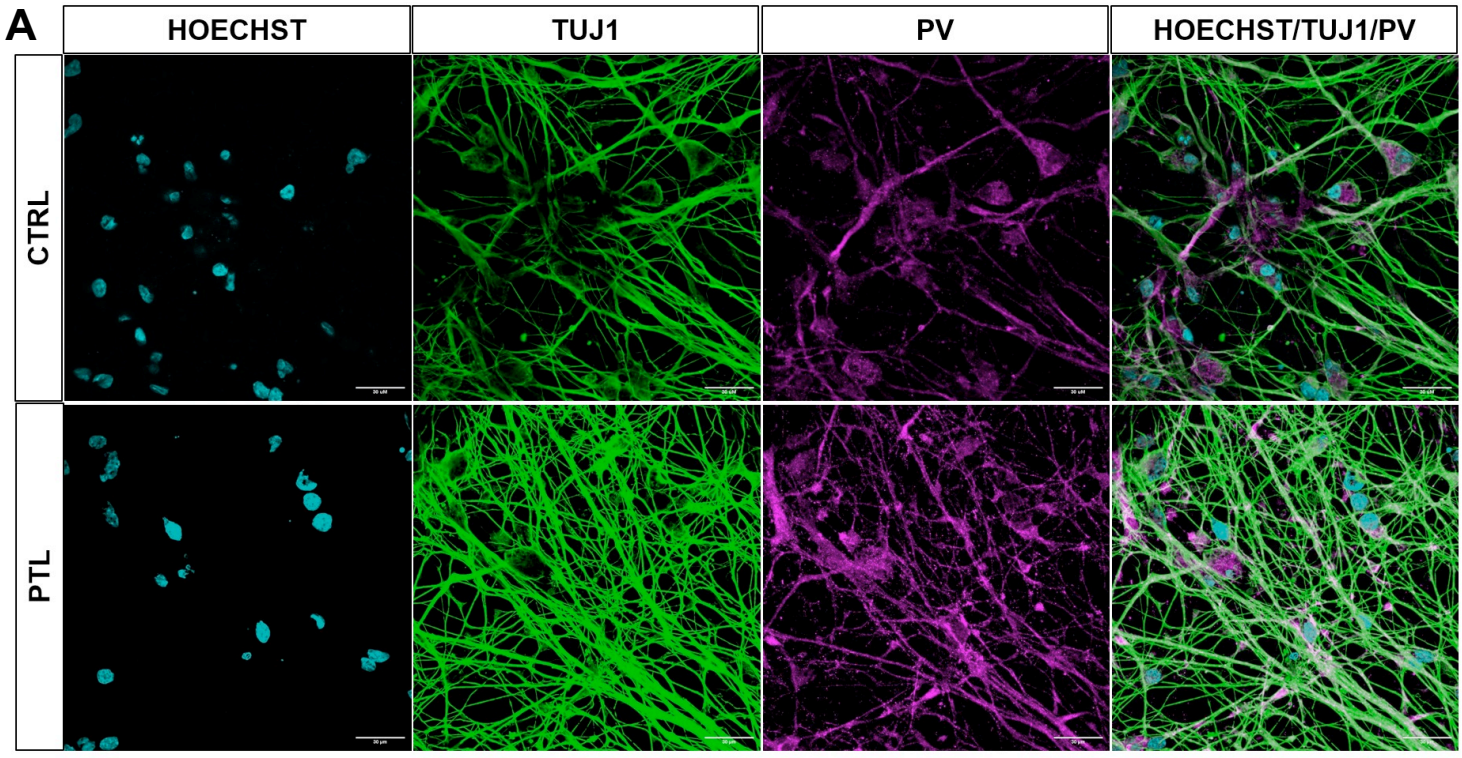

Figure S5. Characterization of iPSCs-derived sensory neurons from healthy control and PTL patient. A. Immunofluorescence on iPSCs-derived sensory neurons at DIV40 from healthy control and PTL patient stained for TUBULIN β3 (green) and PARVALBUMIN (purple) markers. Scale bar 30 um.

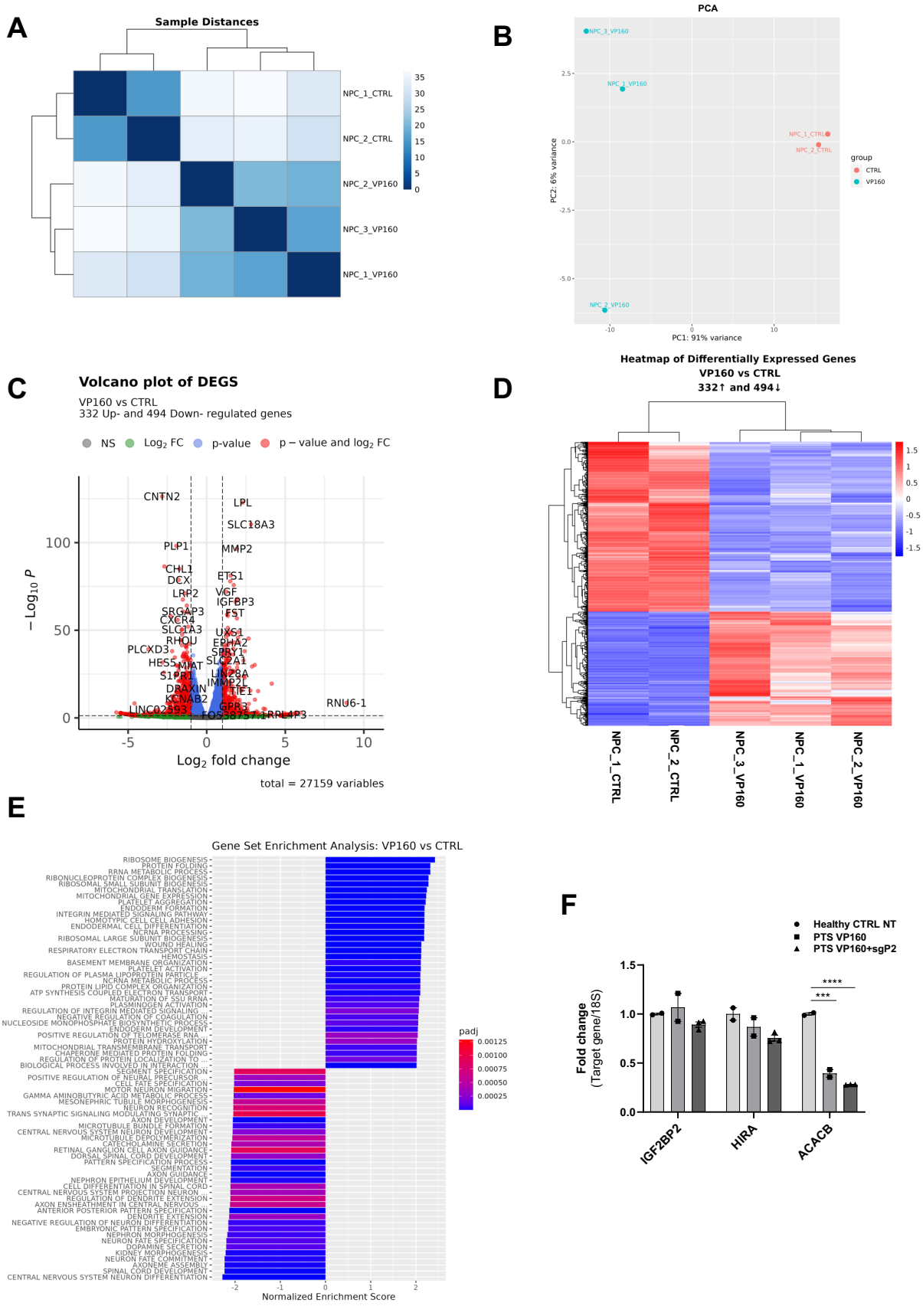
A
Sample Distances
NPC_1_CTRL
NPC_2_CTRL
NPC_2_VP160
NPC_3_VP160
NPC_1_VP160
35
30
25
20
15
10
5
0
B
PCA
NPC_3_VP160
NPC_1_VP160
NPC_1_CTRL
NPC_2_CTRL
NPC_2_VP160
group
CTRL
VP160
PC2: 6% variance
PC1: 91% variance
C
Volcano plot of DEGS
VP160 vs CTRL
332 Up- and 494 Down- regulated genes
NS
Log2 FC
p-value
p – value and log2 FC
CNTN2
LPL
SLC18A3
PLP1
MMP2
CHL1
DCX
ETS1
LRP2
VGF
IGFBP3
SRGAP3
FST
CXCR4
SLC1A3
UXS1
RHOU
EPHA2
PLCXD3
SPRY1
HES5
SLC2A1
MIAT
S1PR1
LINC02693
RNU6-1
Log2 fold change
−Log10 P
total = 27159 variables
D
Heatmap of Differentially Expressed Genes
VP160 vs CTRL
332↑ and 494↓
NPC_1_CTRL
NPC_2_CTRL
NPC_3_VP160
NPC_1_VP160
NPC_2_VP160
E
Gene Set Enrichment Analysis: VP160 vs CTRL
Pathway
padj
Normalized Enrichment Score
F
Healthy CTRL NT
PTS VP160
PTS VP160+sgP2
Fold change
(Target gene/18S)
IGF2BP2
HIRA
ACACB
****
***

Figure S6. RNA sequencing on PTS patient NPCs for transcriptomic analysis. A. Correlation Heatmap showing absolute distances (Pearson R2−1) between transcriptomes of PTS patient NPCs either untreated (NPC CTRL) or transduced with dCas9-VP160 and sgP2 (NPC VP160). The distance between samples is also shown as an unsupervised hierarchical clustered dendrogram on the sides. **B**. Samples transcriptome clustering using the principal component analysis (PCA). **C**. Volcano plot showing differential gene expression between the two groups. Each point represents a gene, with the x-axis showing the log2 fold change (log2FC) between conditions and the y-axis showing the -log10 adjusted p-value (FDR). Genes significantly upregulated are highlighted in red, while significantly downregulated genes are highlighted in blue. Non-significant genes are shown in gray. **D**. Heatmap of differentially expressed genes (DEGs) across all samples, with rows representing genes and columns representing individual samples. Expression values are shown as normalized and scaled counts. Genes and samples are hierarchically clustered based on expression patterns to reveal groups with similar profiles. **E**. Gene set enrichment (GSEA) analysis performed on transcriptomic data from NPCs expressing VP160 compared with control cells. The bar plot displays significantly enriched Gene Ontology biological process pathways ranked by normalized enrichment score (NES), with positive NES values indicating pathways enriched in VP160-treated samples and negative NES values indicating pathways enriched in control samples. Enriched pathways include processes related to ribosome biogenesis, mitochondrial function, and protein metabolism, as well as pathways associated with neural commitment, neuronal differentiation, and neurodevelopment. Bar color represents the adjusted p value (padj), as indicated by the color scale. **F**. RNA-seq data validation by qPCR of three predicted off-target genes. Target gene expression levels relative to 18S, normalized to the untreated healthy control (light grey). Statistical analysis Two-way ANOVA, with multiple comparison analysis by Tukey's test. *** p<0,001. **** p<0,0001. All data are mean±SEM. Statistical analyses were conducted by comparing all experimental groups with one another.

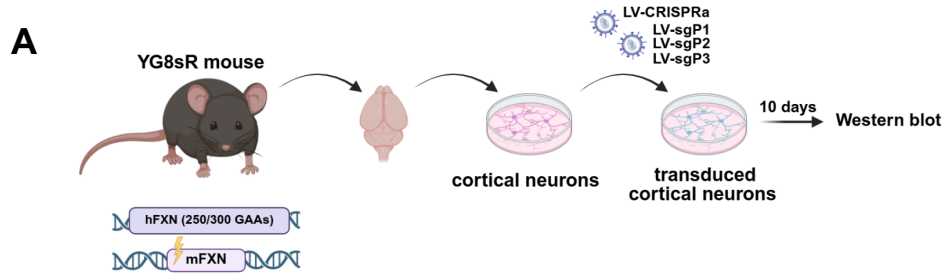
A
YG8sR mouse
LV-CRISPRa
LV-sgP1
LV-sgP2
LV-sgP3
cortical neurons
transduced cortical neurons
10 days
Western blot
hFXN (250/300 GAAs)
mFXN

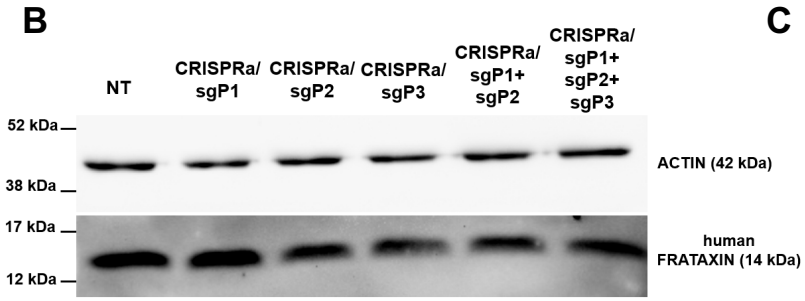
B
NT
CRISPRa/ sgP1
CRISPRa/ sgP2
CRISPRa/ sgP3
CRISPRa/ sgP1+ sgP2
CRISPRa/ sgP1+ sgP2+ sgP3
52 kDa
38 kDa
17 kDa
12 kDa
ACTIN (42 kDa)
human FRATAXIN (14 kDa)

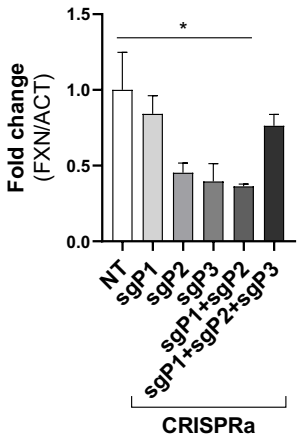
C
Fold change (FXN/ACT)
1.5
1.0
0.5
0.0
*
NT
sgP1
sgP2
sgP3
sgP1+sgP2
sgP1+sgP2+sgP3
CRISPRa

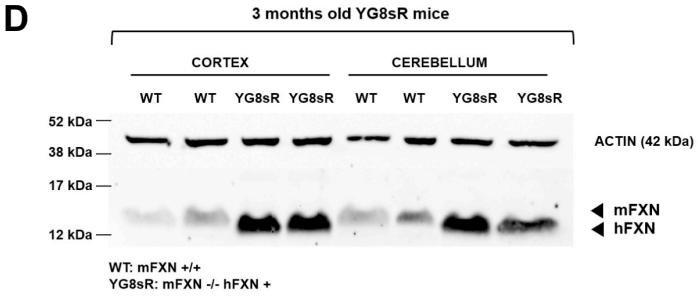
D
3 months old YG8sR mice
CORTEX
CEREBELLUM
WT
WT
YG8sR
YG8sR
WT
WT
YG8sR
YG8sR
52 kDa
38 kDa
17 kDa
12 kDa
ACTIN (42 kDa)
mFXN
hFXN
WT: mFXN +/+
YG8sR: mFXN -/- hFXN +

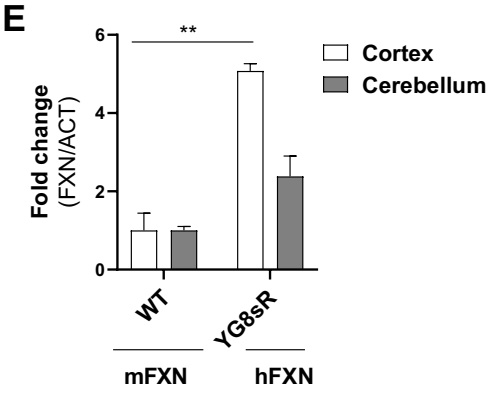
E
Fold change (FXN/ACT)
6
4
2
0
**
Cortex
Cerebellum
WT
YG8sR
mFXN
hFXN

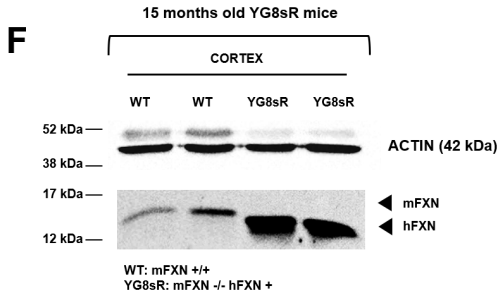
F
15 months old YG8sR mice
CORTEX
WT
WT
YG8sR
YG8sR
52 kDa
38 kDa
17 kDa
12 kDa
ACTIN (42 kDa)
mFXN
hFXN
WT: mFXN +/+
YG8sR: mFXN -/- hFXN +

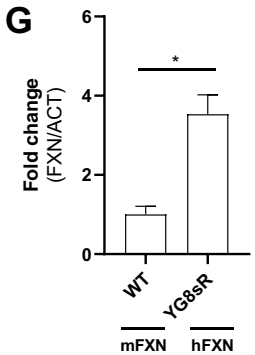
G
Fold change (FXN/ACT)
6
4
2
0
*
WT
YG8sR
mFXN
hFXN

Figure S7. *In vivo* testing of the CRISPRa system. A. Schematic overview of the experimental workflow. YG8sR mice, carrying a human *FXN* (hFXN) transgene with 250/300 GAA repeats on a YAC and lacking the endogenous murine FXN (mFXN), underwent brain dissection to isolate cortical primary neurons. These neurons were transduced with lentiviral vectors encoding dCas9-VP160 and the sgRNAs sgP1, sgP2, and sgP3. Ten days post-transduction, hFXN protein levels were evaluated by Western blot. **B**. Western blot analysis of hFXN protein in YG8sR-derived cortical neurons untreated or treated with lentiviruses carrying dCas9-VP160 and sgP1, sgP2 and sgP3 sgRNAs. B-ACTIN was used as loading control for hFXN protein amounts. **C**. Western blot densitometric quantification of hFXN protein levels in YG8sR-derived cortical neurons untreated or treated with lentiviruses carrying dCas9-VP160 and sgP1, sgP2 and sgP3 sgRNAs, by ImageJ software. Statistical analysis by One-way ANOVA, with multiple comparison analysis by Dunnett's test. * p<0,05. All data are mean±SEM. **D.** Western blot analysis of hFXN or mFXN protein in brain and cerebellum tissues from three months old wild-type (mFXN +/+) and YG8sR (h*FXN* +mFXN -/-) mice. B-ACTIN was used as loading control. **E**. Western blot densitometric quantification of hFXN or mFXN protein in brain (white) and cerebellum (grey) tissues from three months old wild-type (mFXN +/+) and YG8sR (h*FXN* +mFXN -/-) mice, by ImageJ software. Statistical analysis Two-way ANOVA, with multiple comparison analysis by Tukey's test. ** p<0,02. All data are mean±SEM. **F.** Western blot analysis of hFXN or mFXN protein in brain tissues from fifteen months old wild-type (mFXN +/+) and YG8sR (h*FXN* +mFXN -/-) mice. B-ACTIN was used as loading control. **G**. Western blot densitometric quantification of hFXN or mFXN protein in brain tissues from fifteen months old wild-type (mFXN +/+) and YG8sR (h*FXN* +mFXN -/-) mice, by ImageJ software. Statistical analysis by paired t-test. n=4. * p<0,05. All data are mean±SEM. All data are mean±SEM. Statistical analyses were conducted by comparing all experimental groups with one another.

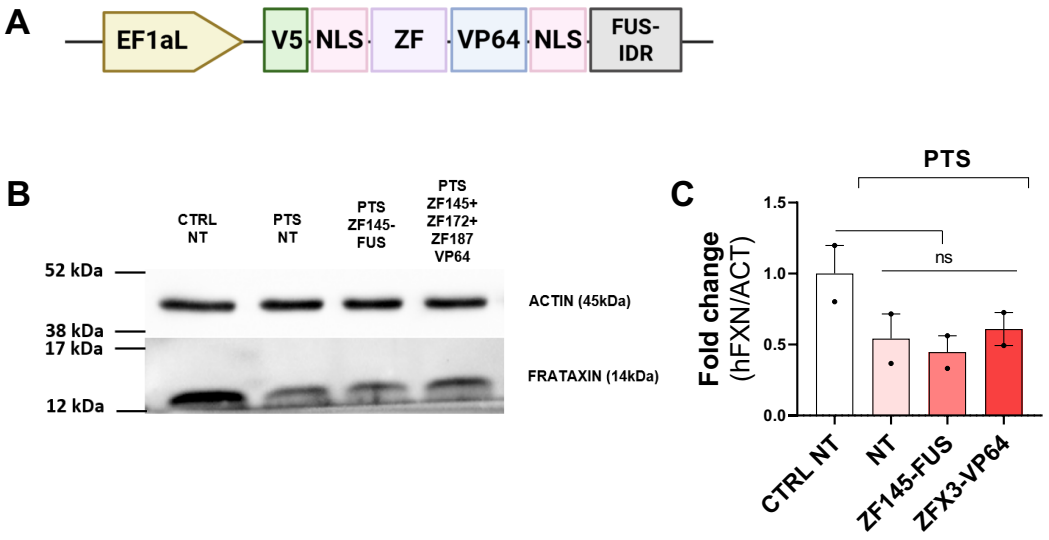

Figure S8. Test of an alternative activation domain FUS-IDR fused to ZF145-VP64. A. Schematic illustration of the lentiviral construct coding for ZF145 fused with the two activation domains VP64 and FUS-IDR, under the control of the EF1a promoter. **B**. Western blot analysis of FXN protein in healthy control and PTS-derived primary fibroblasts transduced with either ZF145-VP64-FUS or the combination of ZF145, ZF172 and ZF187-VP64. B-ACTIN was used as loading control. **C**. Western blot densitometric quantification of FXN protein levels in healthy control and PTS-derived primary fibroblasts transduced with either ZF145-VP64-FUS or the combination of ZF145, ZF172 and ZF187-VP64, by ImageJ software. Statistical analysis by One-way ANOVA, with multiple comparison analysis by Dunnett's test. ns: not significant. All data are mean±SEM. All data are mean±SEM. Statistical analyses were conducted by comparing all experimental groups with the healthy control (white).

Supplementary table 1: sgRNAs sequences

sgRNA	sequence (5'-3')
sgP1 (dCas9) - FW	CACCAGGCTGCAGTCTCCCT TGG
sgP2 (dCas9) - FW	TGCACGAATAGTGCTAAGCT GGG
sgP3 (dCas9) - FW	AGAAGAGTGCCTGCGGCCAG TGG
sg1 (dCas12a) - RV	TTTG TGCAAAGCACGGAGTGCAACCAG
sg2 (dCas12a) - FW	TTTG TTAAATGCACGAATAGTGCTAAG
sg3 (dCas12a) - RV	TTTA ACAAAAATGGAGAGCCTGCTTTG

Supplementary table 2: Zinc fingers activators (ZFAs) binding sites sequences

ZFA	Binding site sequence
ZFA84	GGGGTCGCCGCAGCACCC
ZFA145	TTGGCCGCCGGTATGGGT
ZFA168	GCAACCAGGACCCCTGAC
ZFA172	GCAAAGCACGGAGTGCAA
ZFA187	GGTGGCCACTGGCCGCAG

Supplementary table 3: RT-qPCR primers

Gene	FW primer (5'-3')	RV primer (5'-3')
FXN	AATCTGGAACTTTGGGCCAC	AACGTGTATGGCTTGTCTGC
18s	GAAATTCTTGGACCGGC	GACTTTGGTTTCCGCGAAGC
HIRA	CACAGCCGTCATTGAGAACC	CATCTGCTGTCCGAGTCTCA
IGF2BP2	CACTTCTCAGGCCAGACAGA	TGCAGCTCCAGAGTTCTCTT
ACACB	CGAGTTTGCGGATTCCCAAT	TTGTTCTGGAAGCTCTCGGT

Supplementary table 4: Antibodies

Antibody	Species	Catalog number	Dilution
hFXN	Mouse	Abcam-ab110328	1:200
h/mFXN	Rabbit	Abcam-ab175402	1:1000
β-ACTIN	Mouse	Sigma Aldrich-T4751	1:5000
PAX6	Rabbit	Covanxe PRB-278P	1:200
NESTIN	Mouse	Millipore MAB5326	1:500
SOX2	Mouse	R&D- Ab59776	1:200
TUJ1 (βIII-Tubulin)	Rabbit	Covance PRB-435P	1:500
TUJ1 (βIII-Tubulin)	Mouse	Covance MMS-435-P	1:500
MAP2	Chicken	Abcam-ab92434	1:500
PV	Rabbit	Swant PV27	1:1000
CD56-647	Mouse	BD biosciences 55771	1:50
OXPHOS	Mouse	Abcam-ab110411	1:1000
METTL17	Rabbit	Invitrogen PA5-107173	1:1000
CALNEXIN	Rabbit	Sigma-Aldrich-C4731	1:2000
phospho-S6	Rabbit	Abcam-ab2211	1:1000
Hoechst	/	Thermo Fisher H1399	1:1000
Anti-rabbit-488	Donkey	Thermo Fisher A21206	1:1000
Anti-rabbit-546	Donkey	Thermo Fisher 10040	1:1000
Anti-mouse-488	Donkey	Thermo Fisher A21202	1:1000
Anti-rabbit-647	Donkey	Thermo Fisher A31573	1:1000
Anti-chicken-546	Donkey	Thermo Fisher A11040	1:1000

Supplementary table 5: CRISPOR predicted off-target genes for sgP2

Predicted off-target	# of mismatches	Location
BRE	3	intron
RNF216-Metazoa_SRP	4	intergenic
RP11-554A11.8-RP11-554A11.9	4	intergenic
RN7SKP62-ST8SIA4	4	intergenic
RP11-174G6.1	4	intron
MYO18A-CRYBA1	3	intergenic
RBAKDN/RBAK-RBAKDN-RNU6-215P	4	intergenic
MIR8065-AC012175.1	4	intergenic
RNA5SP428-CDH5	4	intergenic
CPM-RP11-324P9.1	4	intergenic
MGMT	4	intron
RP11-25I9.2-RNA5SP349	4	intergenic
KB-173C10.2-KB-173C10.1	3	intergenic
SNX12-FOXO4	4	intergenic
MIR4768-RP1-60N8.1	4	intergenic
ARHGAP42-AC015600.1	4	intergenic
SEC14L3	4	intron
TANC2-AC037445.1	4	intergenic
KCND3-IT1-KCND3-AS1	4	intergenic
RP11-406A20.4-RP11-30P16.1	4	intergenic
CDH18	4	intron
C1QTNF9B	4	intron
RP11-100K18.1-RP11-451L19.1	4	intergenic
PRR4-PRH1	4	intergenic
IGF2BP2	4	intron
RP11-297L17.4-RP11-467J12.4	4	intergenic
RNU6-1040P-RALYL	4	intergenic
HIRA	4	intron
ACACB	4	intron
TXNDC16	4	intron
RP11-557C18.4-RP11-557C18.3	4	intergenic
AC004014.3-AC002386.1	4	intergenic
LINC01362-RP11-413G15.1	4	intergenic
RASA2	4	intron
SYNDIG1	4	intron
EGFR	4	intron
EFNB1-PJA1	4	intergenic
MLK7-AS1	4	intron
RP11-22D3.2-CBLN1	4	intergenic
RP11-624C23.1-ADAMDEC1	4	intergenic
FGGY	4	intron
MCC	4	intron
RP11-169K17.4	4	exon
RP11-166B2.7-SNX29	4	intergenic
AP006547.3-AC145123.2	3	intergenic
SCAMP1	4	intron
MEGF11	4	intron
MAN2A1	4	intron
RP11-576D8.4	4	exon
Y_RNA-MIR4325	4	intergenic
AC112198.2-RP11-45H22.3	4	intergenic
RN7SL318P-RP5-991O23.1	4	intergenic
UQCRC1	4	intron

CHAPTER 3

Summary and conclusions

Friedreich's ataxia (FA) is a recessive neurodegenerative disorder, affecting 1 over 40000 individuals (Koeppen AH, 2011; Pandolfo M, 2009). Patients predominantly present with limb and gait ataxia, often accompanied by additional neurological manifestations such as dysarthria, areflexia, impaired vibration and proprioceptive sensation (Corben LA, 2010). These clinical features arise from the loss of sensory neurons in the dorsal root ganglia, particularly proprioceptive neurons, as well as degeneration of the Dentate Nucleus of the cerebellum and corticospinal tracts (Harding IH, 2020). FA is caused by a pathogenic GAA trinucleotide repeat expansion in the intron 1 of the *FXN* gene, which leads to its transcriptional silencing (Campuzano CS et al., 1996). Among the therapeutic strategies currently under investigation, transcriptional reactivation of *FXN* represents a particularly promising approach, with broad relevance across multiple areas of neuroscience. In this study, we proposed novel approaches for *FXN* gene reactivation. More specifically, we focused on CRISPR activation (CRISPRa) and zinc-finger activators (ZFAs) strategies. Regarding the CRISPRa approach, we employed a catalytically inactive Cas9 (dCas9) fused to the potent transcriptional activator VP160, together with a single-guide RNA (sgP2), targeting *FXN* promoter. CRISPRa-mediated activation resulted in a robust increase of FXN protein amounts, across multiple disease-relevant neural cell types differentiated from iPSCs, including neural progenitor cells (NPCs), cortical neurons, and sensory neurons, derived from a mildly affected patient (PTS, 330/300 GAA repeats) and a more severely affected patient (PTL, 530/1000 GAA repeats) (Fig. 2A-I). Importantly, *FXN* reactivation was accompanied by the functional restoration of downstream pathways disrupted in FA. Specifically, we observed normalization of cellular redox homeostasis, reflected by the upregulation of detoxifying genes (Fig. 3B) and a concomitant reduction in reactive oxygen species (ROS) levels (Fig. 4B–D). Moreover, given the established role of FXN in iron–sulfur clusters (ISCs) biosynthesis, we assessed whether CRISPRa-mediated activation could rescue this process. Transcriptome analysis showed increased expression of genes encoding the principal components of the pathway for ISCs biosynthesis (Fig. 3B). Additionally, analysis of ISC-containing protein levels in both control and FA-derived neurons demonstrated that CRISPRa treatment restored their levels, indicative of replenished ISCs pools (Fig. 5A-I). Together, these findings demonstrate that transcriptional activation strategies can effectively restore *FXN* expression and ameliorate associated cellular dysfunctions in human neuronal models of FA. As the ultimate aim of this work was to identify the most suitable tool for translational application, we evaluated ZFAs as a clinically more applicable alternative to CRISPRa for FXN reactivation. ZFAs offer distinct advantages, including their relatively small size, facilitating efficient packaging into AAV vectors, and their

derivation from human protein scaffolds, which is expected to reduce immunogenicity. By generating a panel of promoter-targeted ZFAs, we identified a triple combination (ZF145, ZF172, ZF187) that induced *FXN* expression in fibroblasts derived from PTS patient, but not in cells from PTL patient, again suggesting that residual chromatin accessibility influences the efficacy of gene reactivation. Importantly, the ZFA strategy was also effective in iPSC-derived neuronal cells, where FXN protein levels were restored to near-physiological levels in both NPCs and sensory neurons from PTS patient (Fig. 6A-M). However, given that ZFAs were effective only in cells from a mildly affected patient, future studies are needed to assess their efficacy across a broader panel of patient-derived lines to determine their potential for large-scale clinical application. A major advantage of the CRISPRa and ZFAs approaches explored here is their capacity to restore *FXN* expression within physiological ranges, thereby mitigating the risk of toxicity linked to *FXN* overexpression (Belbellaa B et al., 2018; Huichalaf C et al., 2022). This aspect was broadly investigated in the field of gene therapy for FA. Indeed, *in vivo* studies by Belbellaa et al. showed that high-level *FXN* overexpression, particularly in cardiac tissue, induces dose-dependent mitochondrial toxicity characterized by impaired ISCs–dependent enzyme activities, altered mitochondrial ultrastructure, activation of mitochondrial stress responses, cardiomyocyte death, fibrosis, and progressive cardiac dysfunction, despite restoration of FXN levels well above normal. Importantly, these toxic effects emerged when *FXN* expression exceeded approximately 20-fold endogenous levels, whereas more moderate increases were largely tolerated, underscoring a threshold-dependent phenomenon. Complementary work by Huichalaf et al. further elucidated the mechanistic basis of this toxicity, demonstrating that excessive FXN disrupts ISCs biogenesis through its functional interaction with the core assembly machinery, leading to a paradoxical ISCs deficiency and consequent mitochondrial dysfunction. Notably, toxicity was dependent on FXN's ability to engage the Fe-S assembly complex, as expression of a binding-deficient FXN mutant failed to elicit similar deleterious effects, thereby establishing that FXN overexpression toxicity is mechanistically linked to its canonical biochemical role. Together, these studies indicate that excessive FXN perturbs mitochondrial homeostasis and energy metabolism in a manner that phenocopies aspects of FXN deficiency, with tissue-specific sensitivity and systemic consequences observed at high expression levels, highlighting critical considerations for FXN-targeted therapeutic strategies, particularly gene-replacement approaches. Considering this, CRISPRa and ZFAs approaches offer a significant benefit over conventional gene therapy, which has thus far been regarded as the golden standard and the only definitive therapeutic option for FA. Moreover, the systems investigated in the present work present additional advantages over the therapies based on base editing and small molecules treatments that are currently in clinical development. Genome-editing strategies such as CRISPR/Cas9 nucleases and base editors offer the possibility of permanent genetic correction; however, their principal limitation resides in the irreversible nature of DNA-level interventions and the associated risk of unintended genomic alterations. Even in the absence of canonical double-

strand breaks, base-editing approaches can induce off-target nucleotide conversions, bystander edits, and long-term genomic instability, while Cas9 nuclease activity has been shown to generate insertions, deletions, and chromosomal rearrangements due to erroneous DNA repair (Kosicki et al., 2018; Xue et al., 2021; Kalter et al., 2025). In contrast, CRISPRa and ZFAs systems modulate gene expression without altering the underlying DNA sequence, thereby substantially reducing the risk of permanent genomic damage. This non-mutagenic and reversible mode of action represents a major safety advantage, particularly for dosage-sensitive genes, as it allows controlled and tunable upregulation. However, CRISPRa and ZFAs efficacy depends on sustained expression of the transcriptional machinery, chromatin accessibility, and promoter context, which may limit robustness and necessitate continuous or long-term delivery. An alternative, non-genetic strategy involves the use of small molecules to induce gene expression, which offers additional advantages such as ease of administration, dose-dependent reversibility, and established regulatory pathways for clinical translation. Small molecules can enable systemic and adjustable modulation of gene expression without introducing exogenous genetic material; however, their specificity is often limited, as they frequently act through pleiotropic signaling or epigenetic mechanisms, increasing the risk of off-target transcriptional effects. Furthermore, chronic administration may be required to maintain therapeutic efficacy, raising concerns regarding toxicity, variable bioavailability, and patient compliance. Taken together, while base editing provides durable correction at the cost of irreversible genomic modification, CRISPRa/ZFAs and small-molecule approaches offer safer and more flexible alternatives for therapeutic gene upregulation, albeit with trade-offs in durability, specificity, and delivery requirements that must be carefully balanced for clinical application. Despite its favorable safety profile relative to DNA-editing strategies, the clinical translation of epigenome-editing approaches such as CRISPRa faces several important challenges. Achieving efficient, tissue-specific, and durable delivery of the large CRISPRa machinery in humans remains a major obstacle, as previously raised in the Discussion paragraph. Sustained therapeutic efficacy may require long-term expression of epigenetic regulators, raising concerns about immune responses to Cas-derived proteins and the potential consequences of prolonged transcriptional activation. In addition, variability in chromatin state, epigenetic context, and regulatory architecture across cell types and individuals may lead to heterogeneous responses, complicating dose control and predictability of gene activation. Off-target binding of dCas9 to non-canonical genomic sites, while non-mutagenic, could still perturb transcriptional networks in unintended ways, with uncertain long-term effects. Collectively, these challenges underscore the need for improved delivery platforms, refined targeting strategies, and robust safety assessment frameworks before epigenome-editing technologies can be broadly translated into human therapies.

In summary, through a comparative evaluation of CRISPRa and ZFAs approaches, we show that CRISPRa constitutes the most potent and efficient strategy for restoring endogenous *FXN* expression, enabling robust and physiologically relevant reactivation across multiple disease-

relevant neuronal cell types in the context of FA. Importantly, additional studies are necessary to characterize ZFAs, including comprehensive assessment of off-target activity and validation of their efficacy in a broader range of patient-derived cell lines. Moreover, to further demonstrate the therapeutic efficacy of the proposed approach, further characterization of the mitochondrial function in sensory neurons are required, for example through the analysis of ATP production and mitochondrial respiration before and after CRISPRa treatment. Besides, considering the limitations encountered in the *in vivo* validation and the lack of suitable alternative models, the recently developed YG8JR mouse line currently represents the only new option for such studies. This model, an upgraded version of the YG8sR line used in the present work, harbors the human *FXN* gene with more than 800 GAA repeats and has been reported to exhibit substantially reduced human *FXN* expression, alongside earlier disease onset and more pronounced ataxic phenotypes relative to previously available models (Kalef-Ezra et al., 2023). Nonetheless, the reliance on this single model underscores an enduring challenge in the field, namely the scarcity of animal models that faithfully recapitulate the molecular and transcriptional hallmarks of FA and can be robustly employed to evaluate *FXN* reactivation strategies *in vivo*. Taken together, and in light of the additional studies required, our results demonstrate the feasibility of *FXN* reactivation as a therapeutic strategy and provide a solid foundation for its future clinical translation.

References

1. Abeti R, Baccaro A, Esteras N, Giunti P. Novel NRF2-Inducer Prevents Mitochondrial Defects and Oxidative Stress in Friedreich's Ataxia Models. Front Cell Neurosci. 2018 Jul 17;12:188. doi: 10.3389/fncel.2018.00188. PMID: 30065630; PMCID: PMC6056642.
2. Agrò M, Díaz-Nido J. Effect of Mitochondrial and Cytosolic FXN Isoform Expression on Mitochondrial Dynamics and Metabolism. Int J Mol Sci. 2020 Nov 4;21(21):8251. doi: 10.3390/ijms21218251. PMID: 33158039; PMCID: PMC7662637.
3. Al-Mahdawi S, Mouro Pinto R, Ruddle P, Carroll C, Webster Z, Pook M, GAA repeat instability in Friedreich ataxia YAC transgenic mice, Genomics, Volume 84, Issue 2, 2004, Pages 301-310, ISSN 0888-7543, https://doi.org/10.1016/j.ygeno.2004.04.003.
4. Al-Mahdawi S, Pinto RM, Varshney D, Lawrence L, Lowrie MB, Hughes S, Webster Z, Blake J, Cooper JM, King R, Pook MA. GAA repeat expansion mutation mouse models of Friedreich ataxia exhibit oxidative stress leading to progressive neuronal and cardiac pathology. Genomics. 2006 Nov;88(5):580-90. doi: 10.1016/j.ygeno.2006.06.015. Epub 2006 Aug 17. PMID: 16919418; PMCID: PMC2842930.
5. Andrechek ER, Hardy WR, Girgis-Gabardo AA, Perry RL, Butler R, Graham FL, Kahn RC, Rudnicki MA, Muller WJ. ErbB2 is required for muscle spindle and myoblast cell survival. Mol Cell Biol. 2002 Jul;22(13):4714-22. doi: 10.1128/MCB.22.13.4714-4722.2002. PMID: 12052879; PMCID: PMC133917.
6. Anjomani Virmouni S, Ezzatizadeh V, Sandi C, Sandi M, Al-Mahdawi S, Chutake Y, Pook MA. A novel GAA-repeat-expansion-based mouse model of Friedreich's ataxia. Dis Model Mech. 2015 Mar;8(3):225-35. doi: 10.1242/dmm.018952. Epub 2015 Feb 13. PMID: 25681319; PMCID: PMC4348561.
7. Anjomani Virmouni S, Sandi C, Al-Mahdawi S, Pook MA. Cellular, molecular and functional characterisation of YAC transgenic mouse models of Friedreich ataxia. PLoS One. 2014 Sep 8;9(9):e107416. doi: 10.1371/journal.pone.0107416. PMID: 25198290; PMCID: PMC4157886.
8. Ast T, Meisel JD, Patra S, Wang H, Grange RMH, Kim SH, Calvo SE, Orefice LL, Nagashima F, Ichinose F, Zapol WM, Ruvkun G, Barondeau DP, Mootha VK. Hypoxia Rescues Frataxin Loss by Restoring Iron Sulfur Cluster Biogenesis. Cell. 2019 May 30;177(6):1507-1521.e16. doi: 10.1016/j.cell.2019.03.045. Epub 2019 Apr 25. PMID: 31031004; PMCID: PMC6911770.
9. Ast T, Itoh Y, Sadre S, McCoy JG, Namkoong G, Wengrod JC, Chicherin I, Joshi PR, Kamenski P, Suess DLM, Amunts A, Mootha VK. METTL17 is an Fe-S cluster checkpoint for mitochondrial translation. Mol Cell. 2024 Jan 18;84(2):359-374.e8. doi: 10.1016/j.molcel.2023.12.016. Epub 2024 Jan 9. PMID: 38199006; PMCID: PMC11046306.

10. Banfi, F., Rubio, A., Zaghi, M. *et al.* SETBP1 accumulation induces P53 inhibition and genotoxic stress in neural progenitors underlying neurodegeneration in Schinzel-Giedion syndrome. *Nat Commun* 12, 4050 (2021). https://doi.org/10.1038/s41467-021-24391-3.
11. Banks RW. An allometric analysis of the number of muscle spindles in mammalian skeletal muscles. J Anat. 2006 Jun;208(6):753-68. doi: 10.1111/j.1469-7580.2006.00558.x. PMID: 16761976; PMCID: PMC2100235.
12. Banks RW. The innervation of the muscle spindle: a personal history. J Anat. 2015 Aug;227(2):115-35. doi: 10.1111/joa.12297. Epub 2015 Jun 19. PMID: 26095428; PMCID: PMC4523316.
13. Banks RW. The motor innervation of mammalian muscle spindles. Prog Neurobiol. 1994 Jul-Aug;43(4-5):323-62. doi: 10.1016/0301-0082(94)90059-0. PMID: 7816930.
14. Barrangou R, Fremaux C, Deveau H, Richards M, Boyaval P, Moineau S, Romero DA, Horvath P. CRISPR provides acquired resistance against viruses in prokaryotes. Science. 2007 Mar 23;315(5819):1709-12. doi: 10.1126/science.1138140. PMID: 17379808.
15. Basbaum AI, Bautista DM, Scherrer G, Julius D. Cellular and molecular mechanisms of pain. Cell. 2009 Oct 16;139(2):267-84. doi: 10.1016/j.cell.2009.09.028. PMID: 19837031; PMCID: PMC2852643.
16. Bayot A, Reichman S, Lebon S, Csaba Z, Aubry L, Sterkers G, Husson I, Rak M, Rustin P, Cis-silencing of PIP5K1B evidenced in Friedreich's ataxia patient cells results in cytoskeleton anomalies, Human Molecular Genetics, Volume 22, Issue 14, 15 July 2013, Pages 2894–2904, https://doi.org/10.1093/hmg/ddt144
17. Belbellaa B, Reutenauer L, Messaddeq N, Monassier L, Puccio H. High Levels of Frataxin Overexpression Lead to Mitochondrial and Cardiac Toxicity in Mouse Models. Mol Ther Methods Clin Dev. 2020 Sep 1;19:120-138. doi: 10.1016/j.omtm.2020.08.018. PMID: 33209958; PMCID: PMC7648087.
18. Beerli RR, Segal DJ, Dreier B, Barbas CF 3rd. Toward controlling gene expression at will: specific regulation of the erbB-2/HER-2 promoter by using polydactyl zinc finger proteins constructed from modular building blocks. Proc Natl Acad Sci U S A. 1998 Dec 8;95(25):14628-33. doi: 10.1073/pnas.95.25.14628. PMID: 9843940; PMCID: PMC24500.
19. Behunova J, Gerykova Bujalkova M, Gras G, Taylor T, Ihm U, Kircher S, Rehder H, Laccone F. Distal Arthrogryposis with Impaired Proprioception and Touch: Description of an Early Phenotype in a Boy with Compound Heterozygosity of PIEZO2 Mutations and Review of the Literature. Mol Syndromol. 2019 Jan;9(6):287-294. doi: 10.1159/000494451. Epub 2018 Nov 13. PMID: 30800044; PMCID: PMC6381910.

20. Bibikova M, Carroll D, Segal DJ, Trautman JK, Smith J, Kim YG, Chandrasegaran S. Stimulation of homologous recombination through targeted cleavage by chimeric nucleases. Mol Cell Biol. 2001 Jan;21(1):289-97. doi: 10.1128/MCB.21.1.289-297.2001. PMID: 11113203; PMCID: PMC88802.
21. Bidichandani SI, Ashizawa T, Patel PI. The GAA triplet-repeat expansion in Friedreich ataxia interferes with transcription and may be associated with an unusual DNA structure. Am J Hum Genet. 1998 Jan;62(1):111-21. doi: 10.1086/301680. PMID: 9443873; PMCID: PMC1376805.
22. Bitinaite J, Wah DA, Aggarwal AK, Schildkraut I. FokI dimerization is required for DNA cleavage. Proc Natl Acad Sci U S A. 1998 Sep 1;95(18):10570-5. doi: 10.1073/pnas.95.18.10570. PMID: 9724744; PMCID: PMC27935.
23. Blancafort P, Chen EI, Gonzalez B, Bergquist S, Zijlstra A, Guthy D, Brachat A, Brakenhoff RH, Quigley JP, Erdmann D, Barbas CF 3rd. Genetic reprogramming of tumor cells by zinc finger transcription factors. Proc Natl Acad Sci U S A. 2005 Aug 16;102(33):11716-21. doi: 10.1073/pnas.0501162102. Epub 2005 Aug 4. PMID: 16081541; PMCID: PMC1187960.
24. Blecher R, Heinemann-Yerushalmi L, Assaraf E, Konstantin N, Chapman JR, Cope TC, Bewick GS, Banks RW, Zelzer E. New functions for the proprioceptive system in skeletal biology. Philos Trans R Soc Lond B Biol Sci. 2018 Sep 24;373(1759):20170327. doi: 10.1098/rstb.2017.0327. PMID: 30249776; PMCID: PMC6158198.
25. Blecher R, Krief S, Galili T, Assaraf E, Stern T, Anekstein Y, Agar G, Zelzer E. The Proprioceptive System Regulates Morphologic Restoration of Fractured Bones. Cell Rep. 2017 Aug 22;20(8):1775-1783. doi: 10.1016/j.celrep.2017.07.073. PMID: 28834742; PMCID: PMC5575358.
26. Blecher R, Krief S, Galili T, Biton IE, Stern T, Assaraf E, Levanon D, Appel E, Anekstein Y, Agar G, Groner Y, Zelzer E. The Proprioceptive System Masterminds Spinal Alignment: Insight into the Mechanism of Scoliosis. Dev Cell. 2017 Aug 21;42(4):388-399.e3. doi: 10.1016/j.devcel.2017.07.022. PMID: 28829946.
27. Bridwell-Rabb J, Fox NG, Tsai CL, Winn AM, Barondeau DP. Human frataxin activates Fe-S cluster biosynthesis by facilitating sulfur transfer chemistry. Biochemistry. 2014 Aug 5;53(30):4904-13. doi: 10.1021/bi500532e. Epub 2014 Jul 18. PMID: 24971490; PMCID: PMC4215901.
28. Bürk K, Schulz SR, Schulz JB. Monitoring progression in Friedreich ataxia (FRDA): the use of clinical scales. J Neurochem. 2013 Aug;126 Suppl 1:118-24. doi: 10.1111/jnc.12318. PMID: 23859347.

29. Butterfield GL, Rohm D, Roberts A, Nethery MA, Rizzo AJ, Morone DJ, Garnier L, Iglesias N, Barrangou R, Gersbach CA. Characterization of diverse Cas9 orthologs for genome and epigenome editing. Proc Natl Acad Sci U S A. 2025 Mar 18;122(11):e2417674122. doi: 10.1073/pnas.2417674122. Epub 2025 Mar 12. PMID: 40073054; PMCID: PMC11929499.
30. Campuzano V, Montermini L, Moltò MD, Pianese L, Cossée M, Cavalcanti F, Monros E, Rodius F, Duclos F, Monticelli A, Zara F, Cañizares J, Koutnikova H, Bidichandani SI, Gellera C, Brice A, Trouillas P, De Michele G, Filla A, De Frutos R, Palau F, Patel PI, Di Donato S, Mandel JL, Cocozza S, Koenig M, Pandolfo M. Friedreich's ataxia: autosomal recessive disease caused by an intronic GAA triplet repeat expansion. Science. 1996 Mar 8;271(5254):1423-7. doi: 10.1126/science.271.5254.1423. PMID: 8596916.
31. Chan PK, Torres R, Yandim C, Law PP, Khadayate S, Mauri M, Grosan C, Chapman-Rothe N, Giunti P, Pook M, Festenstein R. Heterochromatinization induced by GAA-repeat hyperexpansion in Friedreich's ataxia can be reduced upon HDAC inhibition by vitamin B3. Hum Mol Genet. 2013 Jul 1;22(13):2662-75. doi: 10.1093/hmg/ddt115. Epub 2013 Mar 7. PMID: 23474817.
32. Chang JC, Ryan MR, Stark MC, Liu S, Purushothaman P, Bolan F, Johnson CA, Champe M, Meng H, Lawlor MW, Halawani S, Ngaba LV, Lynch DR, Davis C, Gonzalo-Gil E, Lutz C, Urbinati F, Medicherla B, Fonck C. AAV8 gene therapy reverses cardiac pathology and prevents early mortality in a mouse model of Friedreich's ataxia. Mol Ther Methods Clin Dev. 2024 Jan 22;32(1):101193. doi: 10.1016/j.omtm.2024.101193. PMID: 38352270; PMCID: PMC10862410.
33. Chandran V, Gao K, Swarup V, Versano R, Dong H, Jordan MC, Geschwind DH. Inducible and reversible phenotypes in a novel mouse model of Friedreich's Ataxia. Elife. 2017 Dec 19;6:e30054. doi: 10.7554/eLife.30054. PMID: 29257745; PMCID: PMC5736353.
34. Chavez A, Scheiman J, Vora S, Pruitt BW, Tuttle M, P R Iyer E, Lin S, Kiani S, Guzman CD, Wiegand DJ, Ter-Ovanesyan D, Braff JL, Davidsohn N, Housden BE, Perrimon N, Weiss R, Aach J, Collins JJ, Church GM. Highly efficient Cas9-mediated transcriptional programming. Nat Methods. 2015 Apr;12(4):326-8. doi: 10.1038/nmeth.3312. Epub 2015 Mar 2. PMID: 25730490; PMCID: PMC4393883.
35. Chen R, Shi X, Yao X, Gao T, Huang G, Ning D, Cao Z, Xu Y, Liang W, Tian SZ, Zhu Q, Fang L, Zheng M, Hu Y, Cui H, Chen W. Specific multivalent molecules boost CRISPR-mediated transcriptional activation. Nat Commun. 2024 Aug 22;15(1):7222. doi: 10.1038/s41467-024-51694-y. PMID: 39174527; PMCID: PMC11341856.

36. Cheret C, Willem M, Fricker FR, Wende H, Wulf-Goldenenberg A, Tahirovic S, Nave KA, Saftig P, Haass C, Garratt AN, Bennett DL, Birchmeier C. Bace1 and Neuregulin-1 cooperate to control formation and maintenance of muscle spindles. EMBO J. 2013 Jul 17;32(14):2015-28. doi: 10.1038/emboj.2013.146. Epub 2013 Jun 21. PMID: 23792428; PMCID: PMC3715864.
37. Cherif K, Gérard C, Rousseau J, Ouellet DL, Chapdelaine P, Tremblay JP. Increased Frataxin Expression Induced in Friedreich Ataxia Cells by Platinum TALE-VP64s or Platinum TALE-SunTag. Mol Ther Nucleic Acids. 2018 Sep 7;12:19-32. doi: 10.1016/j.omtn.2018.04.009. Epub 2018 Apr 27. PMID: 30195758; PMCID: PMC6019861.
38. Clayton R, Galas T, Scherer N, Farmer J, Ruiz N, Hamdani M, Schecter D, Bettoun D. Safety, pharmacokinetics, and pharmacodynamics of nomlabofusp (CTI-1601) in Friedreich's ataxia. Ann Clin Transl Neurol. 2024 Mar;11(3):540-553. doi: 10.1002/acn3.51971. Epub 2024 Feb 4. PMID: 38311797; PMCID: PMC10963286.
39. Codazzi F, Hu A, Rai M, Donatello S, Salerno Scarzella F, Mangiameli E, Pelizzoni I, Grohovaz F, Pandolfo M. Friedreich ataxia-induced pluripotent stem cell-derived neurons show a cellular phenotype that is corrected by a benzamide HDAC inhibitor. Hum Mol Genet. 2016 Nov 15;25(22):4847-4855. doi: 10.1093/hmg/ddw308. PMID: 28175303.
40. Colella P, Ronzitti G, Mingozzi F. Emerging Issues in AAV-Mediated *In Vivo* Gene Therapy. Mol Ther Methods Clin Dev. 2017 Dec 1;8:87-104. doi: 10.1016/j.omtm.2017.11.007. PMID: 29326962; PMCID: PMC5758940.
41. Condò I, Ventura N, Malisan F, Rufini A, Tomassini B, Testi R. In vivo maturation of human frataxin. Hum Mol Genet. 2007 Jul 1;16(13):1534-40. doi: 10.1093/hmg/ddm102. Epub 2007 Apr 27. PMID: 17468497.
42. Condò I, Ventura N, Malisan F, Tomassini B, Testi R. A pool of extramitochondrial frataxin that promotes cell survival. J Biol Chem. 2006 Jun 16;281(24):16750-6. doi: 10.1074/jbc.M511960200. Epub 2006 Apr 11. PMID: 16608849.
43. Cook A, Giunti P. Friedreich's ataxia: clinical features, pathogenesis and management. Br Med Bull. 2017 Dec 1;124(1):19-30. doi: 10.1093/bmb/ldx034. PMID: 29053830; PMCID: PMC5862303.
44. Corben LA, Tai G, Wilson C, Collins V, Churchyard AJ, Delatycki MB. A comparison of three measures of upper limb function in Friedreich ataxia. J Neurol. 2010 Apr;257(4):518-23. doi: 10.1007/s00415-009-5352-7. Epub 2009 Oct 13. PMID: 19823893.
45. Cossée M, Puccio H, Gansmuller A, Koutnikova H, Dierich A, LeMeur M, Fischbeck K, Dollé P, Koenig M. Inactivation of the Friedreich ataxia mouse gene leads to early embryonic lethality without iron accumulation. Hum Mol Genet. 2000 May 1;9(8):1219-26. doi: 10.1093/hmg/9.8.1219. PMID: 10767347.

46. Costa FC, Fedosyuk H, Neades R, de Los Rios JB, Barbas CF 3rd, Peterson KR. Induction of Fetal Hemoglobin In Vivo Mediated by a Synthetic γ-Globin Zinc Finger Activator. Anemia. 2012;2012:507894. doi: 10.1155/2012/507894. Epub 2012 Jun 15. PMID: 22778925; PMCID: PMC3384929.
47. Cranfill SL, Luo W. The development of somatosensory neurons: Insights into pain and itch. Curr Top Dev Biol. 2021;142:443-475. doi: 10.1016/bs.ctdb.2020.10.005. Epub 2020 Nov 5. PMID: 33706924; PMCID: PMC8099032.
48. D'Autréaux B, Toledano MB. ROS as signalling molecules: mechanisms that generate specificity in ROS homeostasis. Nat Rev Mol Cell Biol. 2007 Oct;8(10):813-24. doi: 10.1038/nrm2256. PMID: 17848967.
49. De Biase I, Chutake YK, Rindler PM, Bidichandani SI. Epigenetic silencing in Friedreich ataxia is associated with depletion of CTCF (CCCTC-binding factor) and antisense transcription. PLoS One. 2009 Nov 19;4(11):e7914. doi: 10.1371/journal.pone.0007914. PMID: 19956589; PMCID: PMC2780319.
50. Delatycki MB, Bidichandani SI. Friedreich ataxia- pathogenesis and implications for therapies. Neurobiol Dis. 2019 Dec;132:104606. doi: 10.1016/j.nbd.2019.104606. Epub 2019 Sep 5. PMID: 31494282.
51. Delatycki MB, Camakaris J, Brooks H, Evans-Whipp T, Thorburn DR, Williamson R, Forrest SM. Direct evidence that mitochondrial iron accumulation occurs in Friedreich ataxia. Ann Neurol. 1999 May;45(5):673-5. PMID: 10319894.
52. Delle Vedove A, Storbeck M, Heller R, Hölker I, Hebbar M, Shukla A, Magnusson O, Cirak S, Girisha KM, O'Driscoll M, Loeys B, Wirth B. Biallelic Loss of Proprioception-Related PIEZO2 Causes Muscular Atrophy with Perinatal Respiratory Distress, Arthrogryposis, and Scoliosis. Am J Hum Genet. 2016 Nov 3;99(5):1206-1216. doi: 10.1016/j.ajhg.2016.09.019.
53. Deriu F, Tedde Piras A, Montella A. The early development of muscle spindle in human foetus. Ital J Anat Embryol. 1996 Jul-Sep;101(3):163-72. PMID: 9112824.
54. Dietz V. Proprioception and locomotor disorders. Nat Rev Neurosci. 2002 Oct;3(10):781-90. doi: 10.1038/nrn939. PMID: 12360322.
55. Dionisi C, Chazalon M, Rai M, Keime C, Imbault V, Communi D, Puccio H, Schiffmann SN, Pandolfo M. Proprioceptors-enriched neuronal cultures from induced pluripotent stem cells from Friedreich ataxia patients show altered transcriptomic and proteomic profiles, abnormal neurite extension, and impaired electrophysiological properties. Brain Commun. 2023 Jan 18;5(1):fcad007. doi: 10.1093/braincomms/fcad007. PMID: 36865673; PMCID: PMC9972525.

56. Dionisi C, Rai M, Chazalon M, Schiffmann SN, Pandolfo M. Primary proprioceptive neurons from human induced pluripotent stem cells: a cell model for afferent ataxias. Sci Rep. 2020 May 8;10(1):7752. doi: 10.1038/s41598-020-64831-6. PMID: 32385372; PMCID: PMC7210273.
57. Doni D, Cavion F, Bortolus M, Baschiera E, Muccioli S, Tombesi G, d'Ettorre F, Ottaviani D, Marchesan E, Leanza L, Greggio E, Ziviani E, Russo A, Bellin M, Sartori G, Carbonera D, Salviati L, Costantini P. Human frataxin, the Friedreich ataxia deficient protein, interacts with mitochondrial respiratory chain. Cell Death Dis. 2023 Dec 8;14(12):805. doi: 10.1038/s41419-023-06320-y. Erratum in: Cell Death Dis. 2024 Jan 29;15(1):93. doi: 10.1038/s41419-024-06459-2. PMID: 38062036; PMCID: PMC10703789.
58. Doudna JA, Charpentier E. Genome editing. The new frontier of genome engineering with CRISPR-Cas9. Science. 2014 Nov 28;346(6213):1258096. doi: 10.1126/science.1258096. PMID: 25430774.
59. Dürr A, Cossee M, Agid Y, Campuzano V, Mignard C, Penet C, Mandel JL, Brice A, Koenig M. Clinical and genetic abnormalities in patients with Friedreich's ataxia. N Engl J Med. 1996 Oct 17;335(16):1169-75. doi: 10.1056/NEJM199610173351601. PMID: 8815938.
60. Edzeamey FJ, Ramchunder Z, Pourzand C, Anjomani Virmouni S. Emerging antioxidant therapies in Friedreich's ataxia. Front Pharmacol. 2024 Feb 6;15:1359618. doi: 10.3389/fphar.2024.1359618. PMID: 38379897; PMCID: PMC10876797.
61. Ernfors P, Lee KF, Kucera J, Jaenisch R. Lack of neurotrophin-3 leads to deficiencies in the peripheral nervous system and loss of limb proprioceptive afferents. Cell. 1994 May 20;77(4):503-12. doi: 10.1016/0092-8674(94)90213-5. PMID: 7514502.
62. Fil D, Chacko BK, Conley R, Ouyang X, Zhang J, Darley-Usmar VM, Zuberi AR, Lutz CM, Napierala M, Napierala JS. Mitochondrial damage and senescence phenotype of cells derived from a novel frataxin G127V point mutation mouse model of Friedreich's ataxia. Dis Model Mech. 2020 Jul 27;13(7):dmm045229. doi: 10.1242/dmm.045229. PMID: 32586831; PMCID: PMC7406325.
63. Fil D, Conley RL, Zuberi AR, Lutz CM, Gemelli T, Napierala M, Napierala JS. Neurobehavioral deficits of mice expressing a low level of G127V mutant frataxin. Neurobiol Dis. 2023 Feb;177:105996. doi: 10.1016/j.nbd.2023.105996. Epub 2023 Jan 10. PMID: 36638893; PMCID: PMC9901512.
64. Fox NG, Yu X, Feng X, Bailey HJ, Martelli A, Nabhan JF, Strain-Damerell C, Bulawa C, Yue WW, Han S. Structure of the human frataxin-bound iron-sulfur cluster assembly complex provides insight into its activation mechanism. Nat Commun. 2019 May 17;10(1):2210. doi: 10.1038/s41467-019-09989-y. PMID: 31101807; PMCID: PMC6525205.

65. Galea CA, Huq A, Lockhart PJ, Tai G, Corben LA, Yiu EM, Gurrin LC, Lynch DR, Gelbard S, Durr A, Pousset F, Parkinson M, Labrum R, Giunti P, Perlman SL, Delatycki MB, Evans-Galea MV. Compound heterozygous FXN mutations and clinical outcome in friedreich ataxia. Ann Neurol. 2016 Mar;79(3):485-95. doi: 10.1002/ana.24595. PMID: 26704351.
66. Gasiunas G, Barrangou R, Horvath P, Siksnys V. Cas9-crRNA ribonucleoprotein complex mediates specific DNA cleavage for adaptive immunity in bacteria. Proc Natl Acad Sci U S A. 2012 Sep 25;109(39):E2579-86. doi: 10.1073/pnas.1208507109. Epub 2012 Sep 4. PMID: 22949671; PMCID: PMC3465414.
67. Gérard C, Archambault AF, Bouchard C, Tremblay JP. A promising mouse model for Friedreich Ataxia progressing like human patients. Behav Brain Res. 2023 Jan 5;436:114107. doi: 10.1016/j.bbr.2022.114107. Epub 2022 Sep 8. PMID: 36089099.C. Gérard, A.F. Archambault, C. Bouchard, J.P. Tremblay, A promising mouse model for Friedreich Ataxia progressing like human patients, Behav. Brain Res. 436 (2023) 114107.
68. Gerhardt J, Bhalla AD, Butler JS, Puckett JW, Dervan PB, Rosenwaks Z, Napierala M. Stalled DNA Replication Forks at the Endogenous GAA Repeats Drive Repeat Expansion in Friedreich's Ataxia Cells. Cell Rep. 2016 Aug 2;16(5):1218-1227. doi: 10.1016/j.celrep.2016.06.075. Epub 2016 Jul 14. PMID: 27425605; PMCID: PMC5028224.
69. Gervason, S., Larkem, D., Mansour, A.B. et al. Physiologically relevant reconstitution of iron-sulfur cluster biosynthesis uncovers persulfide-processing functions of ferredoxin-2 and frataxin. Nat Commun 10, 3566 (2019). https://doi.org/10.1038/s41467-019-11470-9.
70. Giuffrida R, Rustioni A. Dorsal root ganglion neurons projecting to the dorsal column nuclei of rats. J Comp Neurol. 1992 Feb 8;316(2):206-20. doi: 10.1002/cne.903160206. PMID: 1374085.
71. Gottesfeld JM. Molecular Mechanisms and Therapeutics for the GAA·TTC Expansion Disease Friedreich Ataxia. Neurotherapeutics. 2019 Oct;16(4):1032-1049. doi: 10.1007/s13311-019-00764-x. PMID: 31317428; PMCID: PMC6985418.
72. Groh M, Lufino MM, Wade-Martins R, Gromak N. R-loops associated with triplet repeat expansions promote gene silencing in Friedreich ataxia and fragile X syndrome. PLoS Genet. 2014 May 1;10(5):e1004318. doi: 10.1371/journal.pgen.1004318. PMID: 24787137; PMCID: PMC4006715.
73. Guccini I, Serio D, Condò I, Rufini A, Tomassini B, Mangiola A, Maira G, Anile C, Fina D, Pallone F, Mongiardi MP, Levi A, Ventura N, Testi R, Malisan F. Frataxin participates to the hypoxia-induced response in tumors. Cell Death Dis. 2011 Feb 24;2(2):e123. doi: 10.1038/cddis.2011.5. PMID: 21368894; PMCID: PMC3101705.

74. Gunther K, Profeta V, Keita M, Park C, Wells M, Sharma S, Schadt K, Lynch DR. Safety Monitoring of Omaveloxolone in Friedreich Ataxia: Results from One Year of Clinical Treatment. Neurol Ther. 2025 Jun;14(3):1105-1114. doi: 10.1007/s40120-025-00749-3. Epub 2025 Apr 30. PMID: 40304846; PMCID: PMC12089633.
75. Guo L, Wang Q, Weng L, Hauser LA, Strawser CJ, Mesaros C, Lynch DR, Blair IA. Characterization of a new N-terminally acetylated extra-mitochondrial isoform of frataxin in human erythrocytes. Sci Rep. 2018 Nov 19;8(1):17043. doi: 10.1038/s41598-018-35346-y. PMID: 30451920; PMCID: PMC6242848.
76. Haberberger RV, Barry C, Dominguez N, Matusica D. Human Dorsal Root Ganglia. Front Cell Neurosci. 2019 Jun 19;13:271. doi: 10.3389/fncel.2019.00271. PMID: 31293388; PMCID: PMC6598622.
77. Haliloglu G, Becker K, Temucin C, Talim B, Küçükşahin N, Pergande M, Motameny S, Nürnberg P, Aydingoz U, Topaloglu H, Cirak S. Recessive PIEZO2 stop mutation causes distal arthrogryposis with distal muscle weakness, scoliosis and proprioception defects. J Hum Genet. 2017 Apr;62(4):497-501. doi: 10.1038/jhg.2016.153. Epub 2016 Dec 15. PMID: 27974811.
78. Harding IH, Lynch DR, Koeppen AH, Pandolfo M. Central Nervous System Therapeutic Targets in Friedreich Ataxia. Hum Gene Ther. 2020 Dec;31(23-24):1226-1236. doi: 10.1089/hum.2020.264. PMID: 33238751; PMCID: PMC7757690.
79. Herman D, Jenssen K, Burnett R, Soragni E, Perlman SL, Gottesfeld JM. Histone deacetylase inhibitors reverse gene silencing in Friedreich's ataxia. Nat Chem Biol. 2006 Oct;2(10):551-8. doi: 10.1038/nchembio815. Epub 2006 Aug 20. Erratum in: Nat Chem Biol. 2007 Jul;3(7):432. PMID: 16921367.
80. Hick A, Wattenhofer-Donzé M, Chintawar S, Tropel P, Simard JP, Vaucamps N, Gall D, Lambot L, André C, Reutenauer L, Rai M, Teletin M, Messaddeq N, Schiffmann SN, Viville S, Pearson CE, Pandolfo M, Puccio H. Neurons and cardiomyocytes derived from induced pluripotent stem cells as a model for mitochondrial defects in Friedreich's ataxia. Dis Model Mech. 2013 May;6(3):608-21. doi: 10.1242/dmm.010900. Epub 2012 Nov 7. PMID: 23136396; PMCID: PMC3634645.
81. Hippenmeyer S, Shneider NA, Birchmeier C, Burden SJ, Jessell TM, Arber S. A role for neuregulin1 signaling in muscle spindle differentiation. Neuron. 2002 Dec 19;36(6):1035-49. doi: 10.1016/s0896-6273(02)01101-7. PMID: 12495620.
82. His, W. (1886). Zur Geschichte des menschlichen Reuckenmarkes und der Nervenwurzeln (S. Hirzel).
83. Horne MK, Butler EG. The role of the cerebello-thalamo-cortical pathway in skilled movement. Prog Neurobiol. 1995 Jun;46(2-3):199-213. PMID: 7568913.
84. https://www.clinicaltrials.gov/.

85. https://www.curefa.org/drug-development/.
86. https://www.sangamo.com/.
87. Huichalaf C, Perfitt TL, Kuperman A, Gooch R, Kovi RC, Brenneman KA, Chen X, Hirenallur-Shanthappa D, Ma T, Assaf BT, Pardo I, Franks T, Monarski L, Cheng TW, Le K, Su C, Somanathan S, Whiteley LO, Bulawa C, Pregel MJ, Martelli A. *In vivo* overexpression of frataxin causes toxicity mediated by iron-sulfur cluster deficiency. Mol Ther Methods Clin Dev. 2022 Feb 7;24:367-378. doi: 10.1016/j.omtm.2022.02.002. PMID: 35252470; PMCID: PMC8866050.
88. Ivanusic JJ, Bourke DW, Xu ZM, Butler EG, Horne MK. Cerebellar thalamic activity in the macaque monkey encodes the duration but not the force or velocity of wrist movement. Brain Res. 2005 Apr 18;1041(2):181-97. doi: 10.1016/j.brainres.2005.02.005. PMID: 15829227.
89. Jami L. Golgi tendon organs in mammalian skeletal muscle: functional properties and central actions. Physiol Rev. 1992 Jul;72(3):623-66. doi: 10.1152/physrev.1992.72.3.623. PMID: 1626033.Proske U, Gandevia SC. 2018. Kinesthetic senses. Compr. Physiol. 8(3):1157–83.
90. Jasoliya MJ, McMackin MZ, Henderson CK, Perlman SL, Cortopassi GA. Frataxin deficiency impairs mitochondrial biogenesis in cells, mice and humans. Hum Mol Genet. 2017 Jul 15;26(14):2627-2633. doi: 10.1093/hmg/ddx141. PMID: 28444186; PMCID: PMC6251520.
91. Jinek M, Chylinski K, Fonfara I, Hauer M, Doudna JA, Charpentier E. A programmable dual-RNA-guided DNA endonuclease in adaptive bacterial immunity. Science. 2012 Aug 17;337(6096):816-21. doi: 10.1126/science.1225829. Epub 2012 Jun 28. PMID: 22745249; PMCID: PMC6286148.
92. Jiralerspong S, Liu Y, Montermini L, Stifani S, Pandolfo M. Frataxin shows developmentally regulated tissue-specific expression in the mouse embryo. Neurobiol Dis. 1997;4(2):103-13. doi: 10.1006/nbdi.1997.0139. PMID: 9331900.
93. Kalef-Ezra E, Edzeamey FJ, Valle A, Khonsari H, Kleine P, Oggianu C, Al-Mahdawi S, Pook MA, Anjomani Virmouni S. A new FRDA mouse model [Fxnnull:YG8s(GAA) > 800] with more than 800 GAA repeats. Front Neurosci. 2023 Jan 26;17:930422. doi: 10.3389/fnins.2023.930422. PMID: 36777637; PMCID: PMC9909538.
94. Kalter N, Fuster-García C, Silva A, Ronco-Díaz V, Roncelli S, Turchiano G, Jan Gorodkin, Cathomen T, Benabdellah K, Lee C, Hendel A, Off-target effects in CRISPR-Cas genome editing for human therapeutics: Progress and challenges, Molecular Therapy Nucleic Acids, Volume 36, Issue 3, 2025, 102636, ISSN 2162-2531, https://doi.org/10.1016/j.omtn.2025.102636.
95. Kasemeier-Kulesa JC, Kulesa PM, Lefcort F. Imaging neural crest cell dynamics during formation of dorsal root ganglia and sympathetic ganglia. Development. 2005 Jan;132(2):235-45. doi: 10.1242/dev.01553. Epub 2004 Dec 8. PMID: 15590743.

96. Keita M, McIntyre K, Rodden LN, Schadt K, Lynch DR. Friedreich ataxia: clinical features and new developments. Neurodegener Dis Manag. 2022 Oct;12(5):267-283. doi: 10.2217/nmt-2022-0011. Epub 2022 Jun 29. PMID: 35766110; PMCID: PMC9517959.
97. Khorkova O, Stahl J, Joji A, Volmar CH, Wahlestedt C. Amplifying gene expression with RNA-targeted therapeutics. Nat Rev Drug Discov. 2023 Jul;22(7):539-561. doi: 10.1038/s41573-023-00704-7. Epub 2023 May 30. PMID: 37253858; PMCID: PMC10227815.
98. Kiehn, O. Decoding the organization of spinal circuits that control locomotion. *Nat Rev Neurosci* **17**, 224–238 (2016). https://doi.org/10.1038/nrn.2016.9
99. Klein R, Silos-Santiago I, Smeyne RJ, Lira SA, Brambilla R, Bryant S, Zhang L, Snider WD, Barbacid M. Disruption of the neurotrophin-3 receptor gene trkC eliminates la muscle afferents and results in abnormal movements. Nature. 1994 Mar 17;368(6468):249-51. doi: 10.1038/368249a0. PMID: 8145824.
100. Koeppen AH. Friedreich's ataxia: pathology, pathogenesis, and molecular genetics. J Neurol Sci. 2011 Apr 15;303(1-2):1-12. doi: 10.1016/j.jns.2011.01.010. PMID: 21315377; PMCID: PMC3062632.
101. Konermann S, Brigham MD, Trevino AE, Joung J, Abudayyeh OO, Barcena C, Hsu PD, Habib N, Gootenberg JS, Nishimasu H, Nureki O, Zhang F. Genome-scale transcriptional activation by an engineered CRISPR-Cas9 complex. Nature. 2015 Jan 29;517(7536):583-8. doi: 10.1038/nature14136. Epub 2014 Dec 10. PMID: 25494202; PMCID: PMC4420636.
102. Kosicki M, Tomberg K, Bradley A. Repair of double-strand breaks induced by CRISPR-Cas9 leads to large deletions and complex rearrangements. Nat Biotechnol. 2018 Sep;36(8):765-771. doi: 10.1038/nbt.4192. Epub 2018 Jul 16. PMID: 30010673; PMCID: PMC6390938.
103. Koutnikova H, Campuzano V, Koenig M. Maturation of wild-type and mutated frataxin by the mitochondrial processing peptidase. Hum Mol Genet. 1998 Sep;7(9):1485-9. doi: 10.1093/hmg/7.9.1485. PMID: 9700204.
104. Kröger S, Watkins B. Muscle spindle function in healthy and diseased muscle. Skelet Muscle. 2021 Jan 7;11(1):3. doi: 10.1186/s13395-020-00258-x. PMID: 33407830; PMCID: PMC7788844.
105. Kröger S. Proprioception 2.0: novel functions for muscle spindles. Curr Opin Neurol. 2018 Oct;31(5):592-598. doi: 10.1097/WCO.0000000000000590. PMID: 30095484.
106. Ku S, Soragni E, Campau E, Thomas EA, Altun G, Laurent LC, Loring JF, Napierala M, Gottesfeld JM. Friedreich's ataxia induced pluripotent stem cells model intergenerational GAA·TTC triplet repeat instability. Cell Stem Cell. 2010 Nov 5;7(5):631-7. doi: 10.1016/j.stem.2010.09.014. PMID: 21040903; PMCID: PMC2987635.
107. Le Douarin N, Dulac C, Dupin E, Cameron-Curry P. Glial cell lineages in the neural crest. Glia. 1991;4(2):175-84. doi: 10.1002/glia.440040209. PMID: 1827777.

108. Lee YK, Ho PW, Schick R, Lau YM, Lai WH, Zhou T, Li Y, Ng KM, Ho SL, Esteban MA, Binah O, Tse HF, Siu CW. Modeling of Friedreich ataxia-related iron overloading cardiomyopathy using patient-specific-induced pluripotent stem cells. Pflugers Arch. 2014 Sep;466(9):1831-44. doi: 10.1007/s00424-013-1414-x. Epub 2013 Dec 11. PMID: 24327207.

109. Li Y, Polak U, Bhalla AD, Rozwadowska N, Butler JS, Lynch DR, Dent SYR, Napierala M. Excision of Expanded GAA Repeats Alleviates the Molecular Phenotype of Friedreich's Ataxia. Mol Ther. 2015 Jun;23(6):1055-1065. doi: 10.1038/mt.2015.41. Epub 2015 Mar 11. PMID: 25758173; PMCID: PMC4817761.

110. Lill R, Mühlenhoff U, Iron–sulfur-protein biogenesis in eukaryotes, Trends in Biochemical Sciences, Volume 30, Issue 3, 2005, Pages 133-141, ISSN 0968-0004, https://doi.org/10.1016/j.tibs.2005.01.006.

111. Liu J, Verma PJ, Evans-Galea MV, Delatycki MB, Michalska A, Leung J, Crombie D, Sarsero JP, Williamson R, Dottori M, Pébay A. Generation of induced pluripotent stem cell lines from Friedreich ataxia patients. Stem Cell Rev Rep. 2011 Sep;7(3):703-13. doi: 10.1007/s12015-010-9210-x. PMID: 21181307.

112. Liu XS, Wu H, Ji X, Stelzer Y, Wu X, Czauderna S, Shu J, Dadon D, Young RA, Jaenisch R. Editing DNA Methylation in the Mammalian Genome. Cell. 2016 Sep 22;167(1):233-247.e17. doi: 10.1016/j.cell.2016.08.056. PMID: 27662091; PMCID: PMC5062609.

113. Loutit AJ, Vickery RM, Potas JR. Functional organization and connectivity of the dorsal column nuclei complex reveals a sensorimotor integration and distribution hub. J Comp Neurol. 2021 Jan;529(1):187-220. doi: 10.1002/cne.24942. Epub 2020 Jun 26. PMID: 32374027.

114. Lynch DR, Chin MP, Delatycki MB, Subramony SH, Corti M, Hoyle JC, Boesch S, Nachbauer W, Mariotti C, Mathews KD, Giunti P, Wilmot G, Zesiewicz T, Perlman S, Goldensberry A, O'Grady M, Meyer CJ. Safety and Efficacy of Omaveloxolone in Friedreich Ataxia (MOXIe Study). Ann Neurol. 2021 Feb;89(2):212-225. doi: 10.1002/ana.25934. Epub 2020 Nov 5. Erratum in: Ann Neurol. 2023. Dec;94(6):1190. doi: 10.1002/ana.26808. PMID: 33068037; PMCID: PMC7894504.

115. Lynch DR, Goldensberry A, Rummey C, Farmer J, Boesch S, Delatycki MB, Giunti P, Hoyle JC, Mariotti C, Mathews KD, Nachbauer W, Perlman S, Subramony SH, Wilmot G, Zesiewicz T, Weissfeld L, Meyer C. Propensity matched comparison of omaveloxolone treatment to Friedreich ataxia natural history data. Ann Clin Transl Neurol. 2024 Jan;11(1):4-16. doi: 10.1002/acn3.51897. Epub 2023 Sep 10. PMID: 37691319; PMCID: PMC10791025.

116. Lynch DR, Regner SR, Schadt KA, Friedman LS, Lin KY, St John Sutton MG. Management and therapy for cardiomyopathy in Friedreich's ataxia. Expert Rev Cardiovasc Ther. 2012 Jun;10(6):767-77. doi: 10.1586/erc.12.57. PMID: 22894632.

117. Ma, D., Peng, S. & Xie, Z. Integration and exchange of split dCas9 domains for transcriptional controls in mammalian cells. *Nat Commun* 7, 13056 (2016). https://doi.org/10.1038/ncomms13056

118. Macefield VG, Knellwolf TP. Functional properties of human muscle spindles. J Neurophysiol. 2018 Aug 1;120(2):452-467. doi: 10.1152/jn.00071.2018. Epub 2018 Apr 18. PMID: 29668385.

119. Mahmud AA, Nahid NA, Nassif C, Sayeed MS, Ahmed MU, Parveen M, Khalil MI, Islam MM, Nahar Z, Rypens F, Hamdan FF, Rouleau GA, Hasnat A, Michaud JL. Loss of the proprioception and touch sensation channel PIEZO2 in siblings with a progressive form of contractures. Clin Genet. 2017 Mar;91(3):470-475. doi: 10.1111/cge.12850. Epub 2016 Sep 16. PMID: 27607563.

120. Manuel M, Zytnicki D. Alpha, beta and gamma motoneurons: functional diversity in the motor system's final pathway. J Integr Neurosci. 2011 Sep;10(3):243-76. doi: 10.1142/S0219635211002786. PMID: 21960303.

121. Marchetto MC, Carromeu C, Acab A, Yu D, Yeo GW, Mu Y, Chen G, Gage FH, Muotri AR. A model for neural development and treatment of Rett syndrome using human induced pluripotent stem cells. Cell. 2010 Nov 12;143(4):527-39. doi: 10.1016/j.cell.2010.10.016. PMID: 21074045; PMCID: PMC3003590.

122. Masingue M, Fauré J, Solé G, Stojkovic T, Léonard-Louis S. A novel nonsense PIEZO2 mutation in a family with scoliosis and proprioceptive defect. Neuromuscul Disord. 2019 Jan;29(1):75-79. doi: 10.1016/j.nmd.2018.10.005. Epub 2018 Nov 8. PMID: 30578100.

123. Matsuda S, Kobayashi N, Mominoki K, Wakisaka H, Mori M, Murakami S. [Morphological transformation of sensory ganglion neurons and satellite cells]. Kaibogaku Zasshi. 1998 Dec;73(6):603-13. Japanese. PMID: 9990197.

124. Matthews PB. Where Anatomy led, Physiology followed: a survey of our developing understanding of the muscle spindle, what it does and how it works. J Anat. 2015 Aug;227(2):104-14. doi: 10.1111/joa.12345. PMID: 26179022; PMCID: PMC4523315.

125. Matthews PBC. 1972. Mammalian Muscle Receptors and Their Central Actions. Philadelphia: Williams & Wilkins.

126. Matuszek, Z., Arbab, M., Kesavan, M. *et al.* Base editing of trinucleotide repeats that cause Huntington's disease and Friedreich's ataxia reduces somatic repeat expansions in patient cells and in mice. *Nat* Gene*t* 57, 1437–1451 (2025). https://doi.org/10.1038/s41588-025-02172-8.

127. Mavrinskaya LF. Development of muscle spindles in man. Neurosci Translat. 1968; 2:529–35.

128. Mazzara, P.G., Muggeo, S., Luoni, M. et al. Frataxin gene editing rescues Friedreich's ataxia pathology in dorsal root ganglia organoid-derived sensory neurons. Nat Commun 11, 4178 (2020). https://doi.org/10.1038/s41467-020-17954-3.

129. Medina-Carbonero M, Sanz-Alcázar A, Britti E, Delaspre F, Cabiscol E, Ros J, Tamarit J. Mice harboring the FXN I151F pathological point mutation present decreased frataxin levels, a Friedreich ataxia-like phenotype, and mitochondrial alterations. Cell Mol Life Sci. 2022 Jan 17;79(2):74. doi: 10.1007/s00018-021-04100-5. PMID: 35038030; PMCID: PMC8763788.

130. Meltzer S, Santiago C, Sharma N, Ginty DD. The cellular and molecular basis of somatosensory neuron development. Neuron. 2021 Dec 1;109(23):3736-3757. doi: 10.1016/j.neuron.2021.09.004. Epub 2021 Sep 29. PMID: 34592169; PMCID: PMC8639614.

131. Monfort B, Want K, Gervason S, D'Autréaux B. Recent Advances in the Elucidation of Frataxin Biochemical Function Open Novel Perspectives for the Treatment of Friedreich's Ataxia. Front Neurosci. 2022 Mar 2;16:838335. doi: 10.3389/fnins.2022.838335. PMID: 35310092; PMCID: PMC8924461.

132. Nascimento AI, Mar FM, Sousa MM. The intriguing nature of dorsal root ganglion neurons: Linking structure with polarity and function. Prog Neurobiol. 2018. Sep;168:86-103. doi: 10.1016/j.pneurobio.2018.05.002. Epub 2018 May 2. PMID: 29729299.

133. Nishimasu H, Ran FA, Hsu PD, Konermann S, Shehata SI, Dohmae N, Ishitani R, Zhang F, Nureki O. Crystal structure of Cas9 in complex with guide RNA and target DNA. Cell. 2014 Feb 27;156(5):935-49. doi: 10.1016/j.cell.2014.02.001. Epub 2014 Feb 13. PMID: 24529477; PMCID: PMC4139937.

134. Olausson H, Wessberg J, Morrison I, McGlone F, Vallbo A. The neurophysiology of unmyelinated tactile afferents. Neurosci Biobehav Rev. 2010 Feb;34(2):185-91. doi: 10.1016/j.neubiorev.2008.09.011. Epub 2008 Oct 8. PMID: 18952123.

135. Ouellet DL, Cherif K, Rousseau J, Tremblay JP. Deletion of the GAA repeats from the human frataxin gene using the CRISPR-Cas9 system in YG8R-derived cells and mouse models of Friedreich ataxia. Gene Ther. 2017 May;24(5):265-274. doi: 10.1038/gt.2016.89. Epub 2016 Dec 26. PMID: 28024081.

136. Pacesa M, Pelea O, Jinek M. Past, present, and future of CRISPR genome editing technologies. Cell. 2024 Feb 29;187(5):1076-1100. doi: 10.1016/j.cell.2024.01.042. PMID: 38428389.

137. Pandolfo M. Friedreich ataxia: the clinical picture. J Neurol. 2009 Mar;256 Suppl 1:3-8. doi: 10.1007/s00415-009-1002-3. PMID: 19283344.

138. Parent A., Elduque X., Cornu D. et al. Mammalian frataxin directly enhances sulfur transfer of NFS1 persulfide to both ISCU and free thiols. Nat Commun 6, 5686 (2015). https://doi.org/10.1038/ncomms6686.

139. Paupe V, Dassa EP, Goncalves S, Auchère F, Lönn M, Holmgren A, Rustin P. Impaired nuclear NRF2 translocation undermines the oxidative stress response in Friedreich ataxia. PLoS One. 2009;4(1):e4253. doi: 10.1371/journal.pone.0004253. Epub 2009 Jan 22. PMID: 19158945; PMCID: PMC2617762.

140. Pavletich NP, Pabo CO. Zinc finger-DNA recognition: crystal structure of a Zif268-DNA complex at 2.1 A. Science. 1991 May 10;252(5007):809-17. doi: 10.1126/science.2028256. PMID: 2028256.

141. Payne RM. The Heart in Friedreich's Ataxia: Basic Findings and Clinical Implications. Prog Pediatr Cardiol. 2011 May;31(2):103-109. doi: 10.1016/j.ppedcard.2011.02.007. PMID: 21691434; PMCID: PMC3117664.

142. Perdomini M, Belbellaa B, Monassier L, Reutenauer L, Messaddeq N, Cartier N, Crystal RG, Aubourg P, Puccio H. Prevention and reversal of severe mitochondrial cardiomyopathy by gene therapy in a mouse model of Friedreich's ataxia. Nat Med. 2014 May;20(5):542-7. doi: 10.1038/nm.3510. Epub 2014 Apr 6. PMID: 24705334.

143. Perdomini M, Hick A, Puccio H, Pook MA. Animal and cellular models of Friedreich ataxia. J Neurochem. 2013 Aug;126 Suppl 1:65-79. doi: 10.1111/jnc.12219. PMID: 23859342.

144. Pharaoh G, Kamat V, Kannan S, Stuppard RS, Whitson J, Martín-Pérez M, Qian WJ, MacCoss MJ, Villén J, Rabinovitch P, Campbell MD, Sweet IR, Marcinek DJ. The mitochondrially targeted peptide elamipretide (SS-31) improves ADP sensitivity in aged mitochondria by increasing uptake through the adenine nucleotide translocator (ANT). Geroscience. 2023 Dec;45(6):3529-3548. doi: 10.1007/s11357-023-00861-y. Epub 2023 Jul 18. PMID: 37462785; PMCID: PMC10643647.

145. Pianese L, Tammaro A, Turano M, De Biase I, Monticelli A, Cocozza S. Identification of a novel transcript of X25, the human gene involved in Friedreich ataxia. Neurosci Lett. 2002 Mar 8;320(3):137-40. doi: 10.1016/s0304-3940(02)00048-4. PMID: 11852181.

146. Piguet F, de Montigny C, Vaucamps N, Reutenauer L, Eisenmann A, Puccio H. Rapid and Complete Reversal of Sensory Ataxia by Gene Therapy in a Novel Model of Friedreich Ataxia. Mol Ther. 2018 Aug 1;26(8):1940-1952. doi: 10.1016/j.ymthe.2018.05.006. Epub 2018 May 28. PMID: 29853274; PMCID: PMC6094869.

147. Proske U, Gandevia SC. The proprioceptive senses: their roles in signaling body shape, body position and movement, and muscle force. Physiol Rev. 2012 Oct;92(4):1651-97. doi: 10.1152/physrev.00048.2011. PMID: 23073629.

148. Proske U. The mammalian muscle spindle. News Physiol Sci. 1997; 12:37–42.

149. Przedpelska-Ober E. The development of muscle spindles in human fetuses. Anat Anz. 1982;152(4):371-80. PMID: 7165119.

150. Qi LS, Larson MH, Gilbert LA, Doudna JA, Weissman JS, Arkin AP, Lim WA. Repurposing CRISPR as an RNA-guided platform for sequence-specific control of gene expression. Cell. 2013 Feb 28;152(5):1173-83. doi: 10.1016/j.cell.2013.02.022. Erratum in: Cell. 2021 Feb 4;184(3):844. doi: 10.1016/j.cell.2021.01.019. PMID: 23452860; PMCID: PMC3664290.

151. Rai M, Soragni E, Jenssen K, Burnett R, Herman D, Coppola G, Geschwind DH, Gottesfeld JM, Pandolfo M. HDAC inhibitors correct frataxin deficiency in a Friedreich ataxia mouse model. PLoS One. 2008 Apr 9;3(4):e1958. doi: 10.1371/journal.pone.0001958. PMID: 18463734; PMCID: PMC2373517.

152. Reisman SA, Gahir SS, Lee CI, Proksch JW, Sakamoto M, Ward KW. Pharmacokinetics and pharmacodynamics of the novel NRF2 activator omaveloxolone in primates. Drug Des Devel Ther. 2019 Apr 17;13:1259-1270. doi: 10.2147/DDDT.S193889. PMID: 31118567; PMCID: PMC6475100.

153. Riemann BL, Lephart SM. The Sensorimotor System, Part II: The Role of Proprioception in Motor Control and Functional Joint Stability. J Athl Train. 2002 Jan;37(1):80-4. PMID: 16558671; PMCID: PMC164312.

154. Rodden LN, Chutake YK, Gilliam K, Lam C, Soragni E, Hauser L, Gilliam M, Wiley G, Anderson MP, Gottesfeld JM, Lynch DR, Bidichandani SI. Methylated and unmethylated epialleles support variegated epigenetic silencing in Friedreich ataxia. Hum Mol Genet. 2021 Feb 4;29(23):3818-3829. doi: 10.1093/hmg/ddaa267. PMID: 33432325; PMCID: PMC7861014.

155. Rowitch DH. Glial specification in the vertebrate neural tube. Nat Rev Neurosci. 2004 May;5(5):409-19. doi: 10.1038/nrn1389. PMID: 15100723.

156. Sahdeo S, Scott BD, McMackin MZ, Jasoliya M, Brown B, Wulff H, Perlman SL, Pook MA, Cortopassi GA. Dyclonine rescues frataxin deficiency in animal models and buccal cells of patients with Friedreich's ataxia. Hum Mol Genet. 2014 Dec 20;23(25):6848-62. doi: 10.1093/hmg/ddu408. Epub 2014 Aug 11. PMID: 25113747; PMCID: PMC4245046.

157. Sakamoto N, Ohshima K, Montermini L, Pandolfo M, Wells RD. Sticky DNA, a self-associated complex formed at long GAA*TTC repeats in intron 1 of the frataxin gene, inhibits transcription. J Biol Chem. 2001 Jul 20;276(29):27171-7. doi: 10.1074/jbc.M101879200. Epub 2001 May 4. PMID: 11340071.

158. Salami CO, Jackson K, Jose C, Alyass L, Cisse GI, De BP, Stiles KM, Chiuchiolo MJ, Sondhi D, Crystal RG, Kaminsky SM. Stress-Induced Mouse Model of the Cardiac Manifestations of Friedreich's Ataxia Corrected by AAV-mediated Gene Therapy. Hum Gene Ther. 2020 Aug;31(15-16):819-827. doi: 10.1089/hum.2019.363. PMID: 32646255.

159. Saveliev A, Everett C, Sharpe T, Webster Z, Festenstein R. DNA triplet repeats mediate heterochromatin-protein-1-sensitive variegated gene silencing. Nature. 2003 Apr 24;422(6934):909-13. doi: 10.1038/nature01596. PMID: 12712207.

160. Scott V, Delatycki MB, Tai G, Corben LA. New and Emerging Drug and Gene Therapies for Friedreich Ataxia. CNS Drugs. 2024 Oct;38(10):791-805. doi: 10.1007/s40263-024-01113-z. Epub 2024 Aug 8. PMID: 39115603; PMCID: PMC11377510.

161. Segal DJ, Gonçalves J, Eberhardy S, Swan CH, Torbett BE, Li X, Barbas CF 3rd. Attenuation of HIV-1 replication in primary human cells with a designed zinc finger transcription factor. J Biol Chem. 2004 Apr 9;279(15):14509-19. doi: 10.1074/jbc.M400349200. Epub 2004 Jan 20. PMID: 14734553.

162. Serbedzija GN, Fraser SE, Bronner-Fraser M. Pathways of trunk neural crest cell migration in the mouse embryo as revealed by vital dye labelling. Development. 1990 Apr;108(4):605-12. doi: 10.1242/dev.108.4.605. PMID: 2387238.

163. Shakirova KM, Ovchinnikova VY, Dashinimaev EB. Cell Reprogramming With CRISPR/Cas9 Based Transcriptional Regulation Systems. Front Bioeng Biotechnol. 2020 Jul 28;8:882. doi: 10.3389/fbioe.2020.00882. PMID: 32850737; PMCID: PMC7399070.

164. Sharma N, Flaherty K, Lezgiyeva K, Wagner DE, Klein AM, Ginty DD. The emergence of transcriptional identity in somatosensory neurons. Nature. 2020 Jan;577(7790):392-398. doi: 10.1038/s41586-019-1900-1. Epub 2020 Jan 8. PMID: 31915380; PMCID: PMC7307422.

165. Sherrington CS. On the proprioceptive system, especially in its reflex aspect. Brain. 907;29(4):467–82.

166. Sivakumar A, Cherqui S. Advantages and Limitations of Gene Therapy and Gene Editing for Friedreich's Ataxia. Front Genome Ed. 2022 May 17;4:903139. doi: 10.3389/fgeed.2022.903139. PMID: 35663795; PMCID: PMC9157421.

167. Smeyne RJ, Klein R, Schnapp A, Long LK, Bryant S, Lewin A, Lira SA, Barbacid M. Severe sensory and sympathetic neuropathies in mice carrying a disrupted Trk/NGF receptor gene. Nature. 1994 Mar 17;368(6468):246-9. doi: 10.1038/368246a0. PMID: 8145823.

168. Smith LJ, Norcliffe-Kaufmann L, Palma JA, Kaufmann H, Macefield VG. Impaired sensorimotor control of the hand in congenital absence of functional muscle spindles. J Neurophysiol. 2018 Dec 1;120(6):2788-2795. doi: 10.1152/jn.00528.2018. Epub 2018 Sep 19. PMID: 30230986; PMCID: PMC7199231.

169. Soragni E, Chou CJ, Rusche JR, Gottesfeld JM. Mechanism of Action of 2-Aminobenzamide HDAC Inhibitors in Reversing Gene Silencing in Friedreich's Ataxia. Front Neurol. 2015 Mar 5;6:44. doi: 10.3389/fneur.2015.00044. PMID: 25798128; PMCID: PMC4350406.

170. Tanenbaum ME, Gilbert LA, Qi LS, Weissman JS, Vale RD. A protein-tagging system for signal amplification in gene expression and fluorescence imaging. Cell. 2014 Oct 23;159(3):635-46. doi: 10.1016/j.cell.2014.09.039. Epub 2014 Oct 9. PMID: 25307933; PMCID: PMC4252608.

171. Truong DJ, Kühner K, Kühn R, Werfel S, Engelhardt S, Wurst W, Ortiz O. Development of an intein-mediated split-Cas9 system for gene therapy. Nucleic Acids Res. 2015 Jul 27;43(13):6450-8. doi: 10.1093/nar/gkv601. Epub 2015 Jun 16. PMID: 26082496; PMCID: PMC4513872.

172. Tuthill JC, Azim E. Proprioception. Curr Biol. 2018 Mar 5;28(5):R194-R203. doi: 10.1016/j.cub.2018.01.064. PMID: 29510103.

173. Tycko, J., Van, M.V., Aradhana et al. Development of compact transcriptional effectors using high-throughput measurements in diverse contexts. Nat Biotechnol 43, 1525–1538 (2025). https://doi.org/10.1038/s41587-024-02442-6.

174. Vaubel RA, Isaya G. Iron-sulfur cluster synthesis, iron homeostasis and oxidative stress in Friedreich ataxia. Mol Cell Neurosci. 2013 Jul;55:50-61. doi: 10.1016/j.mcn.2012.08.003. Epub 2012 Aug 11. PMID: 22917739; PMCID: PMC3530001.

175. Wright DE, Zhou L, Kucera J, Snider WD. Introduction of a neurotrophin-3 transgene into muscle selectively rescues proprioceptive neurons in mice lacking endogenous neurotrophin-3. Neuron. 1997 Sep;19(3):503-17. doi: 10.1016/s0896-6273(00)80367-0. PMID: 9331344.

176. Xia H, Cao Y, Dai X, Marelja Z, Zhou D, Mo R, Al-Mahdawi S, Pook MA, Leimkühler S, Rouault TA, Li K. Novel frataxin isoforms may contribute to the pathological mechanism of Friedreich ataxia. PLoS One. 2012;7(10):e47847. doi: 10.1371/journal.pone.0047847. Epub 2012 Oct 17. PMID: 23082224; PMCID: PMC3474739.

177. Xue C, Greene EC. DNA Repair Pathway Choices in CRISPR-Cas9-Mediated Genome Editing. Trends Genet. 2021 Jul;37(7):639-656. doi: 10.1016/j.tig.2021.02.008. Epub 2021 Apr 22. PMID: 33896583; PMCID: PMC8187289.

178. Yandim C, Natisvili T, Festenstein R. Gene regulation and epigenetics in Friedreich's ataxia. J Neurochem. 2013 Aug;126 Suppl 1:21-42. doi: 10.1111/jnc.12254. PMID: 23859339.

179. Zalatan JG, Lee ME, Almeida R, Gilbert LA, Whitehead EH, La Russa M, Tsai JC, Weissman JS, Dueber JE, Qi LS, Lim WA. Engineering complex synthetic transcriptional programs with CRISPR RNA scaffolds. Cell. 2015 Jan 15;160(1-2):339-50. doi: 10.1016/j.cell.2014.11.052. Epub 2014 Dec 18. PMID: 25533786; PMCID: PMC4297522.

180. Zampieri N, de Nooij JC. Regulating muscle spindle and Golgi tendon organ proprioceptor phenotypes. Curr Opin Physiol. 2021 Feb;19:204-210. doi: 10.1016/j.cophys.2020.11.001. Epub 2020 Nov 10. PMID: 33381667; PMCID: PMC7769215.

181. Zeitler, B., Froelich, S., Marlen, K. *et al.* Allele-selective transcriptional repression of mutant *HTT* for the treatment of Huntington's disease. *Nat Med* 25, 1131–1142 (2019). https://doi.org/10.1038/s41591-019-0478-3.

182. Zelena J. Nerves and mechanoreceptors—the role of innervation in the development and maintenance of mammalian mechanoreceptors. New York: Chapman and Hall; 1994. p. 38–137.

183. Zhang Y, Lin S, Karakatsani A, Rüegg MA, Kröger S. Differential regulation of AChR clustering in the polar and equatorial region of murine muscle spindles. Eur J Neurosci. 2015 Jan;41(1):69-78. doi: 10.1111/ejn.12768. Epub 2014 Nov 6. PMID: 25377642.

184. Shengyao Zhi, Yuxi Chen, Guanglan Wu, Jinkun Wen, Jinni Wu, Qianyi Liu, Yang Li, Rui Kang, Sihui Hu, Jiahui Wang, Puping Liang, Junjiu Huang, Dual-AAV delivering split prime editor system for in vivo genome editing, Molecular Therapy, Volume 30, Issue 1, 2022, Pages 283-294, ISSN 1525-0016, https://doi.org/10.1016/j.ymthe.2021.07.011.

185. Zimmerman A, Bai L, Ginty DD. The gentle touch receptors of mammalian skin. Science. 2014 Nov 21;346(6212):950-4. doi: 10.1126/science.1254229. PMID: 25414303; PMCID: PMC4450345.

186. Zotterman Y. Touch, pain and tickling: an electro-physiological investigation on cutaneous sensory nerves. J Physiol. 1939 Feb 14;95(1):1-28. doi: 10.1113/jphysiol.1939.sp003707. PMID: 16995068; PMCID: PMC1393960.

Acknowledgements

I would first like to express my gratitude to Vania Broccoli for giving me the opportunity to begin this path in his lab and for trusting me with this project.

A very special thank you goes to Margherita Rossi and Agostina Di Pizio for their constant help with the experiments, their precious advice, and their support both inside and outside the lab. Working with you has been an inspiring and enriching experience.

I would also like to thank all the members of the lab, past and present, for creating such a stimulating and supportive environment. Your friendship and collaboration made even the hardest moments easier to face and turned this journey into an unforgettable experience. These PhD years, though difficult at times, taught me the importance of perseverance and critical thinking, that will be part of me also in future challenges.